



JASCO Solutions Book
Petro & Chemicals Volume 2

JASCO Europe is in charge for marketing, sales, service and support for all Jasco products throughout **Europe, Middle East and Africa.**



JASCO Europe S.r.l.

Via Cadorna, 1 - 23894 Cremella (LC)

Tel. +39-0399215811

Fax +39-0399215835

jasco@jasco-europe.com

www.jasco-europe.com

Follow us on:



Make the most of your investment with JASCO Service and Support

JASCO Service and Support agreement plans are designed for those laboratories pursuing superior productivity through the highest level of professional services.

The use of automated instrumentation is the right approach to meet today's laboratories productivity requirements, reducing analysis run times, enhancing sample throughput, and increasing analytical accuracy and precision. In this view, preventive maintenance is very important to maximize laboratory uptime and avoid unexpected expenses.

In addition to the analytical goal, proper installation and maintenance are required to achieve optimal performance. JASCO provides flexible service and support management solutions focused on your laboratory real objectives.

With its service network, JASCO is ready to maintain the perfect reliability of customer's instrumentation and minimize the laboratory down time.

- Superior productivity
- Optimized analytical performance
- Lower cost of ownership
- Extended instrument life

If your laboratory has specific Service and Support requirements, JASCO can help you with customized contract agreements. In addition, a full set of Installation Qualification (IQ), Operational Qualification (OQ), and Performance Qualification (PQ) tests are available to verify the system proper installation, operation and performance, respectively.

Get the most from your investment with JASCO Training Courses

JASCO Training Courses ensure maximum skill development for the best value of your laboratory. Our team of highly-experienced specialists can help your staff to get the most from your instrument reducing your analysis run time and improve performance.

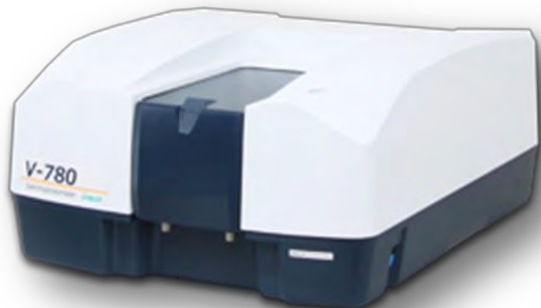
Build your knowledge with JASCO Training Courses:

- Instrument and Software operation
- troubleshooting
- Maintenance
- Calibration
- Applications and Methods developments
- Operating Techniques



V-730 – V-730bio – V-750 – V-760

UV-Vis Spectrophotometers



V-770 – V-780

UV-Vis/NIR Spectrophotometers

With more than fifty years of experience in the design of spectrophotometers, JASCO offers a complete range of UV-Vis/NIR instruments.

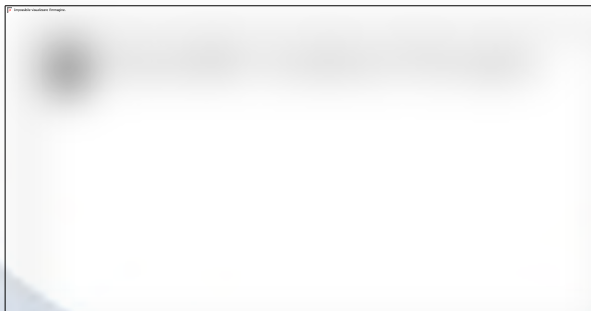
The **V-700 series** consists of six distinct models designed to meet a wide range of application requirements.

From an innovative optical layout to a simple comprehensive instrument control and data analysis software interface, the **V-700 series** does not compromise on accuracy, performance or reliability.

All spectrophotometers are controlled by **Spectra Manager™ II**, JASCO's powerful cross-platform spectroscopy software package with USB communication.

FT/IR-4600 – FT/IR-4700

FT/IR Spectrometers



FT/IR-6600 – FT/IR-6700 – FT/IR-6800

FT/IR Spectrometers

The **FT/IR-4000** and **FT/IR-6000** models represent a broad range of instrumentation that redefine infrared spectroscopy as a powerful yet easy to use technique in a compact and reliable line of instruments with the highest signal-to-noise ratio.

All models are controlled by **Spectra Manager™ II**, JASCO'S powerful cross-platform spectroscopy software package with USB communication.

All models feature an auto-alignment function which maintains instrument optical alignment after beamsplitter changes or instrument movement.

IRT-5100 – IRT-5200

FT/IR Microscopes



IRT-7100 – IRT-7200

FT/IR Microscopes

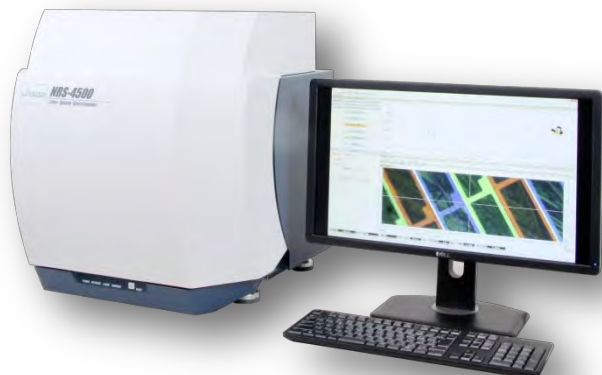
JASCO is proud to release four innovative FT-IR Microscope, the **IRT-5000** and **IRT-7000**, providing several new functions that drastically improve infrared micro-spectroscopy analysis.

Both microscope systems can be easily interfaced with either the FT/IR-4000 or FT/IR-6000 spectrometer, offering the most advanced microscopy and imaging systems available in the market today.

The microscope system automatically scans the specified points or area, rapidly collecting a full spectrum of each point without moving the sample stage.

NRS-4500

Laser Raman Spectrometer



The system offers space-saving, automated switching laser light source and alignment adjustment to assist the analysis, **NRS-4500** is easily used to quality control as well as research and development.

The micro-Raman **NRS-4500** is equipped with measurement assist function that can be easily setup operation and a user advice function that automatically analyzes the spectrum and obtain a high-quality data even at the first time.

QRI – Quick Raman Imaging function (available also on NRS-5000/7000 series) allows imaging speed x50 faster than traditional systems.

High Speed/High Accuracy Automatic Stage combined with High Speed EMCCD detector make it possible to shorten amount of imaging time dramatically.

NRS-5500 – NRS-5600

Laser Raman Spectrometers



NRS-7500 – NRS-7600

Laser Raman Spectrometers

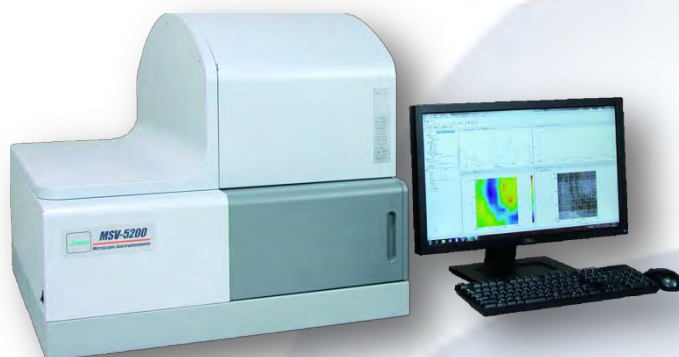
The performance expected on a micro-Raman spectrometer are fully provided with the JASCO **NRS-5000/7000** series Raman systems, assuring consistent performance for rapid acquisition of high quality data with automated system control and minimal optical adjustments.

For application expansion, an automated multi-grating turret, 2 internally mounted detectors and a maximum of 8 lasers ranging from the UV through the NIR are capable of integration with the instrument system.

Spectra Manager™ II for the **NRS-5000/7000** offers revolutionary features to simplify previously difficult measurement and analysis tasks, while adding various user-support tools such as auto-fluorescence-correction, wavenumber correction, intensity correction, and a novel user-advice function.

MSV-5100 – MSV-5200 – MSV-5300

UV-Vis/NIR Microscopes



The MSV-5000 series is a microscopic spectrophotometer system providing transmittance/reflectance measurements of a microscopic sample area with a wide wavelength range from ultraviolet to near infrared.

MSV-5100 Spectrophotometer is a dedicated UV-Vis microscope with a wavelength range of (200-900 nm).

MSV-5200 Spectrophotometer includes a Peltier-cooled PbS detector and has a wavelength range of (200-2700 nm).

MSV-5300 Spectrophotometer incorporates an InGaAs detector to obtain optimized NIR measurements and has a wavelength range of (200-1600 nm).

J-1100 – J-1500 – J-1700

Circular Dichroism Spectropolarimeters



The latest effort in the JASCO commitment to lead the field of Circular Dichroism.

Unparalleled optical performance and optionally available measurement modes are combined in a manner to make the **J-1000 Series Spectropolarimeter**, a true "chiro-optical spectroscopy workbench", **able to work up to 2,500 nm**.

Instrument control and data processing are handled effortlessly by our JASCO's user friendly and innovative cross-platform software, **Spectra Manager™ II**.

FVS-6000

Vibrational Circular Dichroism



The **FVS-6000** not only allows you to easily obtain fingerprint VCD spectra, but also has several unique features such as a measurement range extension option of $4000-750\text{ cm}^{-1}$.

Since the CD signals in the infrared region are one or more orders of magnitude lower than ECD signals in the UV-Vis region, high sensitivity and stability are required for a VCD spectrometer.

The **FVS-6000** is the VCD spectrometer of choice for highly sensitive VCD measurements.

P-2000

Digital Polarimeter

The **P-2000** is designed as a customizable polarimeter with various options for a range of applications and budgetary requirements.

Options such as polarizers, wavelength filters, lamps and photomultiplier detectors provide a wide range of analytical wavelengths from UV-Vis to NIR.

A newly redesigned **intelligent remote module (iRM)** with a color LCD touch screen conveniently guides the operator through routines from data acquisition to data processing. The obtained data can be automatically printed to USB printers, or saved to a compact flash memory card for further processing on a PC.



FP-8200 – FP-8300

FP-8500 – FP-8600 – FP-8700

Spectrofluorometers

Designed with the latest technology, the **FP-8000 Series** spectrofluorometers incorporate the highest sensitivity, fastest spectral scanning capability and excellent analysis-oriented functionality offering integrated solutions for NIR advanced materials research and biochemical analysis applications.

To meet the most stringent analysis demands, a variety of accessories are available for integration with a range of sophisticated control and analysis applications available in the user-friendly **Spectra Manager™ II** software to offer a flexible platform for any fluorescence and phosphorescence application.



RMP-510 – RMP-520 – RMP-530

Portable RAMAN Spectrometers



JASCO's new **RMP-500** Series has been developed to meet the needs of Material Science, Manufacturing and Biochemistry by combining the flexibility of a fiber optic probe with a portable Raman Microspectrometer.

The RMP-500 Series consists of three models, **RMP-510, RMP-520, RMP-530** ranging from small, portable units suitable for in-situ measurements to research-grade systems that will meet even the most difficult application requirements.

The **RMP-500** Series portable Raman spectrometer systems feature an integrated fiber optic probe with a small X-Y-Z stage, a compact laser, a high-throughput spectrograph and CCD detector.

VIR-100 – VIR-200 – VIR-300

Portable FT-IR Spectrometers

The **VIR-100/200/300** series are compact, lightweight, flexible FT-IR systems.

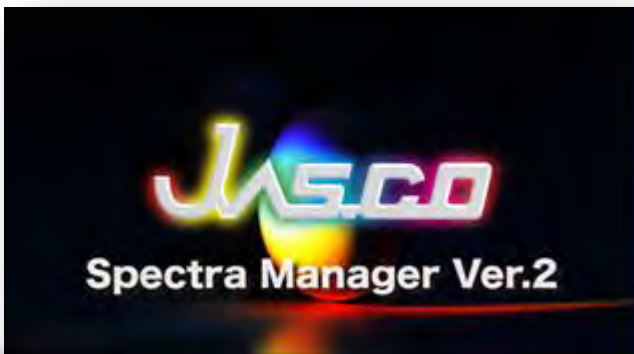
The collimated entrance and exit ports make it an ideal instrument for a wide range of applications.

The standard instrument includes a hermetically sealed interferometer, DLATGS detector, high intensity source, KRS-5 windows and automatic alignment. Options can be added for increased sensitivity, optional spectral ranges including NIR, and battery operation.

For even greater flexibility, external connection optics allows the user to install up to three different attachments in one system, selecting the most appropriate application accessory by simply switching the PC controlled optical configuration.



JASCO is the first manufacturer to develop a powerful, cross-platform software package, "**Spectra Manager**", for controlling a wide range of spectroscopic instrumentation. Spectra Manager program is a comprehensive package for capturing and processing data, eliminating the need to learn multiple software packages and offering the user a shallower learning curve.



Several types of measurement data files (UV-Vis/NIR, FT-IR, Fluorescence, etc.) can be viewed in a single window, and processed using a full range of data manipulation functions.

The latest version, Spectra Manager II, includes four measurement programs, a spectra analysis program, an instrument validation program and the JASCO Canvas program as standard. It is possible to analyze data even during sample measurements.

Spectra Manager CFR provides features to support laboratories in compliance with 21 CFR Part 11.

LC-4000

High Performance Liquid Chromatography



The **LC-4000** Series is the latest in a long history of innovative HPLC systems developed by JASCO reaching all the way back to the start of commercial HPLC in the early 1970s.

The concept of the integrated **LC-4000** series HPLC provides key separation platforms at 50MPa, 70MPa and 130MPa which correspond to **conventional HPLC**, the increasingly popular Rapid Analysis **Fast HPLC** and sub 2 μ m **U-HPLC** respectively.

Each platform is supplied with a dedicated pump and autosampler matched to the operating pressure and share detectors optimized for high-speed 100Hz acquisition and the narrow peak shapes common to both Fast HPLC and U-HPLC.

In the LC-4000 series, SSQD technology (Slow Suction, Quick Delivery) has been re-developed, with a completely new solvent delivery mechanism offering the highest stability in solvent delivery across the entire analytical flow rate range used in the **PU-4100** Fast HPLC and **PU-4200** U-HPLC pump models.

JASCO has the largest range of optical detectors - from **dual wavelength UV** to **diode array** to unique **chiral detectors**. All the detector are designed to meet U-HPLC requirements, data acquisition rate of 100Hz.

SFC-4000

Supercritical Fluid Chromatography

The JASCO **SFC/SFE 4000** integrated Analytical SFC system has been developed for all aspects of analytical SFC; including routine separation, method development and small scale preparation of samples at the mg scale.

With a simple intuitive software and robust engineering, the JASCO SFC system is a powerful tool for analytical separations.



Before separating and collecting the target chiral compound, finding the optimum separation condition is required (column, solvent, etc.).

JASCO offers a wide range of detectors with high pressure cells UV, Diode Array (real-time collection of 3D spectra and chromatogram) and the only CD detector available for SFC.

Especially, **JASCO original CD detector** measures optical isomers with circular dichromatic absorption, and can measure both CD and UV chromatograms as well as g-factor (CD/UV) chromatograms. Since g-factor in particular has a proportional relationship with the compositional ratio of optical isomer sample, the CD detector can perform compositional measurements and high purity fractionation for non-separated peaks.

LC-4500 Compact HPLC



The new **LC-4500** model has been developed taking into account laboratory space requirements.

The **LC-4500** compact HPLC provides outstanding performances in **conventional HPLC**, making effective use of lab space.

PU-4580 enables to configure the various solvent delivery system, **AS-4550** can provide the various sample injection method and **UV-4570** UV-Vis detector offers you an enhanced sensitivity.

LC-4500 model has the key panel, which achieves simple operation.

Combination with existing LC-4000 modules can provides wider application.

Both HPLC and SFC/SFE systems are coupled with **ChromNAV 2.0** data system to offer both HPLC and spectral data handling for most of the detectors even with the dual wavelength UV detector.

A newly added feature of **ChromNAV 2.0** is the automatic e-mail notification on your smartphone/tablet, stay always updated on analysis status of your LC-4000. Full GLP compliance and 21 CFR part 11.



Application	Description	Page	Technique
030-AN-002	Evaluation of crystallization in micro part on plastic (polyethylene terephthalate)	12	RAMAN
030-AN-003	Raman and Photoluminescence Measurements of Glass and Quartz Materials	13	RAMAN
040-AN-004	Qualitative analysis of colorant by Raman Spectroscopy	14	RAMAN
030-AN-005	2D correlation spectroscopy using 2 kinds of spectrum of IR and Raman obtained by time course measurement (Analysis of instant adhesive in cure process)	17	RAMAN
030-AN-006	Determination of ortho and para hydrogen ratio by using Raman spectroscopy Application to fuel cell	19	RAMAN
030-AN-013	Evaluation of cosmetics by Raman micro-spectroscopy	21	RAMAN
260-AN-0010	Measurement of buried foreign material by Raman Spectrometer NRS-4100	23	RAMAN
260-AN-0012	Minimizing fluorescence using a 457nm laser excitation wavelength	25	RAMAN
040-AN-0009	Discernment of the vermilion ink by Raman spectroscopy	27	RAMAN
170-AN-001	Evaluation of Single-Walled Carbon Nanotube (SWNT) by Raman Spectroscopy - For inorganic and high function materials	29	RAMAN
170-AN-007	Distribution Estimation of Polymorphism of Coral Skeleton Component by Mapping Measurement	30	RAMAN
260-SO-0011	Measurement of scattered foreign materials by using Measurement Assist and Sample Search functions	32	RAMAN
220-AN-008	Evaluation of semiconductor materials by Raman spectroscopy - Crystal polymorphism and carrier density of Silicon power semiconductor device -	34	RAMAN
JINC-RM-01	Raman Quantitative Calibration Stability for a Sample Mixture	36	RAMAN
RM-01-02	Dispersive Raman for the Identification of Contaminant Particles in Ink Jet Cartridges	37	RAMAN
RM-08-04	Carbon Nanotube Analysis by Raman Spectroscopy	39	RAMAN
JINC-RM-02	Gemstone Identification Using Raman Spectroscopy	40	RAMAN
JE-RM-1-16	Spatial Resolution and DSF in Micro Raman Spectrometer	47	RAMAN
260AN0014	Rapid measurement of sample in container using macro measurement unit	50	RAMAN
FP-0002-E	Upgrade of simple coumarin analysis system to high sensitivity one	52	FP
FP-01-02	Fluorescence Detection of Counterfeit US Currency	55	FP
FP-0008	Absolute quantum yield measurement of solution using FP-8000 series	57	FP
FP-0018	System evaluation of spectrofluorometer FP-8500 with optical fiber	59	FP
UV-01-04	Automated Sun Protection Factor (SPF) Analysis of Sunscreen using UV-Vis	60	UV-Vis
UV-0011-E	Countermeasure technique against heat island phenomenon - Evaluation of solar reflective paint material -	61	UV-Vis
UV-0036	Evaluation of sun protection fabrics by using a UPF evaluation system	63	UV-Vis
UV-0033	Evaluation of the privacy film using an automated absolute reflectance measurement accessory	66	UV-Vis
UV-0023	Thickness Analysis of natural oxide film on microscopic Si pattern	67	Micro-UV-Vis
JE-Ap-UV1005-0006	Luminous Color Measurement by using UV/Vis Spectrophotometer	68	UV-Vis

Application	Description	Page	Technique
<i>JE-UV-02-16</i>	Bandgap Measurements for Titanium Dioxide Powder	72	<i>UV-Vis</i>
<i>JE-UV-03-16</i>	Reflection Object Color Measurements using Color Diagnosis System	73	<i>UV-Vis</i>
<i>JE-UV-04-16</i>	Gardner Color Measurement System	75	<i>UV-Vis</i>
<i>JE-UV-05-16</i>	Hazen Color Measurement System	76	<i>UV-Vis</i>
<i>UV-0040</i>	Evaluation of antireflection film by using absolute reflectance measurement accessory	77	<i>UV-Vis</i>
<i>UV-0042</i>	Introduction of Haze value measurement system for UV/Vis spectrophotometer	80	<i>UV-Vis</i>
<i>UV-0043</i>	Example of the measurement of a highly reflective material, a dielectric multi-layer mirror using absolute reflectance spectroscopy	82	<i>UV-Vis</i>
<i>UV-0044</i>	Measurement reproducibility of Color Diagnosis System	84	<i>UV-Vis</i>
<i>JE-UV-06-16</i>	Color Analysis System for RGB Color Filters	89	<i>Micro-UV-Vis</i>
<i>UV-0025</i>	Estimation of refractive index of monocrystalline sapphire by polarization measurement using MSV-5000 series	90	<i>Micro-UV-Vis</i>
<i>JE-UV-01-16</i>	Transmittance and Reflectance Measurement System for Minute Lenses	92	<i>Micro-UV-Vis</i>
<i>CD-0030</i>	Verification of [Wavelength Accuracy] and [Wavelength Repeatability] using mercury emission line spectrum	93	<i>CD</i>

Evaluation of crystallization in micro part on plastic (polyethylene terephthalate)

It is reported that the full width at half maximum (FWHM) and crystallization (density) of the carbonyl group. [C=O](1730 cm^{-1}) of polyethylene terephthalate (PET) have the good correlation. 1). In comparison to other analytical methods, the measurement procedure in Raman spectrometry is simple, easy and, it is effective for the measurement of micro part. In this application, the distribution of crystallization on cross-section of plastic (PET) bottle was measured.

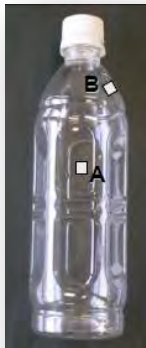
Sample preparation

The A and B part shown in the photo of plastic bottle were cut and then, the cross-section of each part was prepared by a slicer (Model HW-1 Variable angle slicer, JASCO Engineering Co., Ltd.), since the mapping measurement in micro area requires the smooth sample surface. The multi-point measurement was carried out in 50 microns step from outside to inside of crosssection.

Measurement conditions;

Excitation wavelength: 532 nm

Objective; 100x, beam diameter; 1 micron



PET Bottle

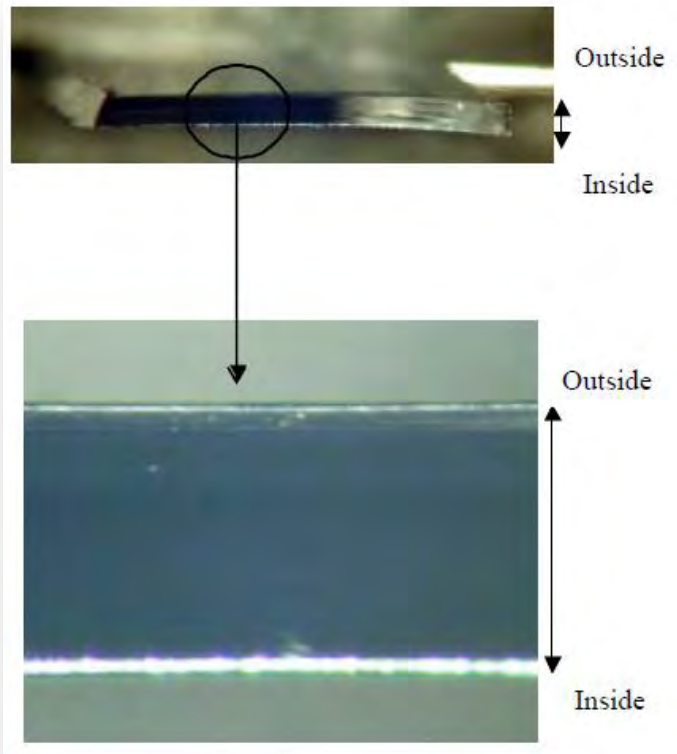
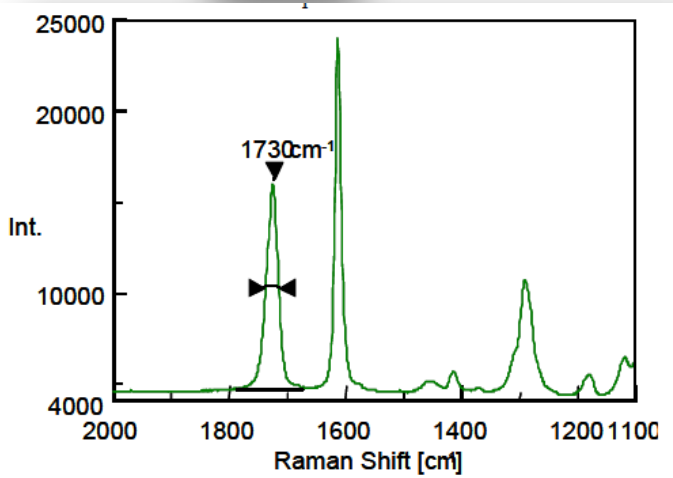


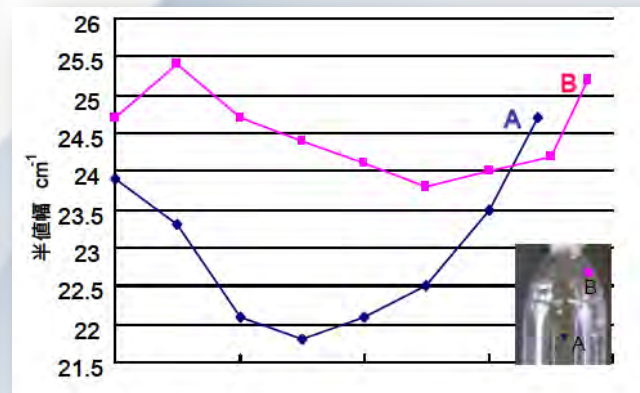
Figure 1 Sampling part and its cross-section

Results

The FWHM of carbonyl group in each sampling part is shown in the below pictures. Since the FWHM and crystallization shows the negative correlation, the crystallization becomes higher when the FWHM becomes narrower. The results indicate that the distribution of crystallization in A and B part is different. In the evaluation of physical properties of plastic (PET) bottle, the crystallization is an important factor. Therefore, the micro Raman spectrometry is an effective analysis method especially for the measurement of micro part.



Raman spectra of PET



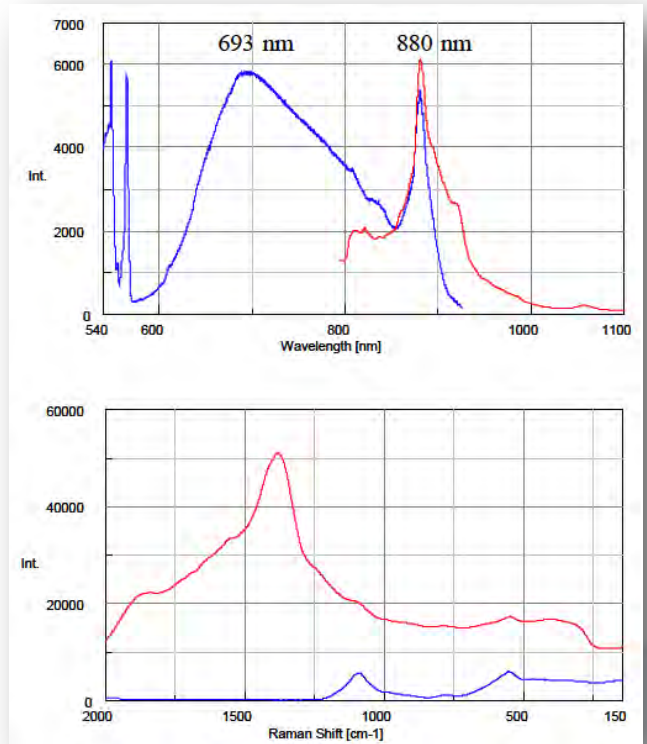
FWHM Calculation result in 1730 cm^{-1}

Raman and Photoluminescence Measurements of Glass and Quartz Materials

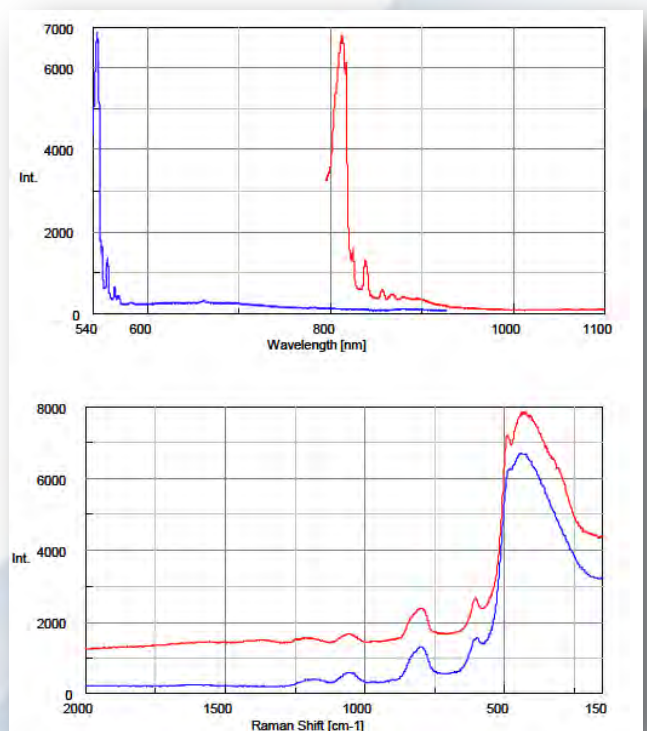
This note is intended to provide important information for users of Raman spectroscopy, specifically discussing measurements using microscope slide glass, cover glasses or glass tubes for holding the Raman sample. A fluorescence free glass is commercially available, however, it can still cause very weak fluorescence. Even though it is very weak, it may significantly disturb the intended Raman measurement, specifically when changing the laser excitation wavelength. To estimate the influence from substrate fluorescence, the Raman and fluorescence spectra of simple microscope slide glass and quartz materials were measured using the laser excitation wavelengths of 532 and 785 nm. The Raman and fluorescence spectra of the various samples are displayed as Figure 1 (horizontal axis – wavelength; vertical axis – Raman shift). For the measurement of slide glass using 532 nm excitation, a Raman peak in the low wave number region was observed in addition to the Fluorescence peaks centered at 693 and 880 nm. Using the 785 nm excitation, the slide glass sample offered a fluorescence peak of 880 nm.

Using 532 nm excitation, the observed peaks of the slide glass may not disturb the Raman spectral measurement (Raman shift: 0 to 4000 cm^{-1}). However, the fluorescence peak of 880 nm at 785 nm excitation may overlap the Raman shift around 1385 cm^{-1} and, it may significantly disturb measurements due to the very strong intensity of the fluorescence as compared to the Raman spectrum. On the other hand, for the quartz materials, only the Rayleigh band was observed at both 532 and 785 nm excitations and there was almost no influence from fluorescence.

These results suggest that the quartz glass must be used for the measurement especially at 785 nm excitation. It is our suggestion that only quartz be used for the majority of Raman measurements, wherever possible. It may be feasible, however, to use glass as a rounded surface (HPLC vials, NMR tubes, capillary tubes, etc.) if measurements using only 532 nm excitation are to be attempted.



Slide glass
(Excitation: 532nm, 785 nm)



Quartz glass
(Excitation: 532 nm, 785 nm)

Qualitative analysis of colorant by Raman Spectroscopy

Introduction

In order to progress Archeology, to study art history and to repair the works of art, it is generally very important to know and analyze what kind materials our ancestors used historically as colorant. Raman spectroscopy is a very useful technique especially for non-destructive analytical tool for qualitative analysis of archaeological ruins and works of art, because the measurement range is much wider than IR spectroscopy, enabling the measurement of not only organic colorant but also inorganic colorant that has absorption peaks in low wave number range below 400 cm^{-1} . It is considered to be difficult in general to obtain good Raman spectrum of the material which has fluorescent characteristic in UV region such as colorant, but it is possible to avoid this fluorescence emission effect without changing the excitation wavelength but keeping away from the absorption band because such materials have strong and sharp absorption peaks in visible region. In this experiment, 12 different color water paint colorants were used as samples, which were excited by the lasers with 3 different wavelengths for comparative study.

Instrument

JASCO NRS-3100 Laser Raman Spectrometer
 Samples: 12 different color water paint colorants
 Objective lens: 20x
 Excitation wavelength: 532 nm, 633 nm, 785 nm



Result and Discussion

Figure 1 shows the spectral data obtained in this experiment. As the result, Raman spectra of White, Yellow, Black colorants samples show the similar level S/N even excited by any of 3 different excitation wavelength. Spectra of Red, Lemon, Indigo blue, Scarlet, Brown and Ocher colorant samples show better S/N when excited by longer wavelength such as 785 nm, On the other hands, the better spectrum of Blue colorant sample was obtained when excited by the shorter wavelength such as 532 nm and also good spectra were obtained for Green, Yellow colorant samples excited by 633 nm. Table 1 shows colorant components of each samples as the result of this analysis. Generally, the color is recognized as the complementary color of absorbed light (Figure 2). As an example, Red colorant sample is considered to irradiate strong fluorescence when excited by 532 nm because it absorbs selectively the light between green and blue region. However, the Green colorant sample which is expected to absorb Red light has actually shown the best S/N condition when excited by 633 nm in Red region.

The cause of this phenomenon can be considered that Raman peak of Phthalocyanine compound (Figure 3) as the component of Green colorant sample is enhanced selectively by Red laser due to Resonance Raman effect. In addition the shapes of spectra of Green, Blue and Indigo Blue samples are different depending on excitation wavelength, which can be considered that the group vibration of Chromophore derived from absorption is enhanced selectively due to Resonance Raman effect. As well as Phthalocyanine, Chlorophyll and Hemoglobin which have similar chemical structure to Phthalocyanine are known as typical compounds that have Resonance Raman effect characteristics depending on excitation wavelength. Any spectra of Organic colorant which obtained in this experience could not be found in the liberally after searching.



Qualitative analysis of colorant by Raman Spectroscopy

This is because the ratio of peak intensity is considered to be different depending on the excitation wavelength, which makes the spectra different from library data obtained by FT-Raman (1064 excitation) and Colorant components contain various crystal polymorph. Physical characteristics such as hue and anti-corrosion are different depending on the type of crystal Polymorph.

As shown in the above, Raman spectroscopy is one of the very useful analysis tool not only for colorant analysis, but also for evaluation of crystal polymorph and patent application for the cutting edge materials such as the luminescence material of Organic EL, absorbing colorant of Blue-Ray disk, and functional colorant as photovoltaic materials of Dye Sensitized Solar Cell.

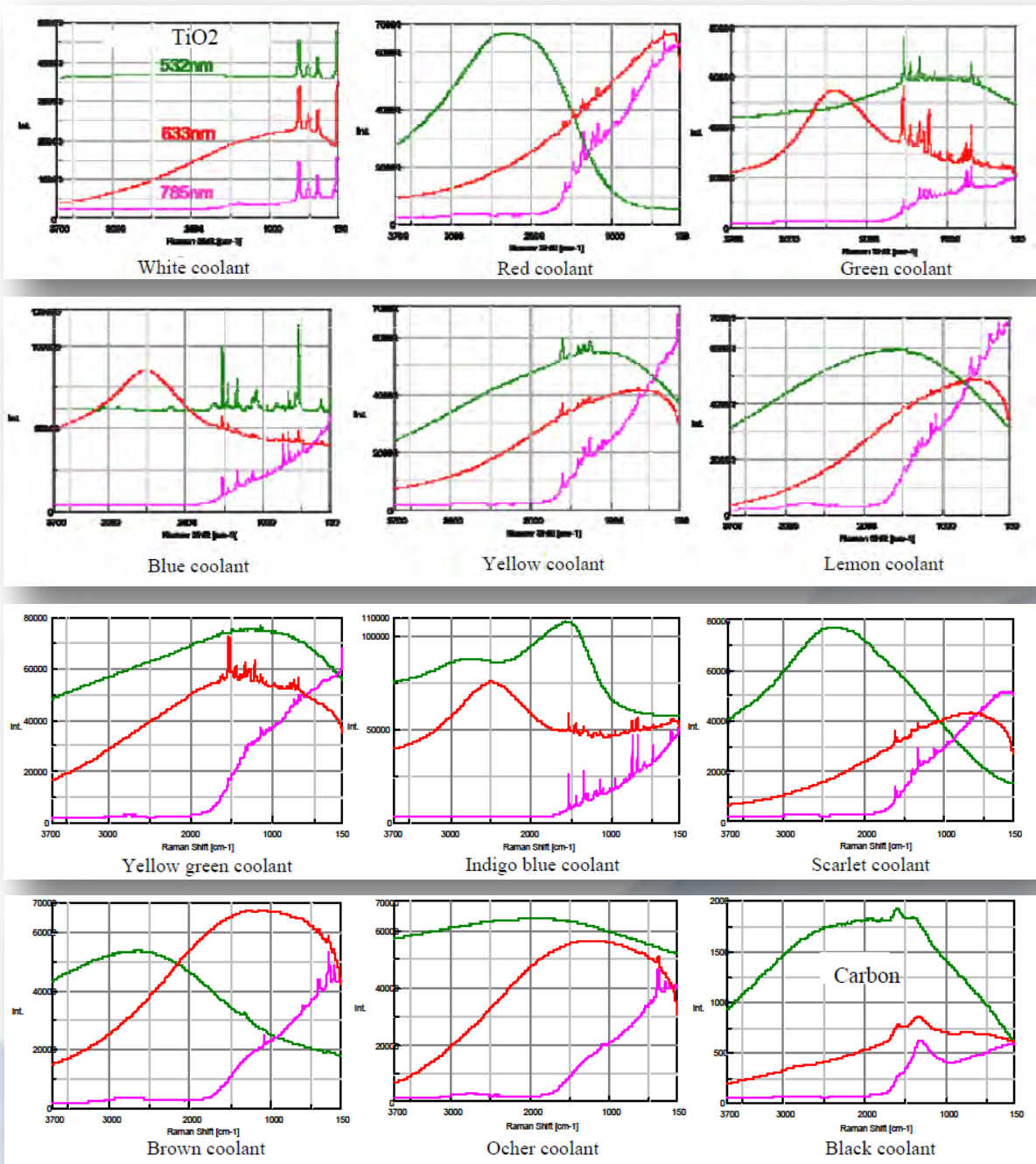


Figure 1 Spectra data of colorant samples

Qualitative analysis of colorant by Raman Spectroscopy

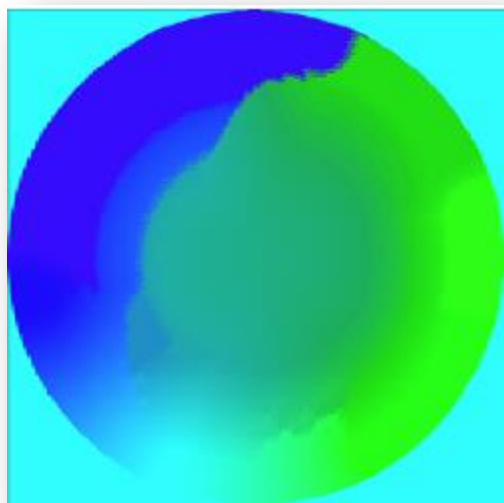


Figure 2 Wheel of hue

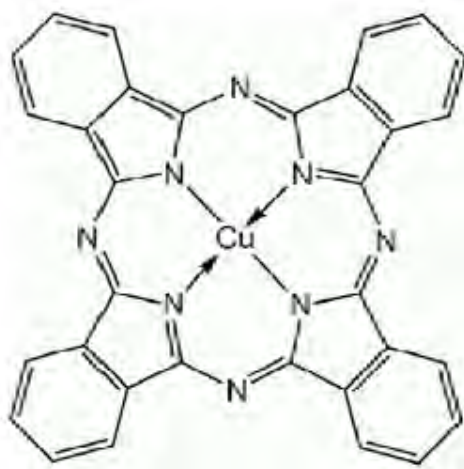


Figure 3 Phthalocyanine complex

<i>Colorant Sample</i>	White	Red	Green	Blue	Yellow	Lemon
<i>Component</i>	Titanium Oxide	Heterocyclic Organic	Phthalocyanine	Phthalocyanine	Heterocyclic Organic	Heterocyclic Organic
<i>Colorant Sample</i>	Yellow Green	Indigo Blue	Scarlet	Brown	Ocher	Black
<i>Component</i>	Phthalocyanine	Phthalocyanine	Heterocyclic Organic	Inorganic	Inorganic	Carbon

Table 1 Analysis result of Colorant component

2D correlation spectroscopy using 2 kinds of spectrum of IR and Raman obtained by time course measurement (Analysis of instant adhesive in cure process)

1. Introduction

2D correlation spectroscopy was proposed in the 1980s as an analytical method for the changes of IR spectra with time. Although 2D correlation spectroscopy is usually used to analyse one kind of spectra obtained by time course measurement, In this experiment, 2D correlation spectroscopy was applied to 2 kinds of time course spectra such as IR and Raman. Instant adhesive was used as a model sample and the changing of the spectrum in cure process was observed. The obtained spectra of both IR and Raman were analyzed by 2D correlation program run on Spectra Manager.

2. Experimental

Commercially available instant adhesive was used as a sample. One of the main components, cyanoacrylate, is reacted with water in the air and the molecules are polymerized, and it becomes hardened (Figure 1). IR spectrum was obtained by thin-film method using KBr windows. The spectrum was obtained by time course measurement with FT/IR-4100 for 60 seconds at intervals of 2 seconds. Raman spectrum was obtained with NRS-3100. A drop of the instant adhesive was put on a glass slide and thinly spread, and it was measured with an objective lens of $\times 20$ for total 60 seconds at intervals of 2 seconds. (Excitation wavelength: 532 nm).

3. Results and Discussion

The obtained IR and Raman spectra by time course measurement were shown in Figure 2 and Figure 3 respectively.

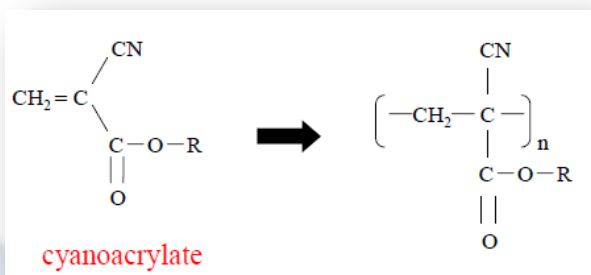


Figure 1 Reaction of instant adhesive in cure process

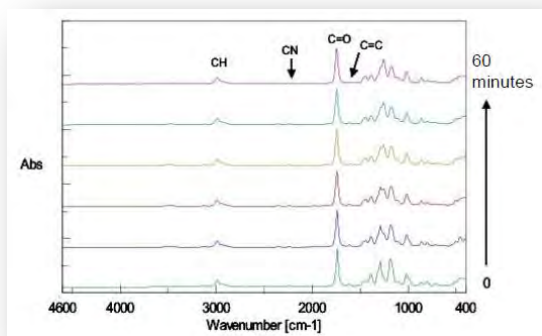


Figure 2 IR absorption spectra

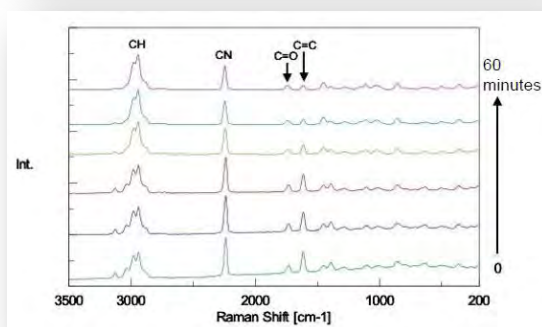


Figure 3 Raman scattering spectra

By comparing Figure 2 with Figure 3, it is seen that the intensity of Raman peak attributed to C=C double bond at 1620 cm^{-1} was decreased (polymerization in progress), while any clear change of IR spectra is not seen with time because the peak intensity was too weak. On the other hand, the peaks in the IR spectra in fingerprint region are changed with time while there is no distinguished change in the peaks in the Raman spectra in such region. Next, the results of simultaneous correlation of the IR and Raman spectra changes with time are shown in Figure 4 and Figure 5 respectively.

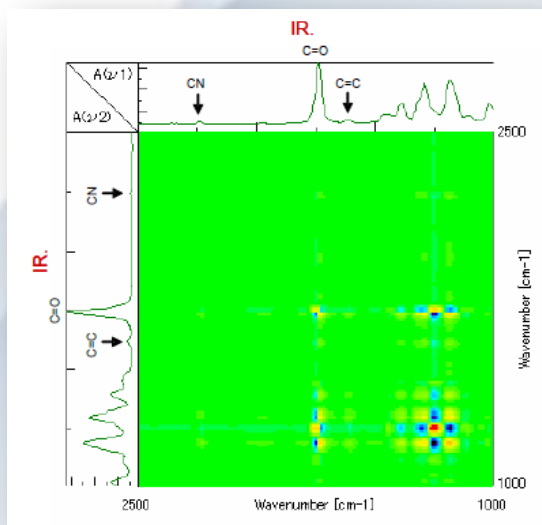


Figure 4 Simultaneous correlation Spectrum with only IR

2D correlation spectroscopy using 2 kinds of spectrum of IR and Raman obtained by time course measurement (Analysis of instant adhesive in cure process)

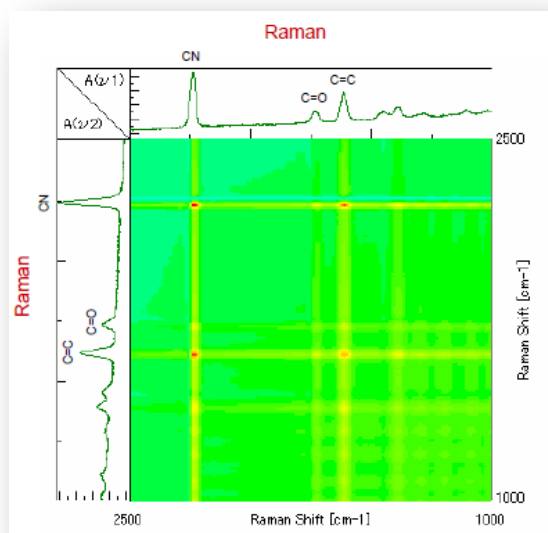


Figure 5 Simultaneous correlation spectrum with only Raman

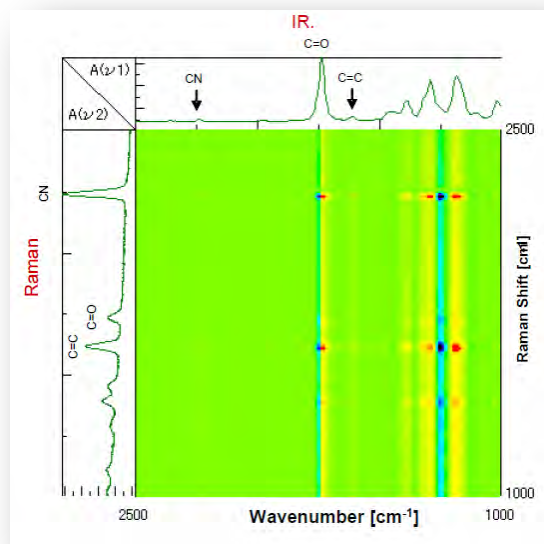


Figure 6 Simultaneous correlation spectrum with IR and Raman

From the simultaneous correlation of IR shown in Figure 4, there is a correlation seen between the peaks from 1100 cm⁻¹ to 1400 cm⁻¹ in the fingerprint region and the peak of C=O at 1735 cm⁻¹ whose significant difference was not seen in Figure 2. In the simultaneous correlation of Raman shown in Figure 5, there is a correlation seen between the peak of C=C double bond at 1620 cm⁻¹ and the peak of C=O at 1735 cm⁻¹. In other words, it is estimated that the peaks of IR spectrum largely changed with time in the fingerprint region from 1400 cm⁻¹ to 1100 cm⁻¹, the peaks of C=C double bond having strong activity on Raman and the peaks of C=O might be correlated with one another.

In order to analyze them in integrated manner, simultaneous correlation analysis was carried out by combining IR spectra with Raman (Figure 6). At the intersection point of the peak of C=C in Raman and the peak of C=O in IR, the peak of C=O in low wavenumber side in blue (minus) and the one in high wavenumber side in red (plus) are correlated. It is considered that the peak of C=O is shifted to high-wavenumber side with time as the peak of C=C is monotonically decreased with time as shown in Figure 7. In addition the peak of C=C in Raman and the peak in the region from 1400 cm⁻¹ to 1100 cm⁻¹ also have correlation. Just like C=C in Raman against C=O in IR, the same correlation is seen for CN group, and accordingly, it is found that the peak intensity of CN group is decreased without shift of the peak.

As explained above, in accordance with the transformation of structure from C=C to C-C by the polymerization reaction, it is presumed that the conformation of functional group not related to the polymerization such as C=O and CN are also changed. Although the results obtained by IR and Raman were used for analysis this time, the combination of the results obtained by other spectroscopic (NIR, UV, VIS, CD etc.) technique and the results by Raman and IR would expand the possibilities for various analysis such as attribution of peaks, lattice vibration and the relation among color, chiral information and intramolecular vibration.

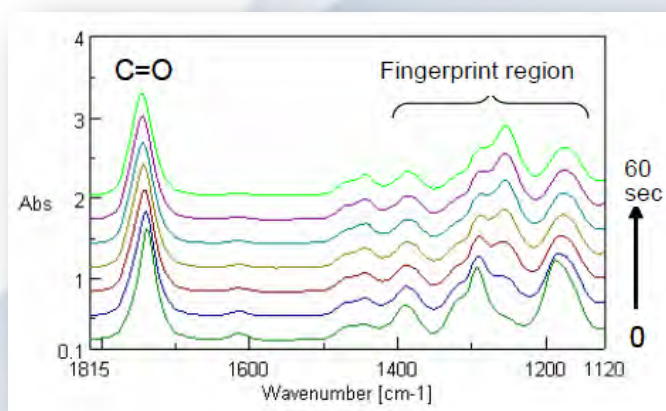


Figure 7 Expanded IR spectra

Determination of ortho and para hydrogen ratio by using Raman spectroscopy - Application to fuel cell -

Introduction

Hydrogen molecule which is now attracting attention as energy source of fuel cell, has two different nuclear spin isomers such as ortho hydrogen (the same direction pair) and para hydrogen (the opposite direction pair). Both ortho and para hydrogen show the same chemical property, while their physical property such as specific heat is different from each other, and since the conversion between ortho and para needs extremely long time, each molecule tends to be handled as different from the other. The abundance ratio of ortho-para in hydrogen gas in ambient temperature is stable as approx. 3: 1, but when it is cooled to liquid state, most hydrogen molecule becomes para hydrogen. However a part of ortho hydrogen also becomes to liquid state, and ortho-para conversion in liquid hydrogen after long time may generate heat, which may affect to storage efficiency. Therefore when hydrogen gas is liquefied industrially, ortho-para conversion catalyst is necessary. In this experiment, we will describe, as an example, simple evaluation of ortho-para abundance ratio by using Raman spectroscopy which is one of the vibrational spectroscopy methods.

Experimental

Laser Raman spectrophotometer NRS-3100 was used for the measurement. 10 cm gas cell with NaCl window which is usually used for FTIR was evacuated by rotary pump, and then hydrogen gas with pressure lower than one atmosphere was encapsulated directly into the gas cell from hydrogen gas cylinder. The gas cell is mounted as shown in Figure 1, and the measurement was done using the objective lens with long working distance by focusing the beam inside of the cell (Excitation wavelength; 532 nm, Laser power at sample point; approx. 10 mW).

Results and discussions

Figure 2 shows the obtained Raman spectrum of hydrogen gas. The peaks due to rotational transition were seen in the spectrum in the range from 350 to 1100 cm^{-1} . The system temperature was estimated from Stokes anti-Stokes ratio using equation (1) to be as approx. 300 K.

$$Z = \sum_j P_j \exp\left(-\frac{BJ(J+1)}{kT}\right) \quad (2)$$

B : Rotation constant, J : Rotation quantum number

$P_j = g_j(2J+1)$

g_j : Each abundance ratio of ortho and para hydrogen

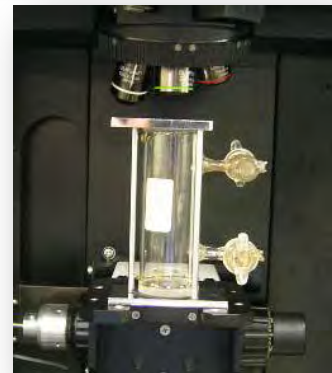


Figure 1

Sample compartment

Ortho-para abundance ratio is calculated from each partition function equation (2) of ortho and para hydrogen by adding the peak height of ortho and para hydrogen in the rotation spectrum and supposing $T = 300\text{K}$ in the equation (2), and then the ratio, approx. 7:3 was obtained. The hydrogen molecular rotation constant B in equation (2) was referred to $B' = 59 \text{ cm}^{-1}$ which was calculated from the equal distance of rotation line $4B$.

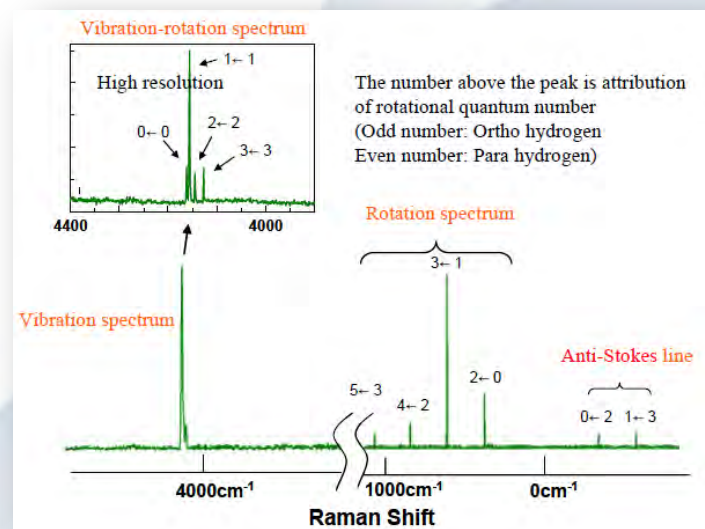


Figure 2 Raman spectrum of hydrogen gas

$$\frac{I_{\text{anti-stokes}}}{I_{\text{stokes}}} = \exp\left(-\frac{h\nu}{kT}\right) \quad (1)$$

Determination of ortho and para hydrogen ratio by using Raman spectroscopy - Application to fuel cell -

Compared to the standard ortho-para ratio of hydrogen in the ambient temperature, 3:1, the ratio of para hydrogen was higher. From this result, it can be recognized that ortho hydrogen was already converted to para hydrogen when hydrogen in the cylinder was liquefied and filled. This time, ortho-para ratio was obtained from the rotation spectrum, but when the rotation spectrum in the wavenumber region in the vicinity of peaks of rotation spectrum is affected from unnecessary light such as fluorescence generated from window, the abundance ratio can be calculated from vibration-rotation spectrum (which is) separated from the change of rotation energy by high resolution measurement of the vibration spectrum region around 4160 cm⁻¹.

Comment

The reason why the difference of the direction of nuclear spin such as ortho and para hydrogen is evaluated by Raman spectroscopy (vibration spectroscopy), can be explained by quantum-mechanics. The wave function of whole hydrogen molecule can be expressed as the product of each wave function of electron, vibration, rotation and nuclear spin as shown in the equation (3).

$$\phi_{\text{Total}} = \phi_{\text{electron}} \phi_{\text{vibration}} \phi_{\text{rotation}} \phi_{\text{nuclear spin}} \quad \text{--- (3)}$$

Equation (4) and (5) show the energy of molecular vibration and rotation respectively calculated from the characteristic value of Schrodinger equation.

$$\text{Vibration energy } E = (v + 1/2) h\nu \quad v=0.1.2... \quad (4)$$

Note, $\nu = (1/2\pi)(k/\mu)^{1/2}$
 (v: vibrational quantum number,
 k: force constant,
 μ : reduced mass)

$$\text{Rotation energy } E = BJ(J+1) \quad B = h^2 / (8\pi^2Ic) \quad J=0.1.2... \quad (5)$$

B : rotational constant,
 J : rotational quantum number,
 I : inertia moment, for diatomic molecule,
 $I = \mu R^2$ (μ : reduced mass, R : distance between nucleus)

Figure 3 shows the energy level of hydrogen molecule using quantum number of rotation J . Generally in electronic ground state, wave function of electron and vibration is symmetric to the displacement of nucleus. On the other hand, wave function of nuclear spin has both symmetric and asymmetric cases to the displacement, and the each case is called as ortho and para. Wave function of rotation must be symmetric in order to satisfy the Pauli exclusion principle. Therefore ortho hydrogen exists only when rotation level J is odd (asymmetric), and para hydrogen exists only when rotation level J is even (symmetric). Nuclear spin information such as ortho and para hydrogen can be obtained from rotation spectrum (or vibration rotation spectrum) of hydrogen molecule. However, in case of Deuterium molecule (D₂), Deuterium atom is Bose particle, so that the relationship between odd - even and ortho - para is contrary to hydrogen molecular case, resulting interesting phenomenon that the shape of rotation spectrum changes drastically.

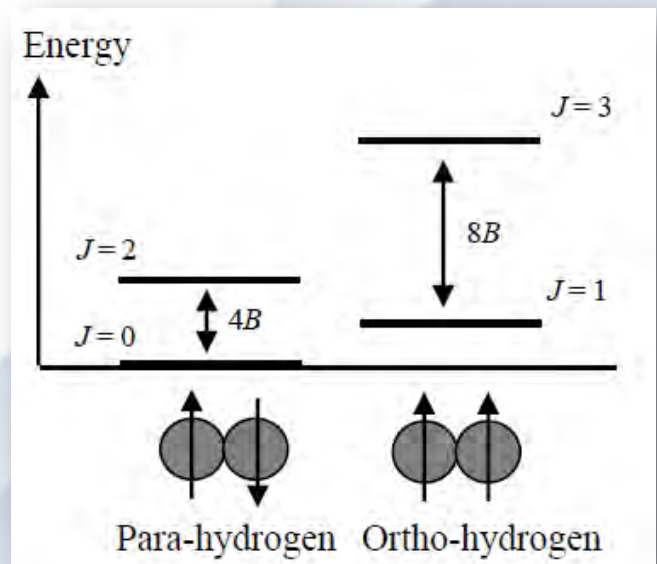


Figure 3 energy level of ortho-para hydrogen

Evaluation of cosmetics by Raman micro-spectroscopy

Introduction

Raman spectroscopy can be used to analyze the molecular or crystalline structure based on various molecular vibrations.

The technique has been applied to analyses of various kinds of organic and inorganic materials such as polymers, chemicals, biological materials, semiconductor or various nanomaterials including graphene and carbon nanotubes.

Due to miniaturization, performance improvement and cost reduction of lasers and other optical devices, the price point of Raman spectrometers has been steadily declining.

As a result, Raman spectroscopy is now being used for materials analysis in many fields such as quality control for pharmaceuticals and in the food industry. In comparison with infrared spectroscopy, there are several advantages in Raman as non-contact, non-destructive, easy sample preparation and small measuring spot down to approx. 1 micron.

An additional (and important) advantage, is that measurement in the low wavenumber range can be easily achieved to obtain precise information on inorganic samples. Cosmetic preparations consist of organic and inorganic materials. This application note shows the method for identification and discrimination of the components in eye shadow samples using Raman micro-spectroscopy NRS-4100.

Experimental

Two kinds of eye shadow products (manufactured by Company A and Company B) were coated onto a metal plate. And these samples were measured with JASCO NRS-4100 Raman micro-spectrometer to get mapping images of it. These data were analyzed and identified by using a search database.

System configuration

- NRS-4100 Raman Spectrometer 532 nm laser
- Automatic imaging system

Measurement conditions

Excitation wavelength: 532 nm

Grating: 900 gr/mm

Laser power: 3.2 mW

Objective lens: 100x

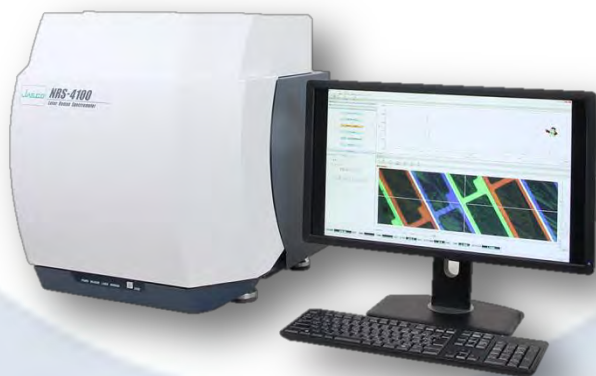
Sampling area: 35 x 35 mm

Measurement points: 35 x 35 with 1 mm interval

Results and discussion

Figure 1 shows observation image of each eye shadow and Figure 2 shows the spectra of the main components of each eye shadow (black spectra are calculated using a PCA model analysis and red spectra are the results of the database search). Figure 3 presents the color mapping images of each eye shadow. The visual differences in the particle size or the color of the two kinds of eye shadow cannot be found in the visual observation image (Figure 1).

The difference between the two kinds of eye shadows can be easily recognized by the spectra difference shown in Figure 2. The eye shadow made by company A contains a surfactant, rutile TiO₂ and pigment. Another sample contains anatase TiO₂ in addition to a surfactant, rutile TiO₂ and the pigment.



Evaluation of cosmetics by Raman micro-spectroscopy

Figure 3 shows the color mapping images of the component distribution for each eye shadow formulation. The differences in component dispersion can be reviewed in the mapping images. Raman microscopy easily highlights the composition differences in chemical formulations that cannot be discerned by optical or infrared microscopy. As an example, the dispersion of inorganic crystals that demonstrate polymorphism can be easily measured by colored mapping images of the spectral peaks. Raman micro-spectroscopy is effective for measurement of composite materials like cosmetics that contain organic and inorganic material dispersed in discrete micron-sized locations within the chemical formulation.

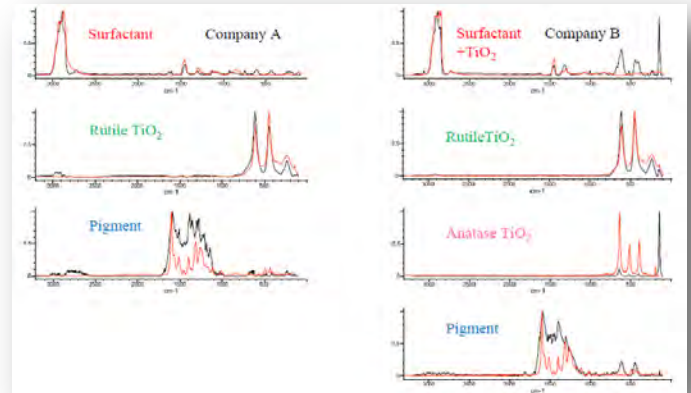
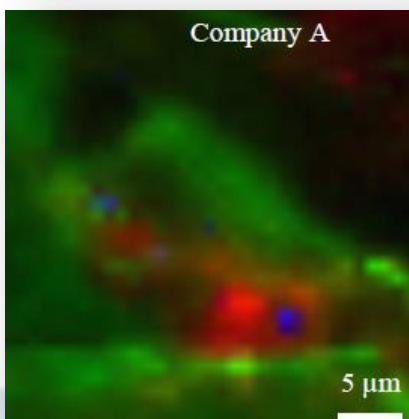
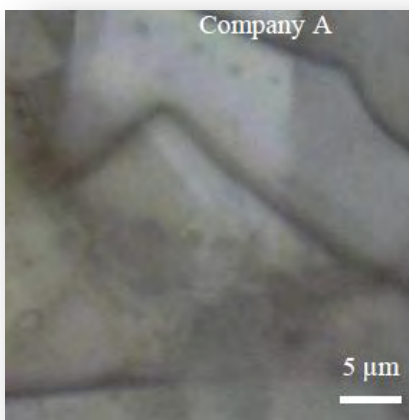
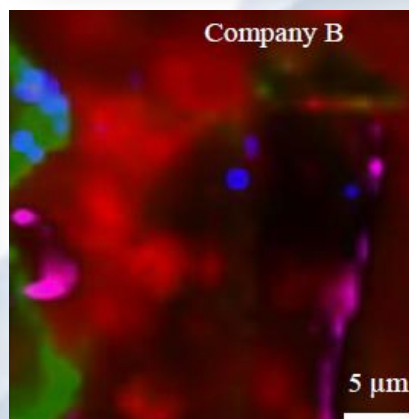


Figure 2 The Raman spectra of each eye shadow



Red: Surfactant
Green: Rutile TiO₂
Blue: Pigment



Red: Surfactant
Green: Rutile TiO₂
Pink: Anatase TiO₂
Blue: Pigment

Figure 3 The color mapping image of each eye shadow application

Measurement of buried foreign material by Raman Spectrometer NRS-4100

Introduction

Currently, the infrared microscope is used extensively as one of the identification approaches for micro foreign materials.

Since in microscopic infrared spectroscopy, there is a huge database, which works very well on the identification of foreign materials, while the infrared microscope has several problems for the measurement such that the spatial resolution is limited to only a few micrometer and the sample preparation is necessary if the foreign material is buried in the sample.

Therefore, the Laser Raman spectrophotometer is now often used for measurement of foreign materials in combination with infrared microscope. Raman spectroscopy is a method to analyze molecular structure by molecular vibration as well as infrared spectroscopy, but there are following advantages in Raman spectrophotometer.

1. The spatial resolution is as small as 1 μm by using visible laser
2. The Raman spectrophotometer allows quick and easy measurement of the sample with non-destructive manner without sample pretreatment
3. For inorganic samples, it is easy to identify because of the easy measurement in low wavenumber range

The potential of measuring foreign materials by using Raman spectrophotometer is expanding, and JASCO has developed a new laser Raman spectrophotometer, NRS-4100 with compact design and ease of use to be used together with FTIR.

In this application note, the features of NRS-4100 and identification of foreign materials buried in the polymer film are illustrated.

Features

The NRS-4100 is a Raman Spectrophotometer, incorporating high performance spectrograph, sample compartment, detector and laser light source in a space as small as 60 cm square, which can be installed on the ordinary laboratory bench other than anti-vibration bed, with no extra space because the door of sample compartment moves up and down for open/close. In addition, the NRS-4100 meets the laser safety standards of Class 1.

Maximum three lasers such as 457nm and 785nm as well as 532nm can be mounted, and the spatial resolution is as small as only 1 μm in XY and 1.5 μm in Z direction, enabling the high spatial resolution and fluorescence minimization, which are important for the foreign material measurement.

The “Measurement assist function” aids the user in setting up the NRS-4100 for sample measurement; a simple sequence guide takes you through setup and optimization of measurement parameters with helpful advice and tips, such as a warning if you have the laser intensity set too high. The new “Sample Search” function is used with the automated XYZ stage.

A new algorithm developed by JASCO (patent pending) analyzes the microscopic image and automatically selects measurement position(s) based on the size, contrast and/or color of the target material described by the user, then simply click the measurement button to execute spectral measurements of the automatically identified sample positions. Spectra Manager II includes a wealth of user-selectable options for data analysis, as well as the usual tools like opening single or multiple spectra, zooming, normalization, a variety of arithmetic data processing functions, there is a variety of Raman specific tools and analysis functions.

Measurement of buried foreign material by Raman Spectrometer NRS-4100

System configuration

- NRS-4100 Raman Spectrometer 532 nm laser
- Automatic imaging system

Foreign material measurement/Analysis

The foreign material buried in the multi layer substrate (Glass/Adhesion layer/Transparent film) shown in Figure 1 was measured. It is difficult to measure such foreign material by using infrared microscope, because it is difficult to cut the foreign material in section due to the presence of glass and the adhesion layer may be picked up together. On the other hand, Raman spectrophotometer with the confocal optical system can obtain the spectrum of laser focused point selectively. As a result, it is possible to measure the inside of the sample in non-contact and non-destructive manner without lousy sample pretreatment. In this report, the position where the target foreign material is located was measured in the depth direction (Z axis direction) and also each layer's information was obtained. The major spectrum obtained from each layer is shown in Figure 2.

Measurement parameters

- Ex wavelength: 532 nm
- Grating: 900 gr/mm
- Exposure time: 5 sec. (Accumulation: 2 times)



Figure 1 Observation Image

In the obtained spectrum of the foreign material, the C-H peak at around 3000 cm^{-1} is not shown, and so it is quite different from the spectrum of transparent film and adhesion layer.

In order to analyze the result in further details, the spectrum of foreign material was tried to be identified by using database as shown in Figure 3, and it was found to be talc (hydrated magnesium silicate).

In addition, it is known that the transparent film is made of cellulose and the adhesion layer is made of terpene resin.

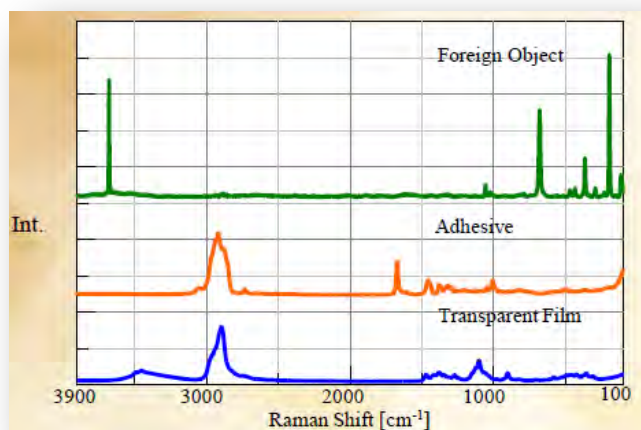


Figure 2 Spectrum for each layer

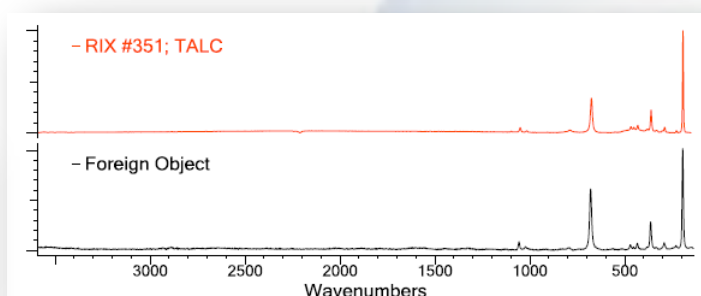
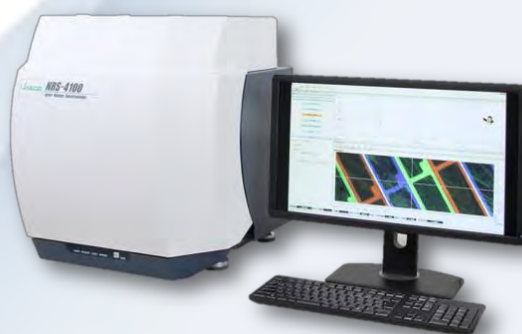


Figure 3 Search result of the database



Minimizing fluorescence using a 457nm laser excitation wavelength

Introduction

Raman spectroscopy is a popular method for analyzing molecular structure and is considered a complementary technique to infrared spectroscopy.

Recently, Raman has been attracting the attention of FT-IR users because it offers several important advantages over FT-IR.

Raman spectroscopy is a non-contact and non-destructive technique and measurements can be made with little to no sample preparation. Samples can be measured with a spatial resolution as small as 1 μm and depth profiling can also be easily performed on transparent samples.

However, in some cases, good quality analysis by Raman spectroscopy can be adversely affected by interference from fluorescence.

The JASCO NRS series of Raman spectrometers have several fluorescence compensation features, which fluorescence elimination algorithm is patented.

This application shows the evaluation of JASCO NRS-4100 mounting 457 nm laser for the measurement of samples that exhibit fluorescence, to determine if this can be a better alternative to red and NIR lasers such as 785 or 1064 nm excitation.

Methods for minimizing fluorescence

Both Raman scattering and fluorescence are phenomena where the wavelengths of light emitted from a sample are different than the wavelength of the input excitation light. If the wavelengths of Raman scattering and fluorescence overlap, it is impossible to obtain good Raman spectra.

The NRS series Raman instruments have three tools for reducing or eliminating unwanted fluorescence.

1. An important method for minimizing fluorescence is the fluorescence correction algorithm (JASCO patent) included with the Spectra Manager II software.
2. When fluorescence is emitted from the surrounding matrix, the most widely used method to reduce this fluorescence is to use higher spatial resolution by reducing the aperture in the confocal optical system.
3. When the sample itself emits fluorescence, the most effective method is to change the wavelength of the excitation laser. The wavelengths of Raman scattering do not change even if the excitation wavelength is changed, while the fluorescence wavelengths are dependent on the excitation wavelength. Therefore, it is possible to minimize or even eliminate the overlap of the Raman scattering and fluorescence by changing the excitation wavelength. As Raman spectra are displayed as a shift value from the excitation wavelength, Raman peaks always appear at the same position independent of the excitation wavelength and so Raman spectra with substantially minimized fluorescence can be obtained. An additional benefit of using the 457 nm laser is that the intensity of Raman scattering is inversely proportional to the fourth power of excitation wavelength, therefore by using a shorter wavelength laser as the excitation source, Raman scattering intensity can be substantially increased while minimizing fluorescence.

The 457 nm laser as shown in Figure 1 has a shorter wavelength than the 532 nm laser and offers two important advantages; the same CCD detector can be used as with the 532 nm laser and the Raman scattering intensity can be up to 1.8 times higher when using a laser of equal power output.

Minimizing fluorescence using a 457nm laser excitation wavelength



Figure 1 457 nm laser spot (a blue-purple color)

System configuration

- NRS-4100 Raman Spectrometer
- 532 nm laser
- 785 nm laser
- 457 nm laser
- Laser switching mechanism
- 900 and 400 gr/mm grating

Wavelength [nm]	Grating [Line/mm]	Measurement time [sec]	Number of scans
457	900	30	2
532	900	5	12
785	400	30	2

Table 1

Excitation Wavelength Measurement Parameters

Measurement and Analysis

A fiber sample was measured using the laser excitation wavelengths of 457 nm, 532 nm and 785 nm; measurement parameters are outlined in Table 1. The spectra in Figure 2 demonstrate that using excitation wavelengths at both 532 nm and 785 nm result in strong fluorescence which completely obscures any peaks of the Raman spectrum. However, by using an excitation wavelength at 457 nm, the fluorescence interference exhibited by the other excitation lasers is quite reduced.

The spectrum obtained using the 457 nm laser and the fluorescence correction software resulted in data which could be compared to a database library spectrum and the measured sample was correctly identified as a nylon-6 fiber (Figure 3).

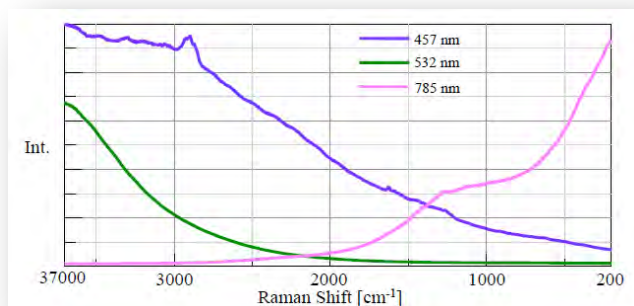


Figure 2 Overlaid spectra for three laser Excitation wavelengths

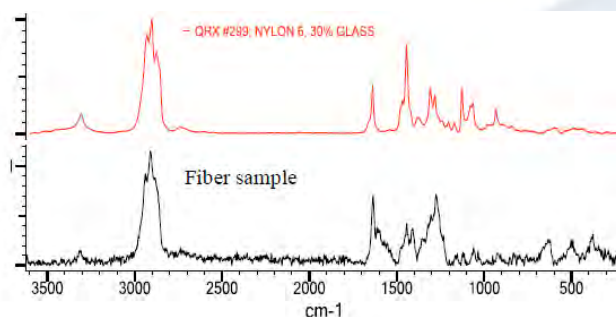


Figure 3 Database Search Result

Summary

A nylon sample fiber was measured using the 'standard' 532 and 785 nm excitation wavelengths and the results for both lasers demonstrate a strong fluorescence emission. However, using the shorter (higher energy) 457 nm laser excitation, which has significantly higher Raman scattering intensity, proves to be an extremely effective method to minimize the effects of fluorescence.

In addition to the nylon test fiber, we used the three-laser NRS-4100 Raman spectrometer (582 nm, 457 nm and 785 nm) to evaluate a range of samples that exhibit strong fluorescence, such as polyimide and biological materials and found that the 457 nm excitation wavelength offers spectra with much lower fluorescence than the 'standard' combination of 532 nm and 785 nm laser excitation wavelengths.

Discernment of the vermilion ink by Raman spectroscopy

Introduction

Raman spectroscopy is a technique to analyze the molecular structure from molecular vibrations as well as infrared spectroscopy. There are several advantages of RAMAN such that much smaller microscopic area can be measured, measurement in low wavenumber range can be easily implemented, a sample can be measured by non-destructive and non-contact method, and precise information on inside of a sample can be obtained selectively. Therefore, RAMAN has been used in the analysis of many fields, such as semiconductor and pharmaceutical as well as chemistry. Recently, more applications to the field of a criminal investigation are now expected. For example, RAMAN is applied to multilateral judgment of a very small piece of evidence and moreover, to identification of the poisonous, deleterious substances and illegal drugs from outside of the container. As explained, Raman spectroscopy is now effectively utilized in a criminal investigation, however there are following two points to be noted for measurement. One is the disturbance by the fluorescence from a sample, and the other, the possible damage to the sample by laser irradiation. The effective method of avoiding fluorescence is changing an excitation wavelength, or improvement in spatial resolution. If an excitation wavelength is changed into longer wavelength such as 785 nm or 1064 nm rather than 532 nm of standard, generally fluorescence will be decreased. Moreover, by narrowing down the laser beam size or using a confocal optical system, the spatial resolution of the xy-direction and even the z-direction improves, and then the influence of fluorescence can be eliminated. In order to avoid damage of the sample by the laser, it is important to set the optimum laser intensity by using attenuator.

As one of the cases which could be identified by Raman spectroscopy, here is a report on the identification of the imprint of a seal placed, which is essential for official documents in Japan. Vermilion ink pad containing the inorganic pigments such as cinnabar and the other ink pad containing organic pigments are generally used for imprint. Both materials can be easily discriminated by the Raman spectra in the low wavenumber range. If the ink material can be specified, it will be quite helpful for investigative information.

Measurement by 532nm laser

Using JASCO Laser Raman Spectrophotometer, NRS-5100 (Figure 1), the seals (Figure 2) on three different papers were measured by standard 532nm laser. In order to avoid the damage to a sample, the laser intensity was raised gradually to be optimized. Moreover, since the fluorescence from vermilion ink or from its surrounding was very strong when measured without using a confocal optical system, it was very difficult to identify Raman peaks. Therefore, in order to increase spatial resolution, the measurement was implemented using the confocal optical system. Figure 3 shows the measurement result. As can be seen, the Raman peaks were confirmed in the spectrum of A Seal, though it was affected by fluorescence. In the spectrum of a Seal B, some small peaks were slightly seen, but it was impossible to see the peaks at all on the spectrum of a Seal C.



Figure 1 JASCO NRS-5100



Figure 2 Microscopic observation image of the seal

Discernment of the vermilion ink by Raman spectroscopy

Measurement by 785nm laser

In order to avoid the influence of fluorescence, 785 nm laser was used for measurement. Figure 4 shows the measurement result. The Raman peaks are seen in the spectrum of Seal A, but the fluorescence is dominant, but the effect from fluorescence was reduced greatly in the spectra of Seal B and Seal C as compared with using 532 nm laser. If the optimum conditions are selected, such as a suitable laser wavelength, better spatial resolution and proper laser intensity, good Raman spectra can be obtained even for a sample like vermilion ink which generates the large background of fluorescence.

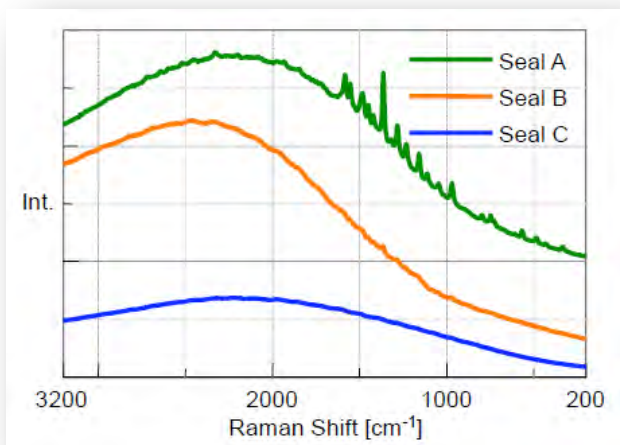


Figure 3 Spectra with excitation wavelength at 532nm

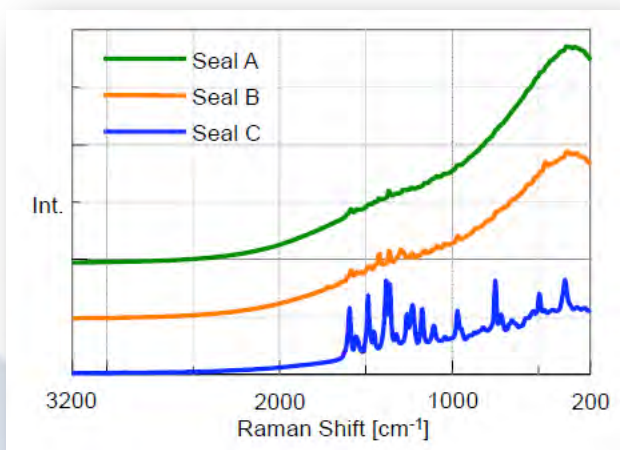


Figure 4 Spectra with excitation wavelength at 785nm

Analysis of the results

In order to analyze the measurement results in details, the measured three spectra (Seal A: excitation wavelength 532 nm, Seal B and C: excitation wavelength 785 nm) were processed by fluorescence correction and normalization in software and shown in Figure 5. Concentrating on the wavenumber range of 2000-600 cm^{-1} , three different peaks have appeared, and all peaks could be identified. These peaks are due to the resin that contains organic pigment. On the other hand, in the low wavenumber range (red frame in Figure 5) where the peaks due to inorganic substances are expected to appear, a peak is hardly seen in the spectrum of a Seal A as compared with the spectra of Seal B and Seal C. Therefore, it is assumed that organic pigments are used primarily in ink of Seal A, while Seal B and Seal C contain inorganic pigment in the resin of vermilion ink pad. If the standard spectral data of multiple vermilion ink pad and other ink are available, by comparing the obtained spectra of imprint with such standard data, the type of ink and the vermilion ink pad used in imprint can be identified.

As mentioned above, in Raman spectroscopy a sample can be measured in a non-contact method with very simple operation. It is an analysis technique to demonstrate it as a powerful tool, when the amount of sample is limited and non-destructive analysis is required.

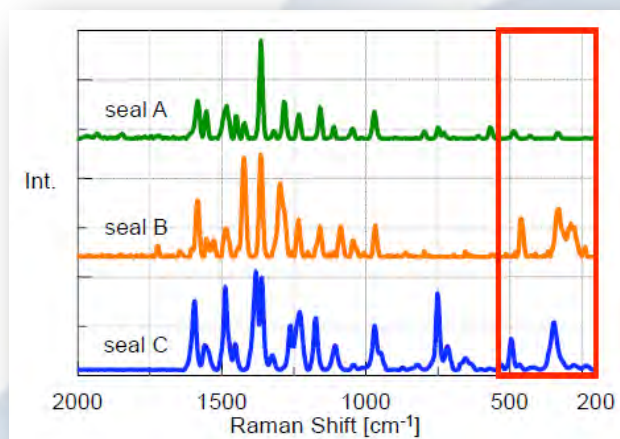


Figure 5 Spectra after fluorescence correction (normalized view)

Evaluation of Single-Walled Carbon Nanotube (SWNT) by Raman Spectroscopy - For inorganic and high function materials

Raman spectroscopy is widely used for the evaluation of carbon materials and can be applied to analysis of single-walled carbon nanotube (SWNT) in order to obtain useful information on carbon nanotube. SWNT shows metallic and also semiconducting characters due to different electronic structure in accordance with chirality and tube radius. Accordingly, by exciting its molecules with the energy corresponding to electronic transition (Resonance Raman Scattering), information about chirality and tube radius can be obtained. Fig. 1 shows Raman spectra of two SWNTs with different synthesis method (Sample A and B). In Raman spectra, three specific bands are seen. G-band observed around 1600 cm⁻¹ corresponds to vibrational mode assigned to graphite. In metal SWNT, BWF (Breit-Wigner-Fano) type spectrum is observed in the lower wavenumber range of G-band. D-band which attributes to defect is often utilized in the evaluation of crystallization. In addition, the band appearing in the low wavenumber region corresponds to the mode called RBM (Radial Breathing Mode), which correlates nanotube stretching diametrically. The peak position is inversely proportional to the tube diameter. From the equation shown in Figure 1, diameter can be estimated by peak position.

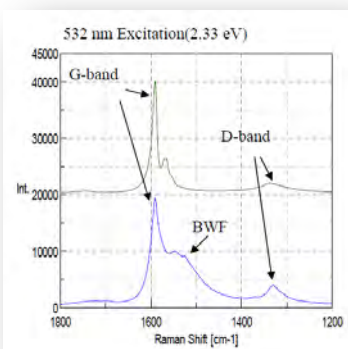
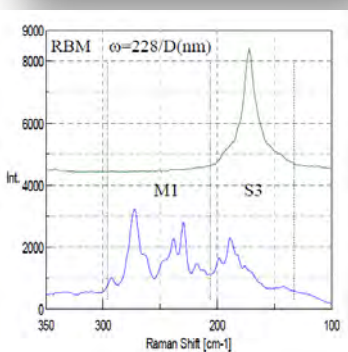


Figure 1 Resonance Raman spectra of SWNT (above: sample A, below: sample B)



(M1 : resonance of metallic SWNT,

S3 : resonance of semiconducting SWNT)

Figure 2 shows excitation wavelength dependence of SWNT (Sample B) Raman spectra. Using Resonance Raman Scattering, SWNT measurement can be done selectively for specific chirality and tube radius, depending on the excitation wavelength. Therefore, the shape of Raman spectra changes drastically depending on the selected excitation wavelength. It is assumed that 532 nm excitation is mainly in resonance with metallic SWNT, 633 nm with both metallic and semiconducting SWNT, and 785 nm with semiconductor SWNT respectively.

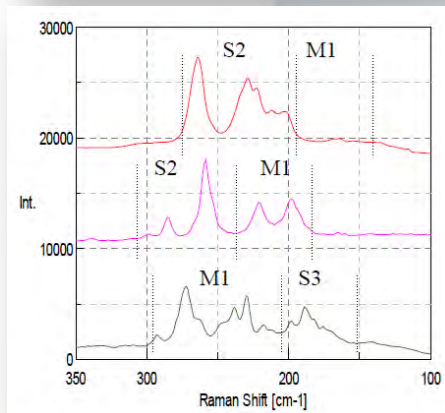
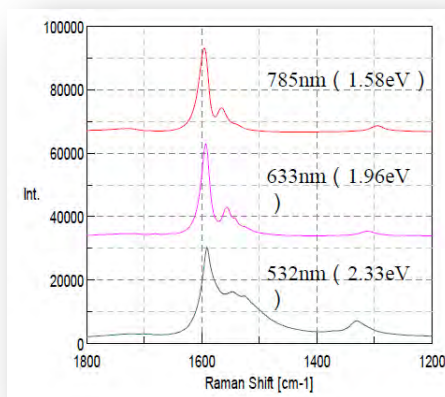


Figure 2 Raman spectrum of SWNT (excitation wavelength dependence)

(M1; resonance of metallic SWNT, S2,S3; resonance of semiconducting SWNT)

As in the above, the usefulness and measurement examples by Raman spectroscopy for single walled carbon nanotube have been described. The best features for Raman spectroscopy are capabilities of simple and non-destructive measurement, even in the air environment.

Distribution Estimation of Polymorphism of Coral Skeleton Component by Mapping Measurement

Introduction

The biogenic mineral of the gallstone, seashell, coral and so on is in many cases made of calcium carbonate. There are two kinds of crystal polymorphism such as calcite and aragonite due to the difference of the crystal structure. The aragonite is more thermally unstable than the calcite at ordinary temperature and pressure, and when heated, the aragonite changes the phase to the calcite. The crystal formation depends on the organism species. On the other hand, in some cases, the calcite and aragonite are formed contiguously in the same species. According to the recent research, if the Mg^{2+} is taken in the calcite crystal as an impurity, the solubility of the calcite is increased, resulting the inhibition of the crystal growth. On the other hand, the aragonite cannot take in the Mg^{2+} in the crystal lattice due to the ionic radius, therefore the solubility is not changed. There are a lot of Mg^{2+} in the sea water these days, so the aragonite is formed more in the sea due to the relation of the crystal formation in the sea and kinetic aspect of the dissolution.

In Raman spectroscopy, it is easier to measure in the low wavelength range, and it is possible to identify the polymorphism by peak pattern of the lattice vibration of the crystal appearing in the low wavenumber range. This time, the coral larva was transferred to the laboratory, then it was grown under the condition of some sea ingredient composition with adjusted the concentration of the each ions for easy growth of the calcite skeleton. The process of the skeletal formation of the calcite was measured by using the mapping measurement with Raman spectroscopy.

Experimental

Instrument: NRS-5100
 Objective lens: 20x
 Interval: 10 μm
 Measurement points: 31 x 31, total 300 x 300 μm
 Ex wavelength: 532 nm
 Laser power at sample point: about 10 mW
 Measurement time: about 1 hour
 Sample: 1 seed coral

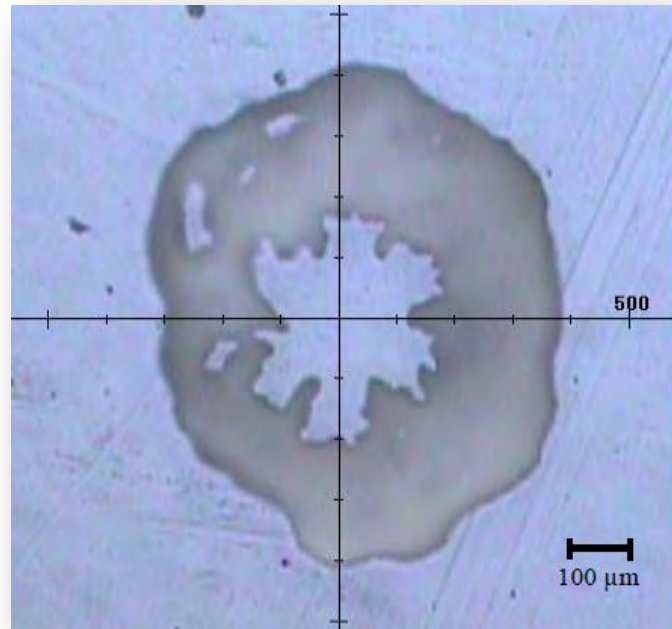


Figure 1 Observation image of 5x Objective lens

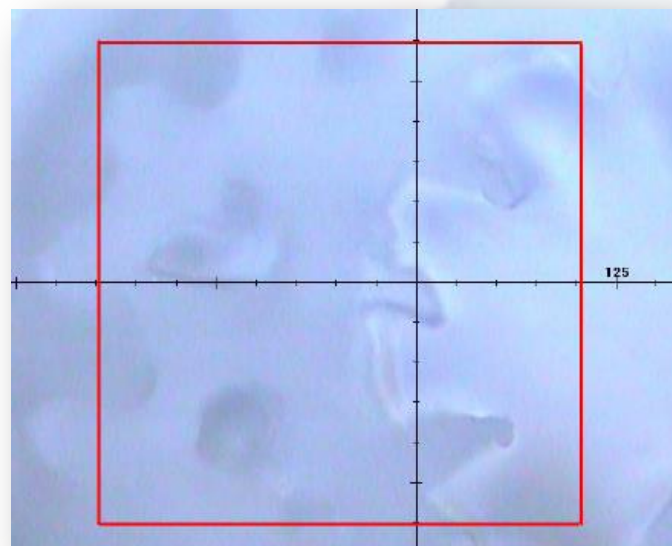


Figure 2 Observation image of 20x objective lens
(300 x 300 μm in the red square)

Distribution Estimation of Polymorphism of Coral Skeleton Component by Mapping Measurement

Results and discussions

Figure 3 Raman spectrum of calcite and aragonite. The peak due to the symmetrical stretch vibration specific to carbonate ion was observed at 1090 cm^{-1} from the result of the mapping measurement. In the wavenumber region below 300 cm^{-1} , the difference of the peak patterns due to the lattice vibration depending on the crystal configuration difference between the calcite and aragonite was seen as shown in Figure 3. The peak specific to the calcite is 285 cm^{-1} and to the aragonite, 210 cm^{-1} . Those peaks are shown as colored-coded plot in Figure 4. As a result, it can be said that 2D image of crystal growth of the aragonite and calcite was visualized.

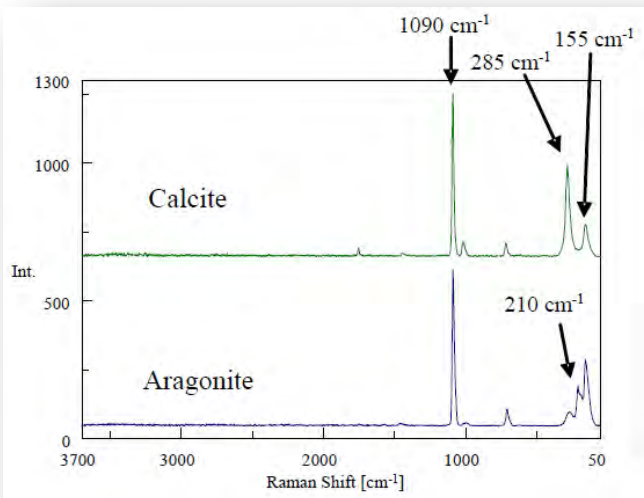


Figure 3 Raman spectrum of calcite and aragonite

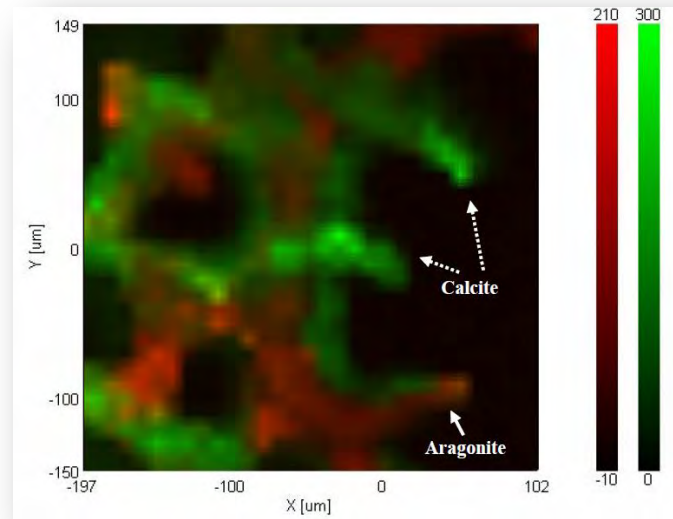


Figure 4

Color-coded plot of peak height of calcite (Green)
Color-coded plot of peak height of aragonite (Red)

The sample has been provided from Dr. Tamotsu Oomori, Dr. Hiroyuki Fujimura, and Dr. Tomihiko Highchi, University of the Ryukyus, Chemistry, Biology and Marine Science.

Measurement of scattered foreign materials by using Measurement Assist and Sample Search functions

Introduction

Recently, foreign material analysis by Raman Spectroscopy is frequently performed (ref.: JASCO Raman application data 260-AN-0010). This is because Raman spectroscopy is a method which enables to obtain the information on molecular structure as well as IR spectroscopy.

In addition, it has several features to allow non-destructive and non-contact measurement without sample preparation, measurement in depth direction with about 1 μm of spatial resolution, and easy identification of the inorganic material because of easy measurement in low wavenumber range. However, some of the users who analyze the foreign material by micro FT/IR are saying that it is difficult to do by the Raman system. Therefore, JASCO developed a special measurement tool on the software of NRS-4100 with intuitive user interface which make it possible to use with ease for user friendly purpose.

For example, it has the functions such as "Measurement Assist" function which enables the easy measurement by supporting at wizard form from focus adjustment to condition setting/measurement, "Real time data processing" for executing the automatic operation such as peak detection, or "User advice" function (patented) for performing in real time basis the operation procedure or advice for spectra.

This time, utilizing the functions of newly-developed software for NRS-4100, the measurement of scattered foreign materials was implemented rapidly and easily as reported below.

System configuration

- NRS-4100 Raman Spectrometer 532 nm laser
- Automatic imaging system

Sample search function

In measurement program of NRS-4100, "Sample search" function is provided which determines the measurement position automatically from size or contrast of observation image when the automatic stage is mounted.

The screen of "Sample search" function is shown in Figure 1, in which the search was implemented so that only foreign materials that is larger than given size were detected. The measurement points were displayed in observation image, and then as a view of search result the images of determined sample position were displayed.

It is also possible to select only the desired position from the result view and to implement the mapping measurement of whole sample region based on searched shape.

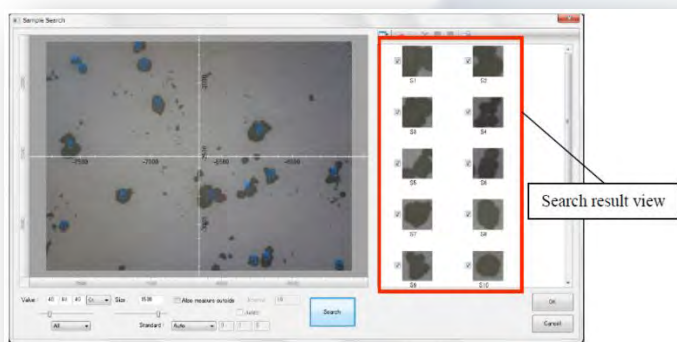
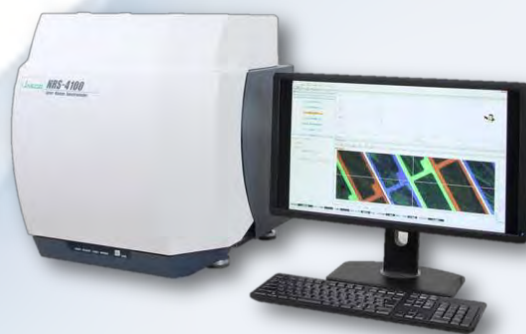


Figure 1 Image of sample search function



Measurement of scattered foreign materials by using Measurement Assist and Sample Search functions

Application of the “Measurement assist” function

The concept of “Measurement assist” function that JASCO developed is to enable anyone to implement Raman measurement easily, by guiding at wizard form the several measurement conditions that are essential to Raman measurement. The screen is configured enabling to operate intuitively using slide bar or tabular form.

This time, the sample search result performed in Figure 1 was regarded as a measurement point, and then the scattered foreign materials on substrate were measured. The foreign materials at 16 positions detected from sample search result were regarded as measurement points. In the setting screen of “Measurement assist” function, the measurement condition setting can be assisted by displaying each point where the measurement condition needs to be set following the “User advice” function, which is shown in Figure 2.

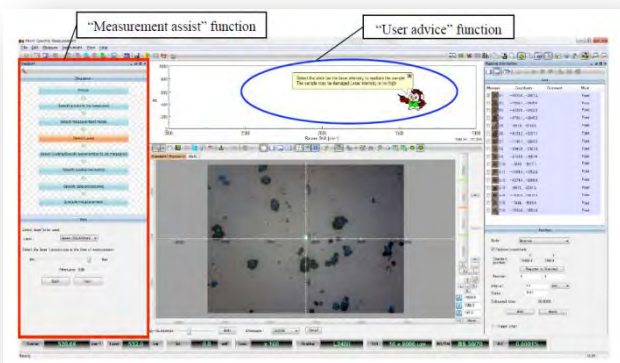


Figure 2 Measurement screen when using “Measurement assist” function (with displaying the “User advice” function)

Three spectra and their mixture spectra were observed as obtained spectra of foreign material. The typical spectra are shown in Figure 3.

From the characteristic of spectra at 16 points, it was determined that 10 points of them are for titanium oxide (anatase type), 2 points of them are for barium sulfate, 2 points of them are for tristearin, and 2 points of them are for the mixture of titanium oxide and tristearin.

It is also possible to analyze such as more specific scattering condition by the mapping measurement of the mixture.

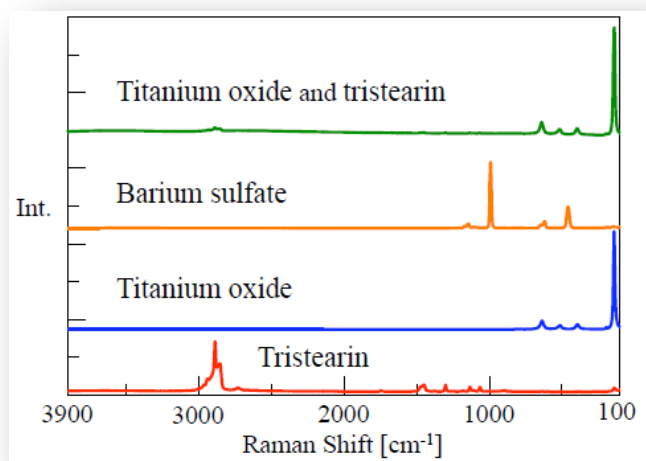


Figure 3 Spectra of foreign materials

Summary

Thus, by using the “Measurement assist” function or “Sample search” function of NRS-4100, it is possible to perform smoothly a sequence of measurement starting from determination of sample position to measurement condition setting and measurement.

Evaluation of semiconductor materials by Raman spectroscopy

- Crystal polymorphism and carrier density of Silicon power semiconductor device -

Introduction

Raman spectroscopy is widely used for evaluating chemical composition, orientation, crystallization, density, stress, temperature of semiconductor materials, and also for various structure-property evaluation such as impurity concentration, defect of semiconductor materials and composition ratio of mixed crystal semiconductor. Hall effect measurement with formed electrode is applied for evaluating electrical characteristics of carrier density in general, while Raman spectroscopy is also utilized for estimating carrier density of group III-V semiconductor. In this application data, we would like to show several measurement results using monocrystal SiC by Raman spectroscopy, such as determination of polymorphism and calculation of carrier density.

Experimental - Evaluating crystal polymorphism

1. Background

It is well known that SiC crystal has more than 200 different types of polymorphism depending on atomic arrangement and these each polymorphism has different physical property. Among such many types of polymorphism, there are the most valuable ones starting from 4H polymorphism which has the biggest band gap and also high mobility and the trials have been attempted to grow crystals selectively as one of hot topics and challenge in field. Raman spectroscopy can evaluate and determine the type of polymorphism by analysis of peak patterns due to lattice vibration of crystals, appearing in low wavenumber region where the measurement is quite difficult by IR spectroscopy.

2. Experiment and result

Two kinds of SiC monocrystal with 0.33 mm thickness that have been prepared by vacuum sublimation method under the different conditions have been measured with 532 nm excitation and backscattering position. As the result of this experiment, by comparing measured spectra in the range of 150-200 cm^{-1} and 700- 800 cm^{-1} with reference spectra in published paper¹), two samples were determined to be 6H and 4H polymorphism respectively.

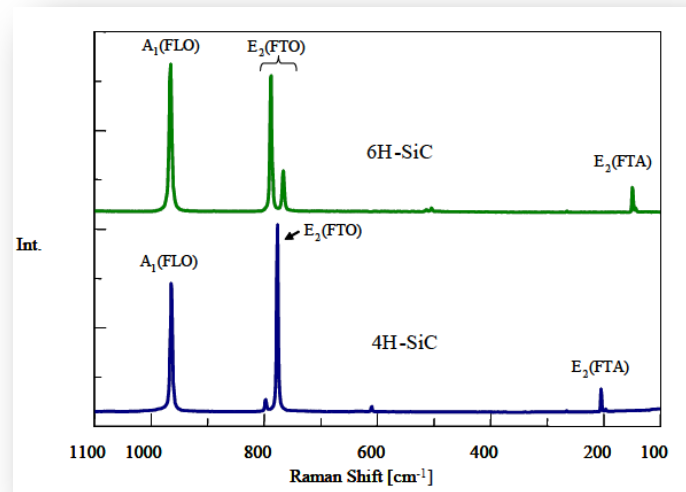


Figure 1 Raman Spectra of 6H-SiC and 4H-SiC

Evaluating carrier density

1. Background

In manufacturing process of semiconductor materials, it is not unusual to dope some impurity material to pure semiconductor to increase the concentration of free electron and electron hole as carrier. Regarding n-type compound semiconductor, Raman spectroscopy is applied as an easy method to estimate the carrier density. In polar semiconductor such as GaN, GaAs, SiC, longitudinal wave and transverse wave due to lattice vibration of crystal can be observed separately in Raman spectra. Collective oscillation of free electron which exists in n-type semiconductor as carrier is called as Plasmon, which is longitudinal wave similar to sound wave. This plasma oscillation is the same kind of wave as the longitudinal wave due to lattice vibration, LO phonon and therefore they interact with each other. This interaction is magnified due to the concentration of carrier and this relevancy makes peak position of longitudinal wave due to lattice vibration shift to higher wavenumber side. Such peak shift is named as $L+$ and $L-$ and shown in Fig. 2. In evaluation of SiC, only the peak of $L+$ can be observed by using of Raman spectroscopy. It is known that this peak shifts to higher wavenumber side with broadening peak shape when carrier concentration is increased, and accordingly, the absolute carrier concentration is evaluated by the peak position.

Figure 2 shows that the energy level of Plasma oscillation, collective oscillation of free electron in semiconductor increases with increase of carrier concentration in compound semiconductor.

Evaluation of semiconductor materials by Raman spectroscopy - Crystal polymorphism and carrier density of Silicon power semiconductor device -

Peak is shifted through interaction between LO phonon, longitudinal wave due to lattice vibration and Plasmon by resonance phenomenon which is generated under the condition that plasma frequency is close to the energy of lattice vibration. However, any peak shift cannot be observed for TO phonon, since TO photon, transverse wave due to lattice vibration does not have any such interaction.

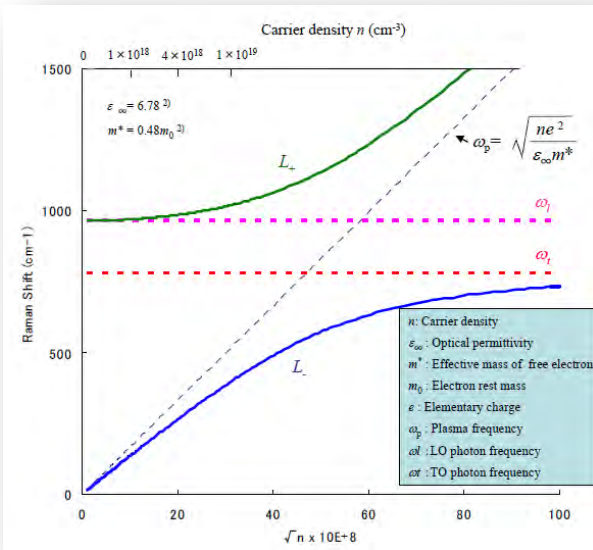


Figure 2 Carrier concentration change vs. wavenumber shift (L+ and L-) in combined mode of Plasmon and phonon

2. Experimental and result

Samples in this experiment are 3 kinds of 4H-SiC monocrystal which have been grown to 0.33 mm thickness by several different conditioned sublimation method. Each sample is measured using JASCO NRS-5100 Raman Spectrometer with 532 nm excitation and backscattering position. Figure 3 shows that peak wavenumber of longitudinal wave is different for each sample. The absolute carrier concentration can be estimated by inputting central wavenumber of each peak to theoretical curve which indicates the relationship between carrier concentration and LO phonon - Plasmon connection mode as shown in Figure 4. As shown in Figure 3, carrier concentration is getting higher in the order of a – b – c, and the higher carrier concentration is, the broader the peak shape becomes, while peak is shifting to higher wavenumber side. As a conclusion, Raman spectroscopy makes it possible to evaluate sample in micron level spatial resolution which is difficult by the technique for Hall measurement, to analyze surface by imaging and also to evaluate depth profile with ease as non-destructive method.

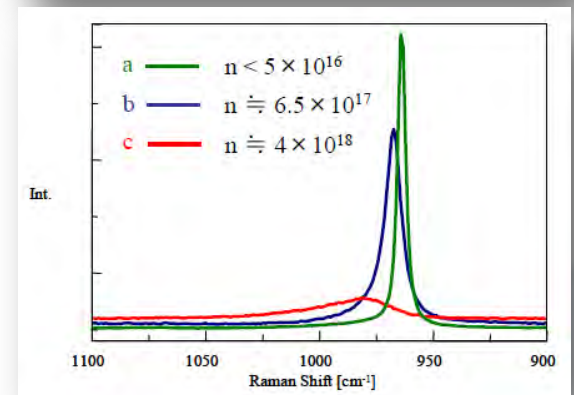
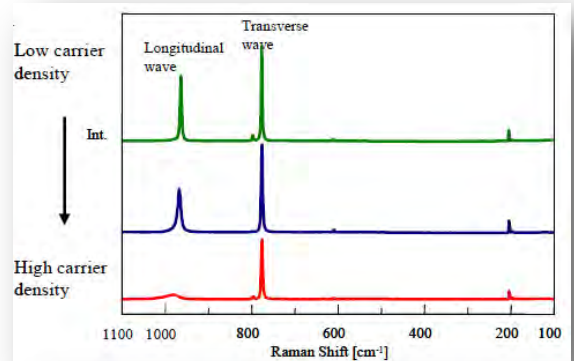


Figure 3 Change of Raman spectrum of 4H-SiC due to carrier - concentration(A), zoomed one (B)

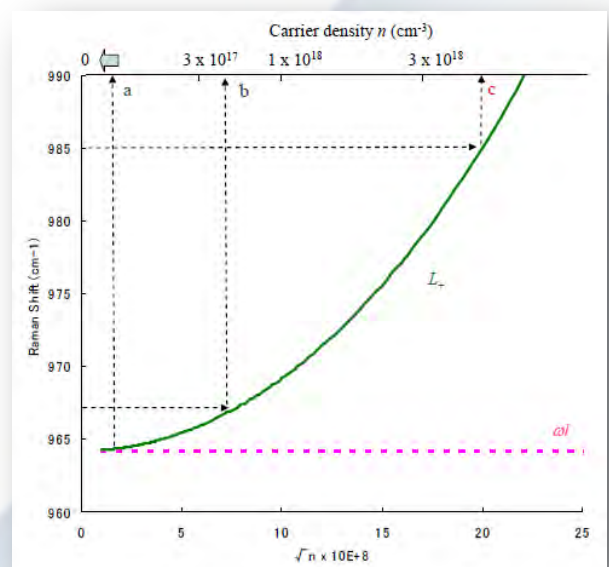


Figure 4 Carrier concentration calculation from central wavenumber

Reference

- 1) S. Nakashima, and H. Harima, *Phys. Stat. Sol. (a)* **162**, 39 (1997).
- 2) H. Harima, S. Nakashima, and T. Uemura, *J. Appl. Phys.*, **78**, 1996 (1995).

Samples in this evaluation had been provided from Prf. Inushima and Mr. Ohta of Course of Electrical and Electronic System in Tokai University.

Raman Quantitative Calibration Stability for a Sample Mixture

John Carriker and Richard A. Larsen, Ph.D., Jasco, Inc

The simplicity of Raman spectroscopy provides an ideal method for the quantitative determination of liquid mixtures.

The use of Raman spectroscopy for routine quantitative analysis is desirable due to the simple sample handling requirements for sample analysis. Due to the many variables associated with Raman spectroscopy, specifically, laser power, Raman cross-section, wavelength and intensity stability, Raman is rarely used for quantitative analysis. Compared to Raman analysis, there are other methods that can provide a repeatable quantitative prediction of unknowns, but these methods can require extensive sample preparation or extended time for analysis. To demonstrate the capabilities of Raman spectroscopy for quantitative analysis, a 2 component mixture of liquid samples was analyzed using a Raman spectrometer and the results reported.

Experimental

Several mixtures of benzonitrile dissolved in ethanol were prepared at 0.1, 0.3, 0.5, 1.0, 3.0 and 5.0% concentration as standards for development of the multi-component calibration model including a 0.2% mixture to be used as an 'unknown' for analysis using the calibration model. A Jasco NRS-3100 Raman spectrometer was used to collect triplicate spectra of the standards using 532 nm excitation and a 60 second integration of the CCD with 2 accumulations to obtain spectra with a spectral resolution of slightly less than 4 cm⁻¹ resolution. Samples were contained within 2 mL HPLC sample vials and a macro accessory used for excitation/collection of the sample volumes. No further correction of the Raman spectra was performed prior to development of the calibration model or analysis of 'unknown' spectra.

Results

The various standard spectra as well as an ethanol 'blank' were used to develop the quantitative calibration model using Jasco's Spectra Manager Quantitative Analysis package. A peak ratio method using the 2234 cm⁻¹ C-N stretch of benzonitrile vs. the 1455 cm⁻¹ C-H bend of the ethanol was used for the development of the linear calibration curve. Initial results based on the initial triplicate spectra of each standard provided a calibration curve with a fit of 0.9998 and an R² of 0.9996, indicating an excellent fit of the data. To evaluate the repeatability of the calibration method, additional spectral data sets of all standards were collected again after 1 and 2 weeks, providing a total of at least nine spectra of each standard for calculation of the calibration curve. The final calibration curve also provided a linear calibration curve with very little scatter, offering a fit of 0.9997 and an R² (residual) of 0.9995 (Figure 1). As well, the analysis of the 'unknown' sample that was prepared indicated errors of less than 0.5% for the replicate analyses conducted over the 2 week period.

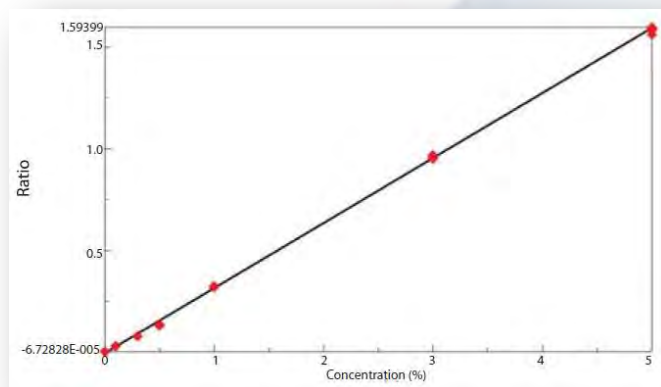


Figure 1 Calibration model for quantitative standard mixtures, including 2nd and 3rd week standards analysis.

Conclusions

The results demonstrate that a reliable calibration model can be developed from Raman spectra of a mixture without further correction. The results demonstrate a correlation of 0.999 or better for the quantitative component over a range of concentrations from approximately 0.1 to 5%. Further, the Raman method provides repeatable, reproducible results and proves to be stable for extended periods.

Dispersive Raman for the Identification of Contaminant Particles in Ink Jet Cartridges

The majority of printing problems are primarily caused by clogged print heads or nozzles, preventing the ink from reaching the paper. Each year billions of dollars in print cartridges are sold, thus, improving the quality and functionality of print cartridges is a priority. Several commercial inkjet cartridges were examined using the Jasco *Ventuno* Raman system to obtain fundamental data on the blockages of print cartridges and some knowledge as to the possible causes.

Introduction

Statistics have long supported the dominance of inkjet printing. From sales of \$500 million in the early 90's to a record-breaking \$14 billion in inkjet cartridge sales projected in 2001. Today, 7 out of every 10 printers sold is an inkjet. The estimated installed base of ink jet printers stands at 130 million worldwide and the numbers continue to climb.

The basic principle of the inkjet system is comprised of a reservoir of ink held in the cartridge, and a method of moving the ink from the reservoir to the paper via the print head, in a very precise and controlled procedure.

Air plays an important part in the whole operation as it replaces the ink as it is used, so there must be a way for the air to get into the cartridge, while not causing the ink to drip out of the cartridge until it is required for printing. The common commercial cartridges all have air vents to allow the passage of air into the cartridge.

To get the ink onto the page, the cartridge print head has many very small (with diameters less than a human hair) nozzles or holes that allow the ink to flow to do the printing. These nozzles hold the ink until an electronic impulse causes the ink to be sent to the paper. The popular method (bubble-jet) is to selectively heat the ink at the nozzles, by resistors. As the ink heats, a bubble forms, the heat source is removed, the formed bubble "bursts" and the resulting ink is transferred to the paper. This is all happening at a very high speed, so that the dots that are being sprayed (up to 6000 per second) onto the paper will form the characters or graphics.

Another method is the "piezoelectric" method, where crystals are subjected to an electric field, which causes them to expand and contract. The movement this generates then allows a precise amount of ink to be put down onto the paper.

Experimental

The JASCO *Ventuno* micro-Raman system equipped with a 532nm diode laser and two interchangeable gratings was used to collect the Raman spectra of the print cartridge. An Andor CCD detector cooled to -75C, and an integration time of 60 seconds was used for collection of sample spectra. Samples were visualized using the 100x magnification of the microscope. The *Ventuno* was also equipped with a MS-2000 motorized joystick controlled sample stage. The typical range for the measurement was from 470 - 2,390 cm^{-1} with a 1200 g/mm grating. Figure 1 shows a representative microscope image of one of the printer cartridge nozzles, the contamination around the nozzle clearly visible. The green spot is the laser. Three distinct particle types were collected and identified from the inside of the cartridge openings: organic matter with resolved Raman peaks; an amorphous or highly complex organic mixture, possibly carbonized due to heat; and almost pure crystalline silicon.



Figure 1 Microscope view of the inkjet hole using a 20X lens. Scale (yellow) is 250 μm . The green spot is the laser focus.

Figure 2 shows the Raman spectra from one of these particles. The organic material was identified as being polymeric with nitrogen and carboxylic groups. Amide and urea are likely candidates. However, so many organic compounds, including commercial polymers such as poly(chloroprene), have Raman lines in the 1,700-1,000 cm^{-1} region, that making an unambiguous determination is difficult without more information on the processing.

Dispersive Raman for the Identification of Contaminant Particles in Ink Jet Cartridges

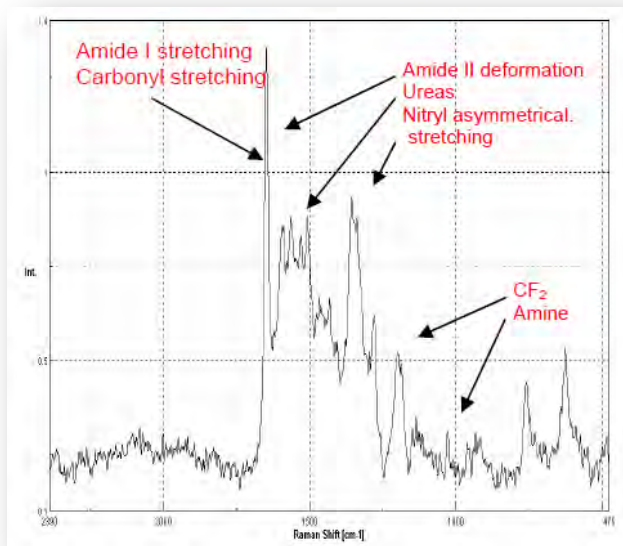


Figure 2 Raman spectrum from 475-2390cm⁻¹ of a typical organic particle in the cartridge opening.

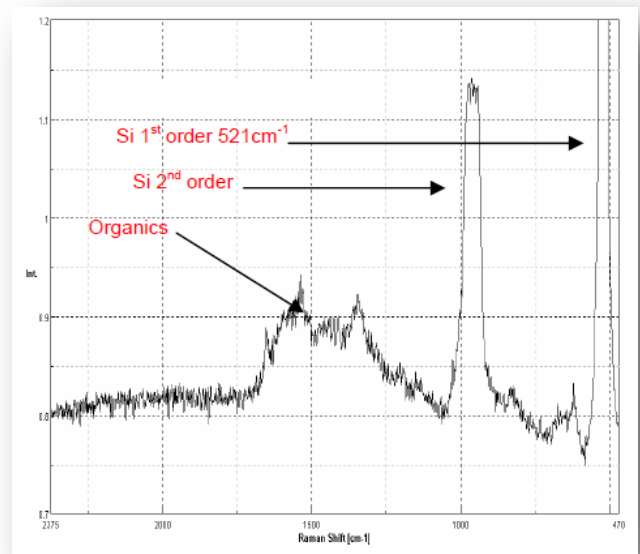


Figure 4 Raman spectrum from 470-2375cm⁻¹ of a typical silica particle found in the cartridge opening.

A representative microscope image of a silicon particle found in the cartridge opening is shown in Figure 3. The 2 micron green laser spot highlights the particle which is not much bigger than the laser spot. The Raman spectrum of the particle is shown in Figure 4. The first and second order peaks used to identify the silicon particle are labeled. Silicon is sometimes used in inkjets and this is a likely origin of the small silicon particles.

One of the major problems faced with refilling ink cartridges is the clogging of ink jets. Many black ink cartridges contain pigmented ink. Pigmented ink is not water soluble (like dye based inks) often contain solid microscopic particles of a carbon-polymer compound. The pigmented ink that remains in a cartridge forms a paste that eventually hardens and strongly adheres to the inside of the cartridge. Every printer cartridge opening that was examined contained some type of particulate matter. Most of these contaminant particles were in the micron size range. Identification of the compounds that create the blockages can lead to their elimination and make ink cartridges less susceptible to clogs.



Figure 3 20M microscope image of a silica particle found in the opening. Scale (yellow) is 50um.

Conclusions

The Raman spectra and representative microscope images were used to characterize the nozzle contaminants. Preliminary peak assignments for some of the organic materials were suggested and the silicon particles positively identified. Examination of the compounds that create the blockages may provide data to improve the inkjet printing mechanism and enhance the development of inkjet cartridges that are less susceptible to the clogging that plagues most systems.

Carbon Nanotube Analysis by Raman Spectroscopy

Carbon nanotubes are unique nanostructures with remarkable electronic and mechanical properties. Nanotubes have been considered prototypes for a one dimensional quantum wire. As other useful properties have been discovered, particularly strength, interest has grown in potential applications, such as, nanometer-sized electronics or stronger polymer materials. Theory suggests that carbon nanotubes will have a variety of useful properties. Experiments validating this is just beginning. One primary method for the analysis of these nanostructures is Raman Microspectroscopy.

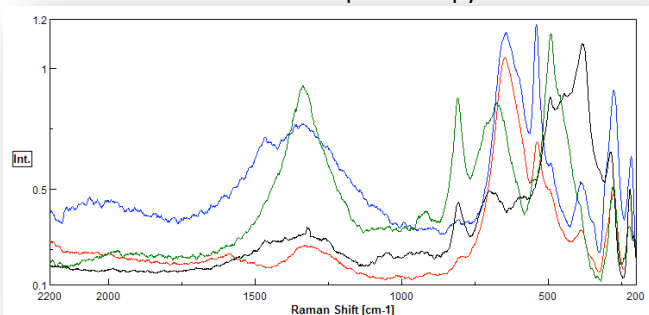


Figure 1 Raman spectra of granular nanotube sample.

Introduction - Carbon nanotubes are fullerene-type structures which consist of graphene cylinders closed at either end. A nanotube can be thought of as a hexagonal network of carbon atoms that has been rolled up to make a seamless cylinder. Nanometer across, the cylinder can be tens of microns long, with each end "capped" with half a fullerene molecule. Studies have predicted that nanotubes can be conducting or insulating depending on their structure, which leads to applications in electronics. They also suggest that nanotubes should be immensely strong, becoming "the ultimate carbon fibers". Single-walled tubes have remarkable adsorptive and catalytic properties, and can be used as components of a new generation of fuel cells. This molecular nature is unprecedented for devices of this size. The challenge exists to find a method capable of finding these tiny particles and non-destructively analyze them for structural composition. Raman microspectroscopy is capable of doing that and more.

Experimental - Nanotube coated glass slides and nanotube granules were synthesized by various laboratories and submitted for analysis. They were imaged using the 20x objective under the microscope and the Raman collected using the Ventuno Raman system. Several areas of each sample were evaluated. The instrument was equipped with a 532 nm diode laser; 2 gratings and an air cooled CCD detector. The integration times for spectral collection were 20 seconds per acquisition. The confocal aperture used (50mm), gives an approximate 1mm (x,y) and 2mm (z) sample volume. The laser power at the sample was 10 mW or less.

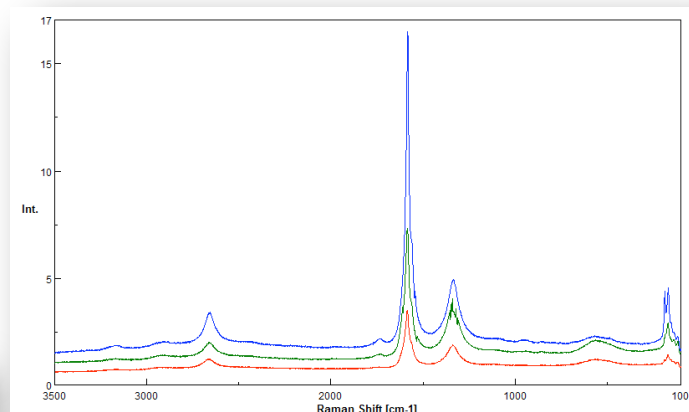


Figure 2 Raman spectra of carbon nanotubes on glass slides.

Results and Discussion - Figures 1-3 show various nanotube spectra. The spectra are being used with the permission of the researchers. The spectra indicate that the purity and structure of the nanotubes can be determined using the raman spectra. The spectra in Figures 1 and 3 were collected using both 532nm while Figure 2 was collected using 633nm excitation. Both excitation wavelengths appeared to be effective for analysis.

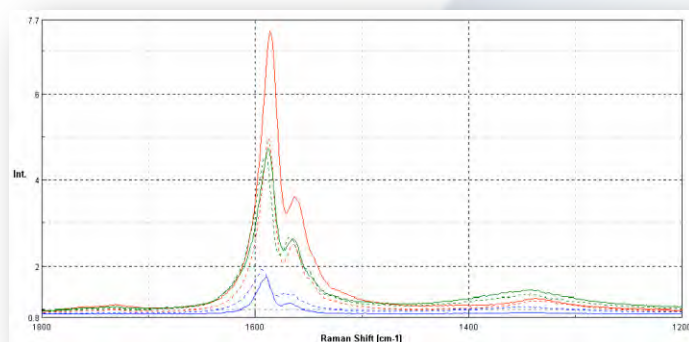


Figure 3 Raman of nanotubes on glass showing the G/D region

The primary concern in the analysis of the nanotubes was burning of the samples under prolonged laser exposure. The switching of the wavelengths was one method used to help reduce this effect. Additionally a laser attenuator was added to reduce the power on the sample and allow for longer collection times. Many of the nanotube samples were thin layers on microscope slides did not exhibit signs of burning. The more impure nanotube samples seemed to suffer the most from absorption of the laser.

Conclusions - Raman is an effective way to screen nanotubes that is reliable, non-destructive and requires little sample preparation.

Gemstone Identification using Raman Spectroscopy

Amanda L. Jenkins and Richard A. Larsen Jasco, Inc

Raman micro-spectroscopy is an ideal method for the examination of marketable gemstones because of the lack of sample preparation involved and the nondestructive nature of Raman analysis.

In recent years, the gemstone market has been flooded with stones of questionable origin. Frequently, even thorough analysis by a qualified jeweler cannot reveal unequivocally whether the gemstone is genuine or fake. In the worst case, sophisticated analytical methods struggle to differentiate modified diamonds, causing considerable concern to the international gemstone trade. Raman micro-spectroscopy is an ideal method for the examination of marketable gemstones because of the lack of sample preparation involved and the nondestructive nature of Raman analysis. The micro-Raman study of a stone also provides a unique record for identification purposes. This article discusses the variety of Raman spectra that can be obtained from different families of gemstones, comparing and contrasting spectra from genuine and artificial minerals.

Color in gemstones is caused by light of specific wavelengths being absorbed inside the stone. Such absorption is a characteristic of the gemstone material, the molecular structure, and extraneous impurities or inclusions within the crystalline structure (1). The human eye perceives the different light wavelengths as colors. As white light enters a stone, the wavelengths are affected by the chemical and structural properties of the stone, some wavelengths being absorbed, others reflected.

A combination of different wavelengths radiate from the stone, changing the white light that entered into emitted light of various colors (2). Materials formed in different configurations can have very few similarities. For example, both diamond and graphite are essentially pure carbon but the crystal structure of the carbon in diamond is completely different. For colored gemstones the quality of the color is worth at least 50% of the valuation of the gemstone (3). Color also comes from sources other than absorption of bands of light. Structural properties can cause various types of phenomena.

The first is play of color, an effect caused by diffraction of light. In opal, which is made up of regularly stacked small spheres of silica, these layers of spheres act similar to a diffraction grating producing colors from the refracted light. The colors are determined by the sphere size and spacing. Iridescence is somewhat similar to a play of color in that the interference colors are created by light refracting from very thin layers of a gemstone material such as fire agate or ammonite. Orient is another interference phenomenon that occurs in pearls and is caused by the thin layer structure of the outer pearl and by undulations in nonspherical pearls.

Asterism is caused by needle inclusions along crystallographic lines. This effect is seen in star rubies, sapphires, and some other stones. Chatoyancy is similar to asterism, but produces a single band of light caused by the needle inclusions creating the phenomena known as a catseye effect. Aventurescence is a sparkle effect caused by small plate-like inclusions and is common in aventurine quartz, sunstone feldspar, and Goldstone glass (4, 5).



Gemstone Modification and Enhancement

Gemstones and semiprecious stones have been modified for centuries to make them more colorful, more eye-catching, and easier to work with. One such technique is heat-treating (the most common) to enhance, clarify or create color in a stone. Amethyst is heated to obtain citrine. Zircon is heated to clarify the stone to clear white. Sapphires are heated to get amazing pinks and blues. Rubies lose a purplish tint while iolite might be turned a deep blue. Heat-treating also can be used to enhance the "color change" of gems such as tanzanite. Dying of stones also is a very common practice. Agate is dyed to get pinks, purples, oranges, and blues. Although chalcedony is often dyed, black chalcedony usually is sold as onyx. Irradiation with UV light is another common treatment.

Gemstone Identification using Raman Spectroscopy

Amanda L. Jenkins and Richard A. Larsen Jasco, Inc

the most commonly irradiated gemstone (to get various shades and tones of blue). This also is how fabulously colored diamonds are obtained. In fact, diamond was the first gemstone to be color treated by UV radiation (1, 3–6). Another gemstone enhancement technique is stabilization.

Stabilization traditionally was accomplished by filling the stone with natural oils; however, modern synthetic resins such as Opticon (Hughes Associates, Wayzata, MN) are being used now. Resin filling often is more permanent than the use of natural oils. Opals often are stabilized and emeralds have a long history of fracture filling due to the popularity of the gem and a tendency for the stones to be highly included or fractured. Another commonly used technique is diffusion, which embeds a very thin layer of an element into the surface to improve color.

Laser drilling also is done to obtain access to enclosed crystal inclusions and remove them with acid. Stones also are bleached, dyed, waxed, coated, and painted (4–6). One of the most controversial modification techniques is the so-called creation of gemstones. Synthetic gems are made on an industrial scale like chemicals and have been around since the late 1800s when ruby first was synthesized. Laboratory grown crystals of ruby, sapphire, diamond, emerald, and star sapphire bear the name of the mineral species they resemble because they have an identical appearance, atomic structure, and a similar (not always identical) chemical composition. Simulants or imitations are gemstones or other materials that alone or in combination with others are made to look like more valuable gemstones. Assembled stones are made by gluing layers of different gem materials together to create an apparently colored composite or to increase stone size. Glass and plastics, manufactured with a wide range of color, specific gravity and index of refraction can be used to simulate natural stones. Cubic zirconia, synthetic rutile, strontium titanate, zircon, and white sapphire include both synthetic and natural gemstones that are used to simulate natural gemstones, usually diamonds (3). From a buyer's point of view, the most important issue with these simulants is proper disclosure (7–9).

Gem Examination and Identification

Gems often are examined by trained personnel using a variety of methods. The most common instrument in gem identification is the eye. Vision alone can be used to observe color, transparency, cut, phenomena, polish luster, dispersion, heft, fractures, and cleavage. However, a variety of analytical instruments also is available and some are explained here. The refractometer probably is the most common instrument in gemstone identification. A special light source is used to project a beam of light into the refractometer and into a hemicylinder of very soft, highly leaded glass. A small drop of a special liquid with a high refractive index is used to form an optical bond (not physical) between the sample stone and the hemicylinder. Observation through a calibrated scale allows the observer to see a partially shaded scale where the boundary defines the refractive index of the stone. If a yellow sodium light source is used, the observer can move the stone around to view different facets and determine both the upper and lower limits of the refractive index on doubly refractive stones and therefore the birefringence. Careful use of the refractometer with the stone in many positions also will allow determination of the optical characteristics (doubly or singly refractive) and the optical sign (positive or negative). These tests must be done with a well-polished, clean stone and great care must be taken so as not to scratch the hemicylinder (3, 10). A thermal impedance tester is used to measure the thermal conductivity of a stone. It is of little value except for separating diamond from other stones.

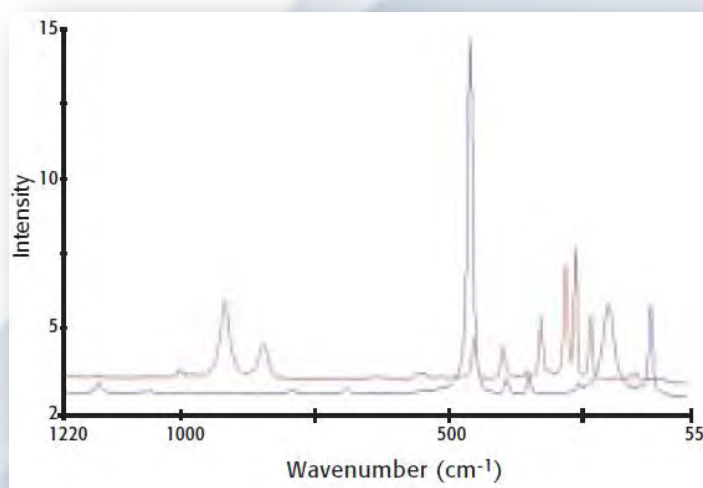


Figure 1 Citrine (bottom), a yellow colored natural quartz, can be passed off as the more expensive topaz (top) by unscrupulous gem dealers.

Gemstone Identification using Raman Spectroscopy

Amanda L. Jenkins and Richard A. Larsen Jasco, Inc

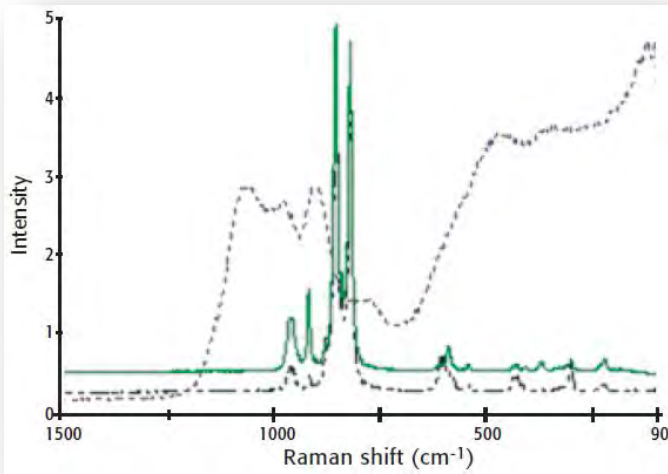


Figure 2 The normalized Raman spectra of peridot from a necklace, (solid) ring, (dots/dashes) and the fake peridot from a bracelet (dotted)

However, imperfections can be filled readily with synthetic materials or the stone can be processed to alter the color and increase market value, with the unsuspecting consumer convinced that he has purchased a stone of greater value (7, 11). With lesser gemstones the analytical techniques are much less established and more reliant on long experience with mineralogical identification methods. Raman spectroscopy provides an ideal method for the examination of gemstones and semiprecious stones. Raman spectroscopy is a measurement of the reemission of light from interaction with an incident light source, usually a laser. Raman spectra result from vibrational motions of the molecular bonds in the material. As opposed to infrared spectra, which are a result of a change in the molecular dipole moment during the molecular vibration, Raman spectra result from a source-induced change in the polarizability of the molecular bond during the vibrational motion. With the ability to microscopically examine both loose and mounted stones, Raman can distinguish not only real versus artificial gemstones, but also can discriminate those that have been adulterated in addition to providing details of the alteration.

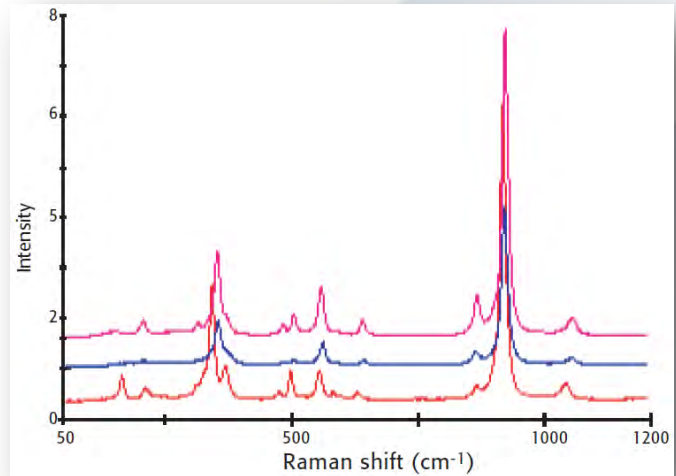


Figure 3 The Raman spectra of several cuts of garnet: square cut (top), oval (middle), and round (bottom).

However, even a positive test using thermal impedance must be augmented by other gemological observations to differentiate diamond from moissanite. A UV cabinet uses both short- and longwave UV light bulbs to illuminate the samples. Testing for UV fluorescence is useful in separating several gemstone types and is particularly useful in separating some synthetic materials from natural counterparts. Occasionally a gemstone will have phosphorescence, a persistent release of light for a short time after exposure to ultraviolet light. This is caused by a slower return of electrons from their excited state to the normal, or ground, state. In adequate darkness, such phosphorescence can be observed easily. A spectroscope is used to reflect a strong light source off the surface of a gemstone or project it through the stone. Either way, the gemstone will leave its spectral fingerprint on the light beam, which is spread into the visible spectrum for observation. The gemologist notes the wavelengths (spectral position) of the absorption line and bands, and compares them to known materials. Microscopes are used for close-up examination of the external and internal characteristics of gemstones (3, 10). In some well-studied cases such as diamond, these techniques usually will suffice.

Gemstone Identification using Raman Spectroscopy

Amanda L. Jenkins and Richard A. Larsen Jasco, Inc

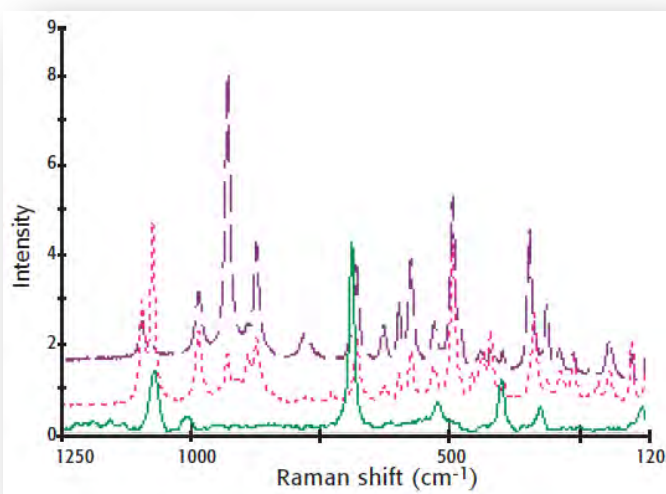


Figure 4 The Raman spectra of emerald (solid) And two tanzanites (dotted and dashed)

Experimental

Loose and mounted gemstones in different types of platinum gold jewelry settings (rings and pendants) were borrowed or purchased from various dealers. In several instances these gemstones had professional appraisals. Each gemstone then was placed into the sample compartment of a Jasco Ventuno, a benchtop-mounted fully integrated confocal micro-Raman spectrometer. The instrument was equipped with a 488-nm argon ion laser (Melles Griot, Carlsbad, CA) and a 532-nm diode laser (Torsana Laser Technologies AVS, Skodsborg, Denmark); two gratings and an Andor (South Windsor, CT) air-cooled, frontilluminated CCD detector. The integration time for spectral collection was 20 s per acquisition. The confocal aperture of 50 mm gives an approximate 1 mm (x, y) × 2 mm (z) sample volume. The laser power at the sample was approximately 10 mW or less.

Results and Discussion

Citrine, Topaz, and Amethyst. The most commonly occurring form of silica (SiO₂) is quartz, which appears in impure form as amethyst, citrine, onyx and jasper (12). Citrine is the most valuable quartz gem. Almost all citrine on the market is heat-treated amethyst (13).

Natural citrine is yellow to orange, and occurs in much lighter hues than the heat-treated material. Amethyst traditionally is purple. The color in both amethyst and citrine is due to impurities of iron at parts per million levels. The iron substitutes for silica in the quartz structure. The iron is trivalent and gives the yellow color seen in citrine. If it is irradiated, most of it will turn purple, but not all citrine will change color (11). In some amethyst deposits, the amethyst has been partially or fully changed to brown citrine by geothermal heating. Citrine also can be produced by heat-treating smoky quartz from certain localities. Citrine also closely resembles topaz (14). Unfortunately, unscrupulous dealers label citrine in such a way that unassuming buyers think they are buying the more valuable topaz. It should be understood that any “topaz” labeled with a prefix (such as gold topaz, Brazilian topaz, and citrine topaz) is heat-treated citrine. The Raman spectra in Figure 1 clearly indicate the differences between citrine and topaz.

Peridot, Emerald, Garnet, and Tanzanite.

Peridot is the well-known gem variety of olivine ([Mg,Fe]₂SiO₄), a species name for a series of magnesium-iron rich silicate minerals known for their green color (12). The ancient Egyptians called peridot “the Gem of the Sun” because it supposedly was too bright to be visible in the sunny Egyptian desert. Legend also suggests that peridot can glow at night which made it easier for the Egyptians to see (and mine it) after sunset (11–15). We analyzed several peridot stones in various shapes and settings. The first two stones were trillion cut, one mounted in a ring and the other in a pendant. Two oval peridot stones from a ring and a pendant also were evaluated. Finally a series of peridot stones from a tennis bracelet were examined by Raman spectroscopy. The Raman spectra from each of the first four stones were almost identical, independent of stone cut. Figure 2 shows the Raman spectra from the oval peridot pendant and the triangular peridot ring. Some minor variations in some of the weaker bands are indicative of the stone cut. The peridot spectra from the tennis bracelet, however, had a large fluorescence and were missing the peridot bands. Instead, these so-called peridot exhibited the characteristic silicon bands from 900–1150 cm⁻¹, which indicated that these stones were merely green glass. Thus Raman analysis proved the peridot in this bracelet to be a fake.

Gemstone Identification using Raman Spectroscopy

Amanda L. Jenkins and Richard A. Larsen Jasco, Inc

Another orthosilicate gemstone is garnet, which is a group of compounds with the structure, $M^2_3M^3_2(SiO_4)_3$ where M^2 are eight-coordinate (Ca, Mg, Fe) and M^3 are six-coordinate (Al, Cr, Fe) (12). The name garnet can be applied to six similar mineral species, namely almandine, pyrope, spessartine, grossular, andradite, and uvarovite. To further complicate matters, many garnets actually are a combination of these minerals. Rhodolite, for instance, is a combination of almandine and pyrope (13). There also are many trade names and other commonly used names which only adds to the confusion, such as Rhodolite, Tsavorite, Malaya, Mozambique, Mandarin, Melanite, Topazolite, and Thai (2, 15). The most common forms of garnet all contain iron and adopt one of the spinel structures (12). We evaluated several different garnets, including two oval shaped garnets mounted as pendants, two square garnets mounted as earrings, and several small round garnets in an earring cluster. Figure 3 illustrates the Raman spectra from each garnet shape. The top square garnet was identified as being spessartine-zz. The middle spectrum of the round stone was determined to be an almandine-xx, while the bottom spectrum of the oval garnet is an example of the pyrope-zz. Tanzanite is a unique gemstone as it occurs in only one specific location in the east African state of Tanzania. It has a characteristic blue color that shimmers in a slightly purplish hue. Tanzanite is a blue variety of zoisite gemstone. However, this hydrated calcium aluminum silicate mineral $Ca_2Al_3Si_3O_{12}(OH)$ achieves only hardness 6.5 – 7 on the Mohs' scale, and is thus not very resistant to abrasions (16, 17). Tanzanite is a natural gemstone whose color is enhanced by heat-treating. When found in nature, tanzanite crystals are a muddy reddish-brown color. The crystals then are heated to approximately 650–700 °F to bring out the permanent rich blue, purple, and violet colors. Tanzanite is one of the few gemstones that are pleochroic, meaning it exhibits two or more separate colors when viewed at different angles. The more common colors are blues and purples but one might also see flashes of red, green, yellow, orange, or brown.

The color that gemologists predominantly speak of is the “deep royal blue” (18–21). Tanzanites, which are more blue than purple, usually are more expensive because the crystals tend to form with the blue color axis oriented along the width of the crystal instead of the length (22). Several synthetic gemstones and nongem materials have been offered as substitutes for tanzanite. For example, synthetic fosterite simulates the color and look of tanzanite but is significantly less expensive. Synthetic sapphires also have been offered as imitators of the bluer varieties of tanzanite (18). We evaluated several tanzanite stones and compared them with a reference database (21). One stone was a triangular shaped stone, two others were oval, and one was round. The Raman spectrum of tanzanite has a characteristically complex spectrum from about 50 to 2000 cm^{-1} (Figure 4). All four tanzanite examined had spectra with identical peak locations, but the individual spectra exhibited different peak height ratios. These slight intensity differences are attributed to the alignment of the crystals along the color axis.

Emerald is in the beryl family (beryllium aluminum metasilicate) with a chemical formula of $Be_3Al_2Si_6O_{18}$. The emerald differs from other beryls in its deep green color (7). Its intense green coloring is due to a trace of chromium or vanadium replacing the aluminum in the beryl structure. Because of the nature of this replacement, almost no emeralds with intense color are free from inclusions. Imitation emeralds are found most commonly as composite stones, which are jewelry pieces comprising more than one stone bonded together. False emerald doublets consist of a thin slab of emerald that is glued on top of a colored glass bottom to form a large composite emerald. Soude emeralds are false emerald doublets that consist of a colorless spinel top and bottom pieces fused together with a green bonding agent. Emerald triplets can be detected by immersing the stone in a liquid such as alcohol — the top and bottom pieces seem to disappear and all that is visible is the green bonder at the girdle. Another common emerald imitator is green glass (19). We examined emeralds in an antique platinum ring consisting of 10 square cut emeralds surrounding a round diamond. The emerald Raman spectra are shown in Figure 4 along with the tanzanite.

Gemstone Identification using Raman Spectroscopy

Amanda L. Jenkins and Richard A. Larsen Jasco, Inc

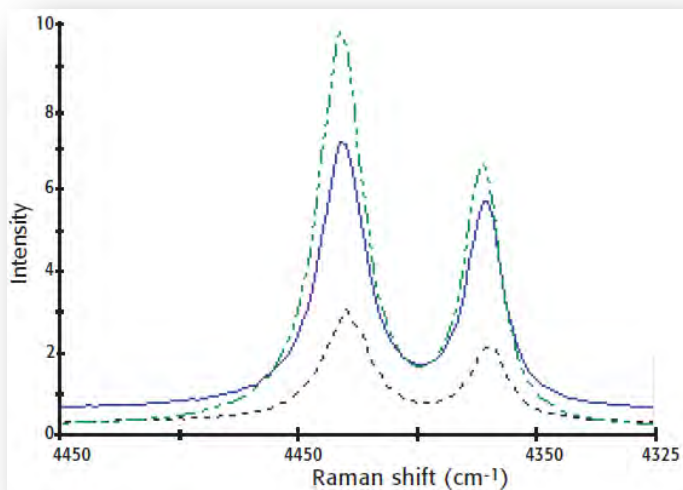


Figure 5 Three rubies: maternal stone (dot/dash), paternal stone (solid), and ruby ring (dashed). All have the same characteristic ruby peaks.

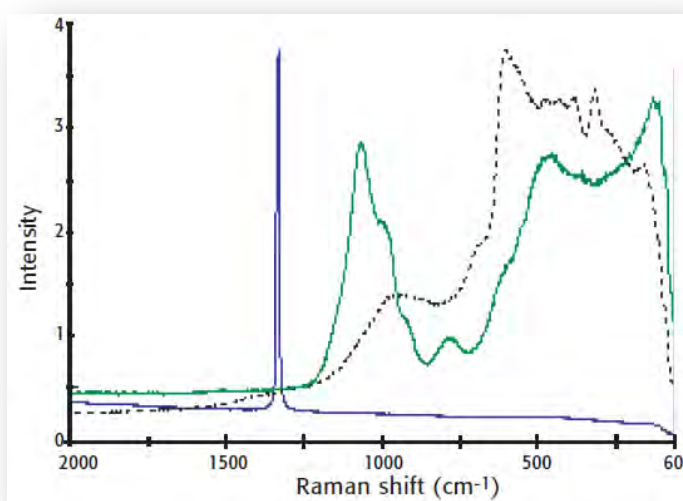


Figure 6 The 1332 cm^{-1} diamond Raman band (bottom) is clearly distinguishable from the luminescence of the glass imposters (top solid and dashed).

Tale of Two Rubies. We examined two large blue–purple gemstones mounted in separate rings. The amethyst from the first ring was a large teardrop shape and mounted in 14- karat yellow gold. It was purchased at an antiques store in rural Maryland and had been appraised independently twice by two separate lapidaries as amethyst. The stone from the second ring was a large round stone with the same blue–purple color mounted in 18-karat rose gold.

It was purchased in Egypt and was sold as alexandrite. This ring also was appraised due to the rarity of the alexandrite. This stone was determined to be amethyst. This seemed reasonable because the other ring with the similar stone was also appraised as amethyst. Raman analysis of both stones provided an interesting discovery. Neither stone had the characteristic amethyst Raman bands; however both stones did display the strong bands at 4392 and 4360 cm^{-1} , characteristic of ruby. Comparison of the spectra of these stones versus that of a known ruby, proved that these two amethysts were indeed rubies despite their purple coloring (Figure 5). In this instance three separate lapidaries gave three incorrect appraisals of the stones. We also evaluated two synthetic rubies and found them to be indistinguishable from their natural counterparts. Throughout history, ruby has been considered the most prized of red gemstones and is considered to be the medium-to-dark orangey red to purplish red variety of corundum, a mineral composed of aluminum oxide (Al_2O_3) (20). Colored metal ion impurities create the gemstone color, such as Cr^{3+} -ruby, and $\text{Fe}^{2/3}$, Ti^{4+} -sapphire (12). The sapphires that we evaluated had spectra virtually indistinguishable from the ruby (11).

Diamonds. Diamond has been prized for centuries as a gemstone of exceptional brilliance and for its range of exceptional chemical properties. When compared with almost any other material, diamond is almost always the most valuable. As well as being the hardest known material, it is also the least compressible, the stiffest, the best thermal conductor with an extremely low thermal expansion, chemically inert to most acids and alkalis, and transparent from the deep UV through the visible to the far infrared, and it is one of the few materials known with a negative electron affinity (or work function) (22). All natural diamonds are flawed, often by color or impurities. Most diamonds have some yellow or brown color. Defects mark the diamond as unique. Color centers in diamond photoluminesce when excited by laser light. A Raman spectrometer used to measure photoluminescence is a powerful characterization tool to identify artificially reprocessed, so-called exotic colored diamonds.

Gemstone Identification using Raman Spectroscopy

Amanda L. Jenkins and Richard A. Larsen Jasco, Inc

The diamond grading system is as follows: D and F are colorless, G through J are near colorless, K through M are faint yellow or brown, N through Z are light yellow, brown or grey, and Z is fancy yellow or brown. Cubic zirconia is now one of the most common substitutes for diamond. The original manufacturing process was developed in Russia and now is performed all over the world. Cubic zirconia can be manufactured in several different colors due to the addition of other minerals, but only the clear white is preferred as a substitute for diamond. With a distinctly different Raman spectrum, cubic zirconia gemstones can be distinguished easily from diamond. Common glass also is a cheap substitute for diamond. Glass is distinguished easily from the diamond in the Raman spectra because glass has a large photoluminescence. Diamond is characterized readily by a sharp Raman band at 1332 cm^{-1} (Figure 6).

Conclusions

Raman spectroscopy has been demonstrated as an ideal method for the analysis of gemstones, both real and fake. With the ability to examine both loose and mounted stones of any size or configuration, Raman can be used to rapidly distinguish various gemstones that do not readily lend themselves to identification by other, more traditional gemological identification methods. Raman spectra also can provide a unique fingerprint of the gemstone with the ability to distinguish any future alteration of the gemstone. The photoluminescence of colored diamonds offers a method for the determination of the color of diamonds and provide a further discrimination of the diamond color scale.

References

1. www.trappgem.com
2. http://www.attawaygems.com/NMFG/causes_of_color.html
3. Richard T. Liddicoat, *Handbook of Gem Identification* (The Gemological Institute of America, Los Angeles, 1951).
4. Robert M. Shipley, *Dictionary of Gems and Gemology* (The Gemological Institute of America, Los Angeles, 1948).
5. <http://www.jewelrystore.com/stones/>
6. <http://www.emporia.edu/earthsci/amber/go340/treat.htm>
7. <http://www.professionaljeweler.com/archives/articles/1998/jun98/0698gg1.html>
8. http://www.palagems.com/quality_4cs.htm
9. <http://www.gemshopper.com/fraud.html>
10. <http://www.trappgem.com/instruments.html>
11. <http://www.fis.unipr.it/~bersani/raman/raman/spettri.htm>
12. N.N. Greenwood and A. Earnshaw, *Chemistry of the Elements* (Pergamon Press, New York, 1989).
13. <http://minerals.gps.caltech.edu/data>
14. Charles W. Chesterman, *Field Guide to Rocks and Minerals* (published for the National Audubon Society by Alfred A. Knopf, New York, 1979).
15. <http://www.mindat.org/min-1651.html>
16. http://www.aist.go.jp/RIODB/rasmin/E_index.htm, Ceramics Institute, AIST, JAPAN
17. <http://www.gemstone.org/gem-bygem/english/tanzanite.html>
18. <http://www.jewelryexpert.com/articles/Tanzanite-Article.htm>
19. <http://www.diamonds-gemstones-jewelry.com/emerald-grading/imitationemeralds.aspx>
20. <http://www.egemstonesjewelry.com/data>
21. <http://cwjewelers.com/stonetanz.htm>
22. <http://www.bris.ac.uk/Depts/Chemistry/MOTM/diamond/diamond.htm>

Amanda L. Jenkins is a senior applications specialist at Jasco, Inc. (Easton, MD). E-mail: Jenkins@jascoinc.com.

Richard A. Larsen is an applications chemist at Jasco.

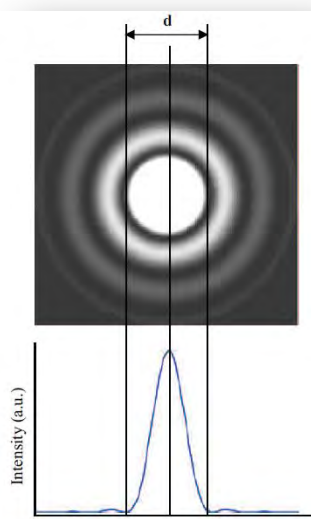
Spatial Resolution and DSF in Micro Raman Spectrometer

Raman micro-spectroscopy has been widely used due to the ability to provide rapid and non-destructive measurements of micron sized samples. Also, Raman spectroscopy can provide similar information as compared to FT-IR micro-spectroscopy offering enhanced capabilities for the analytical laboratory. A primary advantage of Raman micro-spectroscopy is better spatial resolution as compared to FT-IR microspectroscopy. Comparatively, the minimum spatial resolution for FT-IR measurements is about 10 μm , while Raman can easily achieve a spatial resolution of 1 μm .

In this note, the spatial resolution of micro Raman spectroscopy, its general definition, and evaluation methods will be described as well as an explanation of the Dual Spatial Filtration (DSF) system that is a standard feature of the JASCO NRS-5000/7000 series micro-Raman spectrometers.

Definition of Spatial Resolution

A laser, of a specific wavelength, is used as the excitation source for Raman micro-spectroscopy. As the laser beam spot size on the sample is reduced, the spatial resolution on the XY plane becomes higher. When light having a constant intensity distribution is introduced into an objective lens, the diffraction pattern shown as Figure 1 appears. The bright center area is called the 'Airy-disk' and, its size "d" can be determined by the wavelength "l" and the numerical aperture "N.A." (equation 1). The "d" term refers to the diffraction limit that determines the spatial resolution of an optical microscope.



$$d = 1.22\lambda / \text{N.A.} \text{ (equation 1)}$$

(λ : wavelength, N.A.: numerical aperture of objective lens)

Figure 1 Airy-disk resulting from diffraction with a circular aperture

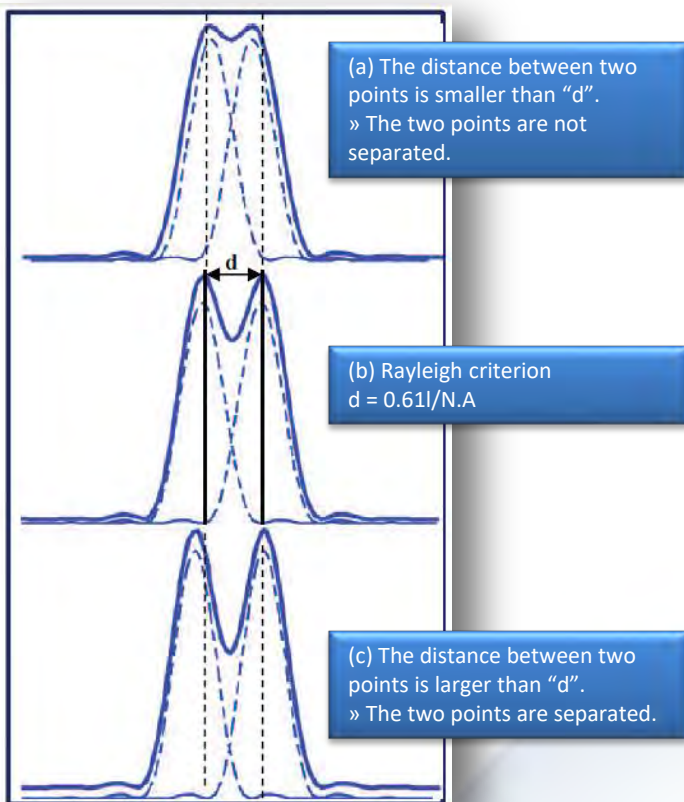


Figure 2 Spatial resolution defined by the Rayleigh criterion

On an XY plane, the definition of spatial resolution is based on the distance between two points close to each other, the 'Rayleigh criterion'. In the standard configuration of the JASCO NRS-5000/7000 (532 nm laser, the 100X objective lens with a N.A. = 0.90), the laser spot size at the diffraction limit is calculated as " d " = 720 nm and the spatial resolution according to the Rayleigh criterion is then equal to 360 nm. As equation 1 suggests, if the laser wavelength is getting shorter (lower wavelength), the spatial resolution then becomes higher. Also, if an objective lens such as an oil-immersed lens having a larger N.A. is used, one can expect a comparative increase in the spatial resolution. However, the definition based on FWHM (full width at half maximum) of the intensity of the interference ring has also been recognized. Therefore, in the comparison of spatial resolution for the Raman micro-spectrometers prepared by different manufacturers, the definition of 'spatial resolution' which has been applied should be confirmed. For the NRS-5000/7000 series, each of the values calculated from the two different definitions is shown in Table 1.

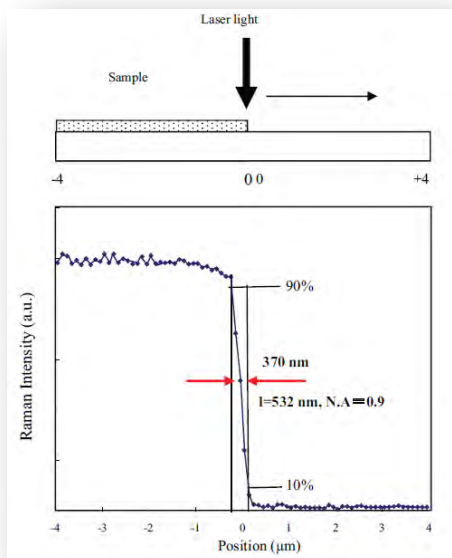
Spatial Resolution and DSF in Micro Raman Spectrometer

Table 1 Spatial resolution on an XY plane measurement

	Equation	532 nm, N.A= 0.90 configuration	355 nm, N.A=1.4 configuration
Rayleigh criterion	$0.61\lambda/N.A$	360 nm	154 nm
FWHM	$0.51\lambda/N.A$	301 nm	129 nm

Evaluation of Spatial Resolution in Confocal Optics

Theoretically, one can calculate the spatial resolution for confocal optics as shown in Table 1, however, the actual value for optical microscopes may become larger due to lens aberrations, the intensity distribution of the incident laser light to the objective lens, etc. The actual spatial resolution can be evaluated by measuring the distance for the Raman intensity profile when it changes from 10 % to 90% by the measurement of a sample having a sharp edge as illustrated in Figure 3. This evaluation method was applied to the NRS-5000/7000 series instruments with the standard configuration of a 532 nm laser and an objective lens of N.A. = 0.9, resulting in a very close value of 370 nm compared to the theoretical value of 360 nm, as calculated according to Table 1.


Figure 3

Measured spatial resolution in NRS-5000/7000 (532 nm laser , objective lens 100x)
(upper – illustration for measurement of silicon sharp edge; lower – Raman intensity profile of silicon peak)

Resolution in Depth in Confocal Optics

In a confocal optical system, a pin hole aperture is located at a reciprocal focal point of the optical system. Therefore, light rays coming from points other than the focus of the objective lens are eliminated. The depth resolution (Z resolution) “dz” can be determined by the excitation wavelength “λ”, the refractive index “n” of the substrate and the numerical aperture “N.A.” of the objective lens (equation 2).

$$dz = \frac{0.88 * \lambda}{n - \sqrt{n^2 - NA^2}} \quad (\text{equation 2})$$

Inserting the values of “λ”=532nm, “n” =1 (atmosphere) and N.A.=0.90, a calculated “dz” of 830 nm is obtained. The actual depth resolution can again be estimated by measuring the FWHM of the Raman intensity profile for a silicon crystal when it is scanned in the Z direction. In a standard confocal optical system, available with most of the commercially available micro Raman spectrometers, a 1.5 to 2.0 μm of FWHM is expected. In the NRS-5000/7000, a FWHM of 1 μm can be expected that is much closer to the theoretical value as shown in Figure 4. This number can be achieved by the use of an improved confocal aperture optimized for Raman spectroscopy.

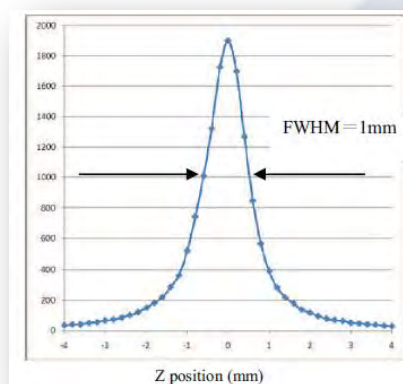
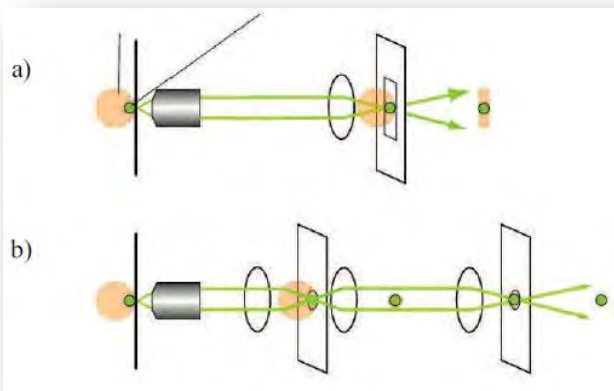


Figure 4 Raman intensity profile of silicon in Z depth profiling (532 nm laser, objective lens 100x, N.A=0.9)

Dual Spatial Filtration(DSF)

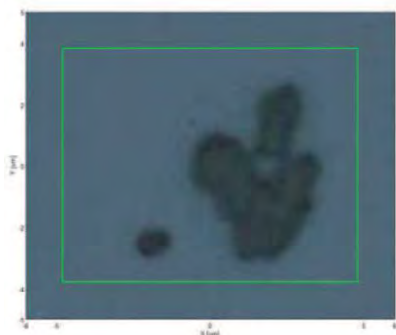
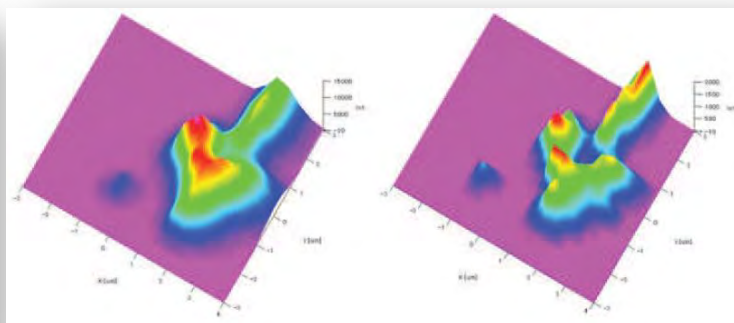
The standard Dual Spatial Filtration (DSF) optical system in the NRS-5000/7000 instruments has a dual aperture system for confocal optics. Therefore, the DSF system can eliminate any stray light that was not removed using the first aperture. The DSF method can improve the Z resolution and at the same time, one can expect an improvement of the spatial resolution for the XY plane.

Spatial Resolution and DSF in Micro Raman Spectrometer


Figure 5

- (a) standard confocal optics with pinhole aperture
(b) JASCO DSF confocal optics

The standard single aperture system ('a' of Figure 5) and the JASCO DSF optics ('b' of Figure 5) were applied to the measurement of oxidized titanium (TiO₂) particles on a silicon substrate. The Raman imaging of the peak intensity profile for both results are shown in Figure 7. As seen in the figure, the spatial resolution in the XY plane was improved by use of the DSF optics (right image in Figure 7) and, the image intensity profile was closer to the microscope image of the sample (Figure 6)


Figure 6 Microscope image of a TiO₂ particle on a silicon substrate

Figure 7 Raman imaging of a TiO₂ particle on a silicon substrate (Intensity profile of the TiO₂ peak height) (left; by ordinary confocal system ('a' of Figure 5), right; the JASCO DSF system ('b' of Figure 5))

Also, the single aperture confocal system and the DSF system were applied to the non-destructive Z scan of a polyvinylalcohol (PVA) layer of a polarizer film to observe the change of the Raman peak intensity of an iodide compound (25 μm thickness) that is sandwiched in the PVA layers. (Figure 8) Theoretically, the intensity of the iodide compound peak will rapidly increase when reaching the iodide compound layer then, rapidly decrease when again reaching the PVA layer as shown in the blue dashed line in the Raman intensity profile displayed as Figure 8. The results demonstrate that the profile by the DSF optics (solid red line in Figure 8) is closer to the theoretical profile than the standard confocal system (solid green line in Figure 8). These results clearly indicate that the DSF optical system can greatly improve the Z resolution of the confocal optical system.

Conclusion

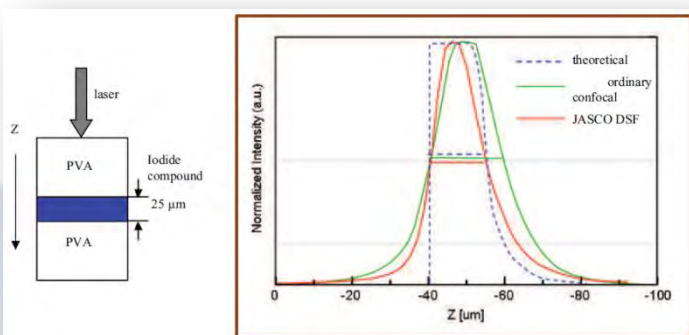
As outlined above, the NRS-5000/7000 offers a high spatial resolution close to the theoretical diffraction limit. Also, the maximum performance in the confocal optical system can be realized by use of the DSF optical system. If high spatial resolution is not required for specific experiments, the larger pin hole aperture can be used such that better energy throughput can be obtained for better S/N results.

NOTE

The measurement position in the Z scan becomes shallower (thinner) than the actual sample position (thickness) due to the influence from the refractive index of the substrate. In the case of a 25 μm thickness of the iodide compound layer, the apparent thickness will be approximately 15.3 μm when the refractive index is 1.64. In the NRS-5000/7000, a [Refractive Index Correction] function is available in the mapping data analysis program so that a correction for the difference between the true and measured values can be performed.

Reference

- 1) T. Wilson and C. J. R. Sheppard: Theory and Practice of Scanning Optical Microscopy, Academic Press (1984)
- 2) G. Kino: Confocal Scanning Optical Microscopy and Related Imaging Systems, Academic Press (1996)
- 3) Confocal Laser Scanning Microscopy Principles: ZEISS
- 4) H. Kubota: Hado-Kougaku (written in Japanese) (1971)
- 5) Neil J. Everall, Applied Spectroscopy, Vol. 54, Issue 6, pp. 773-782 (2000)


Figure 8 Z scan profile of polarizer film (PVA) (left: cross section of multi-layer; right: peak intensity profile of an iodide compound)

Rapid measurement of sample in container using macro measurement unit

Introduction

Laser Raman spectroscopy is a method which enables to obtain the information on molecular structure as well as IR spectroscopy, but by adopting a confocal optical system, it is possible to selectively acquire information on only the part where the laser was focused. With this system, non-destructive and noncontact measurement without sample pre-treatment can be performed, and imaging measurement in the depth direction in a minute area becomes possible. The confocal optical system is also effective in macroscopic measurements. It is also applied for measuring bulk sample in a container such as a bottle without taking it out. We developed a macro measurement unit (figure 1) as an accessory for such measurements. The macro measurement unit has an L-shaped structure with a condenser lens at the tip of the lateral direction. In measurement, users can use the unit easily by just attaching the unit to the revolver in the same procedure as the objective lens.

In this application note, rapid measurement of the liquid/solid samples in the bottle without opening the bottle were performed by using the macro measurement unit.

Comparison with the conventional method

In liquid measurement, a method which requires to remove a sample from a container such as dropping a sample onto a plate or introducing it into a capillary tube has been widely used. Therefore, it was difficult to measure volatile samples and anaerobic samples. Meanwhile, since the macro measuring unit emits the laser beam in the sideways direction, the sample can be measured as with the container in an upright position and without opening. In addition, since the unit has condenser lens at the tip of the L-shaped lateral direction, even a powdery solid sample in a bottle can be measured by focusing on the surface.

As mentioned above, by using the macro measurement unit, it is possible to analyse solid and liquid sample in a non-open, non-contact and rapid manner. Additionally, because the unit is installed in the sample chamber of Raman spectrometer compatible with laser safety standard Class 1, anyone can use this system with confidence without taking countermeasures such as laser exposure.

System configuration

- NRS-4500-532 Raman Spectrometer
- 532nm Laser power upgrade (100mW)
- RMC-457-115 Macro measurement unit

* 100 mW laser was used in this application note, but a similar measurement can be performed by adjusting the exposure time even with a standard 20 mW laser.

* Depending on the cells and samples, optional lasers may be required.

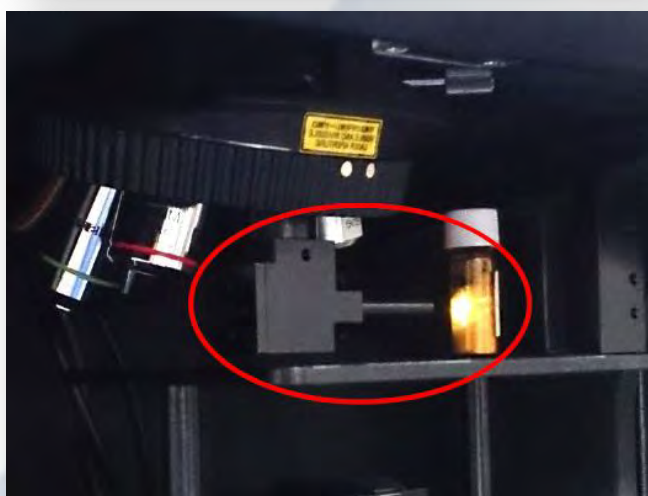
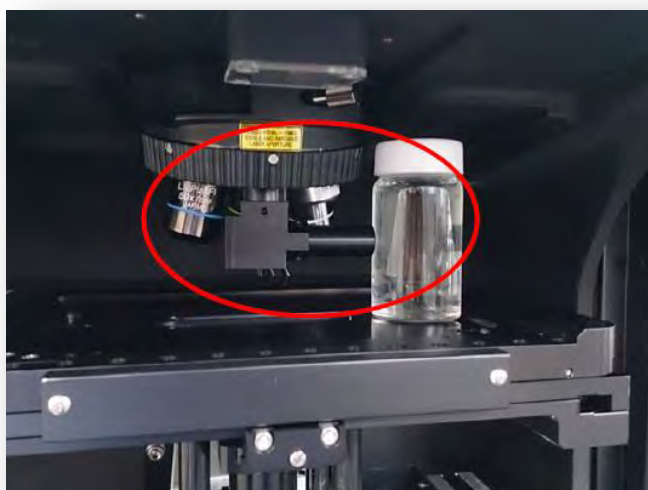


Figure 1 - Macro measurement unit and sample installation image (Up: Liquid, Down: Solid)

Rapid measurement of sample in container using macro measurement unit

Sample measurement

The colorless transparent liquid in a commercially available sample bottle and the white solid in a brown bottle were measured without taking out from the bottle as shown in figure 1. The database search results of the obtained spectra were shown in figures 2 and 3.

The liquid was identified as ethanol (figure 2). The solid sample was able to measure over the bottle without opening the lid, just by set the sample bottle close to the unit. In addition, high quality spectrum was acquired with only two seconds of the exposure time.

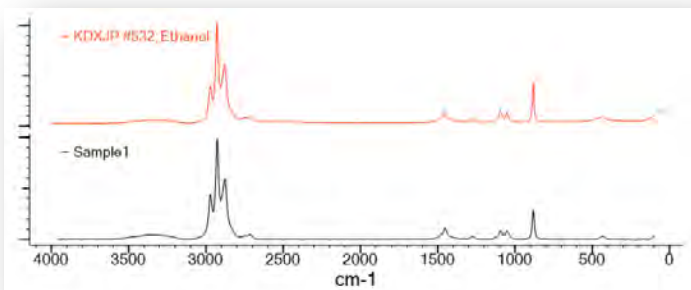


Figure 2 - The result of non-opening measurement of liquid sample by using macro measurement unit
(Top: Database, Bottom: Measurement result)

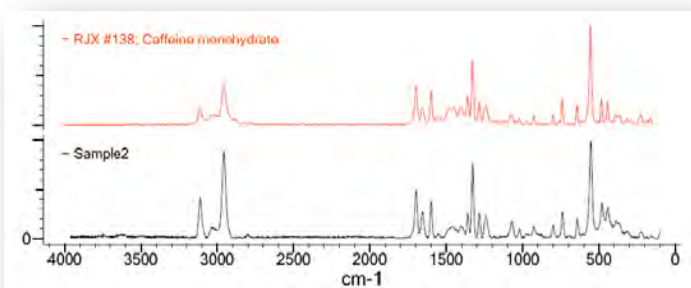


Figure 3 - The result of non-opening measurement of solid sample in a brown bottle by using macro measurement unit
(Top: Database, Bottom: Measurement result)

Conclusion

As described above, using the revolver-installed macro measurement unit, it is possible to measure the bulk sample quickly and easily. In addition, it is considered that this system is useful for the measurement of samples that can not be measured in open system such as hazardous materials, and for analysis of solution components.

Moreover, our software is equipped with easy-to-use functions for routine measurements like quality control, such as a function to support measurement condition setting in wizard format (see more detail: Raman Application data 260-AN-0011) and a function to compare the degree of coincidence with already measured spectrum in real time.

A synergistic effect of software and hardware will enable more efficient analysis.

Upgrade of simple coumarin analysis system to high sensitivity one

In order to prevent from producing illegal light diesel oil which contains kerosene or heavy oil, 1 ppm of coumarin is added in the related oils of the diesel (kerosene or A heavy oil) as discrimination label. The analysis procedures to determine mixing with the discrimination label and its mixing concentration are standardized by Advisory body in National Petroleum Dealers Association. Simple analysis using test tube and quantitative analysis using separating funnel are described in the instruction manual of the procedure. We have already introduced simple quantitative analysis system incorporating easy-to use simple analysis and accuracy of quantitative analysis with the preparation performed using test tube, detecting fluorescence intensity and judging concentration using spectrofluorometer. Usual coumarin determination purpose is to analyze quantitatively more than a couple of percent of the related oils, while there is another analysis case which needs to analyze quantitatively to less than 1 percent. We would like to introduce a system to upgrade the above simple analysis system to high sensitivity system with improved detection limit and quantitation limit drastically.

1. Measurement principle

Coumarin is hydrolyzed in alkaline solution and becomes Cis-O-hydroxycinnamic acid. In addition, the Cis-O-hydroxycinnamic acid is isomerized by ultraviolet radiation and becomes Trans-O-hydroxycinnamic acid. The Trans-O-hydroxycinnamic acid radiates green fluorescence (Ex 360 nm, Em 500 nm). In this quantitative analysis procedure, this green fluorescence is detected.

2. Measurement system

Filters on both EX and EM sides are used to reduce scattering light, enabling the analyzing system to assure high sensitivity measurement.

- FP-6300 Spectrofluorometer
- Test tube holder for coumarin measurement
- U330 filter (EX side), WG305 filter (EM side) *1)

3. Tools to be used

- Round-bottom screw cutting test tube (18 mm outer diameter x 160 mm length)
- Stirrer bar (3 mm diameter x 10 mm length)
- Shaker

4. Preparation of reagents

1) Alkaline solution reagents

Dissolve 10 g of sodium hydroxide and 20 g of sodium nitrate into Millipore water, and prepare 100 mL solution. The alkaline solution is kept in polyethylene vessel.

2) Alcohol solution

Mix 40 mL of 1-butanol and 30 mL of ethanol in this proportions.

3) Undiluted coumarin solution [1000 ppm]

Dissolve 100 mg of the coumarin into aromatic solvent (such as n-propyl benzene).

4) Standard coumarin solution [0.1 ppm]

Dilute 100 μ L of the undiluted coumarin solution using n-dodecane (1 ppm). Take 100 μ L of the 1 ppm coumarin solution, and dilute it using the n-dodecane and prepare 100 mL solution.

5) Standard sample

Mix each of solutions in accordance with the following ratio.

Concentration of additive [%]	Standard coumarin solution [0.1 ppm] (mL)	n-Dodecane (mL)	Alkaline solution (mL)	Alcohol solution (mL)
0%	0	4.2	3	4.8
1%	0.06	4.14	3	4.8
2%	0.12	4.08	3	4.8
4%	0.24	3.96	3	4.8
6%	0.36	3.84	3	4.8
8%	0.48	3.72	3	4.8
10%	0.96	3.24	3	4.8

Table 1

Mixing ratio of standard solution



Figure 1

Hydrolysis and photoisomerization of coumarin

Upgrade of simple coumarin analysis system to high sensitivity one

5. Measurement procedure

Prepare test tubes containing standard samples which were prepared in the [4. Preparation of reagents 5) Standard sample]. Shake these test tubes to hydrolyze coumarin in the test samples, and the coumarin is extracted in the alkaline solution. Then, perform photoisomerization reaction by radiating excitation light (360 nm) of spectrofluorometer on the alkaline solution, and detect fluorescence intensity at 500 nm and generate calibration curve.

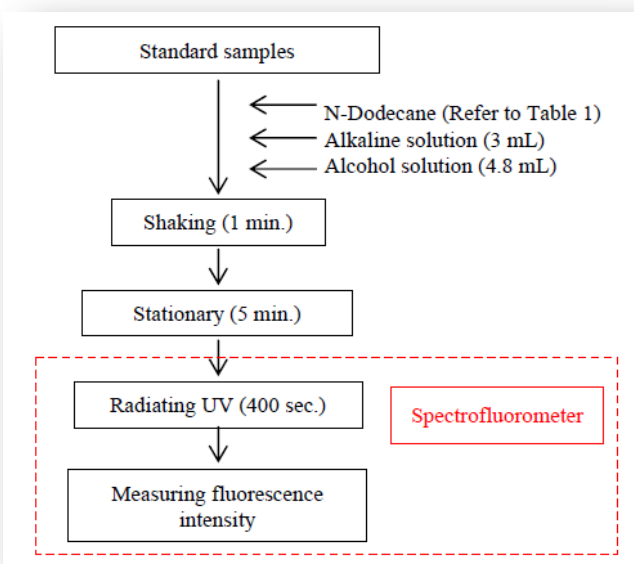


Figure 2 Flow chart of analysis procedure

- 1) Put each of standard samples into test tubes ^{*1)}.
- 2) Add n-dodecane (refer to Table 1), 3 mL of alkaline solution and 4.8 mL of alcohol solution.
- 3) Put stoppers on the test tubes, and shake 1 minute using shaker to hydrolyze coumarin and extract to alkaline solution.
- 4) Keep stationary for 5 minutes after the shaking. By keeping stationary, the above extracted solutions are separated as lower layer of alkaline solution, middle layer of alcohol solution and upper layer of diesel oil.
- 5) After keeping stationary for 5 minutes, put a stirrer into test tube and set it to test tube holder for spectrofluorometer. Radiate UV light (360 nm) on the alkaline solution layer for 400 seconds with rotating the stirrer, for photoisomerization reaction. Stop rotating the stirrer and read fluorescence intensity with EX 360 nm, EM 500 nm and generate calibration curve.

*1) Regarding low concentration coumarin measurement, it is necessary to wash thoroughly those test tool such as test tube.

6. Measurement condition

After monitoring the process of photoisomerization by using [Time course measurement] program, the spectra were measured using [Spectrum measurement] program and fluorescence intensity was detected at Em wavelength = 500 nm.

Time course measurement	
Ex bandwidth ^{*2)}	20 nm
Em bandwidth	10 nm
Response	2 sec
Sensitivity	High
Measurement range	0 - 400 sec
Data acquisition interval	2 sec
Ex wavelength	360 nm
Em wavelength	500 nm

Spectrum measurement	
Ex bandwidth	10 nm
Em bandwidth	10 nm
Response	Fast
Sensitivity	High
Measurement range	380 - 650 sec
Data acquisition interval	1 nm
Ex wavelength	360 nm
Scan speed	1000 nm/min

*2) Ex bandwidth was set at 20 nm to perform photoisomerization effectively for the Time course measurement. Ex bandwidth was set at 10 nm for the Spectrum measurement in order to suppress reduction of fluorescence intensity due to photolysis.

Upgrade of simple coumarin analysis system to high sensitivity one

7. Calibration curve

Time course measurement data and spectral measurement data of standard samples with additive materials concentration of 0 ~ 10 % are shown in the Figure 3 and 4. From the Figure 3, it is observed that photoisomerization finished in 150 seconds from starting UV light radiation.

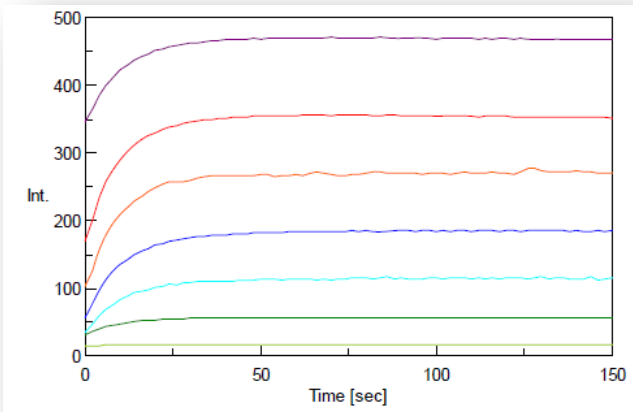


Figure 3 Photoisomerization situation

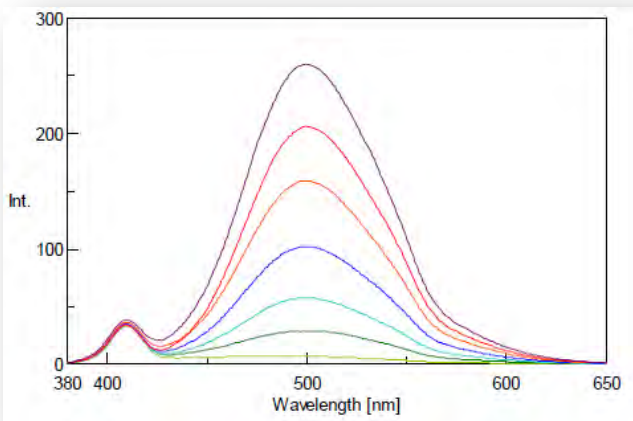


Figure 4 Spectra after finishing photoisomerization

Calibration curve plotting fluorescence intensity at spectrum peak wavelength of 500 nm with additive material concentration is shown in Figure 5. 0.9993 of correlation coefficient for the calibration curve was obtained, showing good linearity.

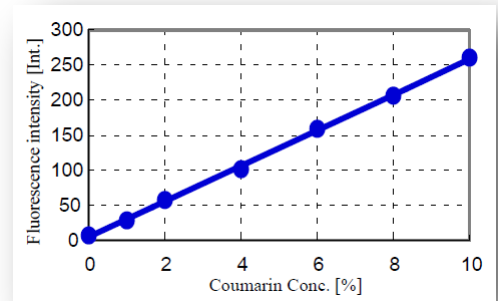


Figure 5 Calibration curve

Additive conc. [%]	Fluorescence intensity
0	6.7077
1	28.7548
2	57.3873
4	101.829
6	158.903
8	205.882
10	260.236

Calibration curve information

$$y = 25.367x + 4.7604$$

$$R^2 = 0.9993$$

The measurement using 0% and 1 % concentration standard solution was repeated 5 times, and standard deviation for fluorescence intensity was 0.4357 and standard deviation for coumarin concentration was 0.0172. Considering such results, it is possible to perform analysis with 0.06% detection limit and 0.2 % quantitation limit. *3)

*3) Detection limit was calculated by 3 sigma and quantitation limit was calculated by 10 sigma.

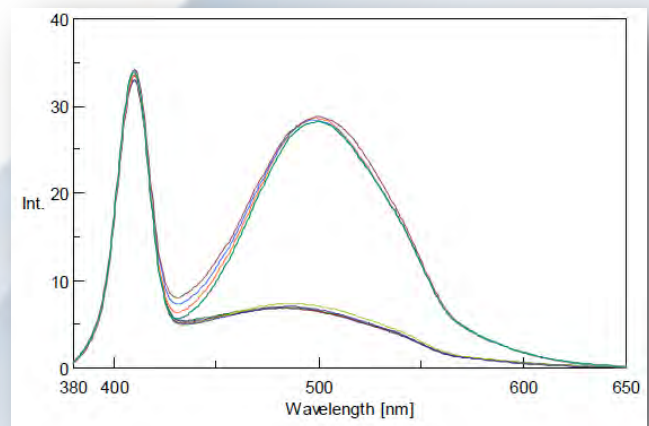


Figure 6 Spectra of conc. 0 and 1 % coumarin solution (5 spectra each)

Fluorescence Detection of Counterfeit US Currency

Each year, significantly more money is stolen with a pen than with a gun. Much of the fraud is due to counterfeiting since the current technology available for personal computers, scanners, and color copiers have attained the capability to accurately reproduce paper currency. Counterfeit currency costs governments and businesses billions of dollars a year. During fiscal year 1997 alone, a total of \$136,205,241 in counterfeit U.S. currency appeared worldwide. This application demonstrates how a simple fluorescence instrument can be used to verify the identity of currency through the presence of the security thread and the background fluorescence of the bill. This fluorescence intensity can also be used to study the aging and manufacturing reproducibility of currency.

Introduction

United States currency is the most counterfeited currency in the world with Canadian money a close second, these currencies popular due to their status as a 'hard' currency, similar to gold. Large numbers of bills in all denominations are counterfeited and passed (given as payment) to unsuspecting merchants and banking institutions. In the past, only large denominations like the \$100 and \$50 bill were counterfeited. Currently, however, numerous businesses report the receipt of counterfeit \$5, \$10, and \$20 notes with the \$20 note being passed with the highest frequency. One of the most common types of counterfeit detection is provided by ultraviolet (UV) light. The operating principle is simple; if the bill being checked has fluorescence then it is genuine. The idea behind this is that the paper used in the printing of real currency has a high starch content making it appear dull under UV light. Counterfeiters generally use bond paper that has virtually no starch and is bleached. The bleached bond paper fluoresces under UV light. The characteristic background fluorescence of all the US currency studied is shown in Figure 1. UV detection of counterfeit currency has been in use since approximately 1976, and has been fairly effective. Recently, a new security measure, the security thread, has been implemented to prevent counterfeiters from passing off a bill as one of a higher denomination.

A security thread is a thin thread or ribbon running through a bank note substrate. The thread in U.S. currency has printing and on the new \$50 note, micro-printing and graphics. The thread in the new notes glows when held under an ultraviolet light. In the \$100 note will glow pink, and in the \$50 note it glows yellow. In addition, it is visible in transmitted light, but not in reflected light.

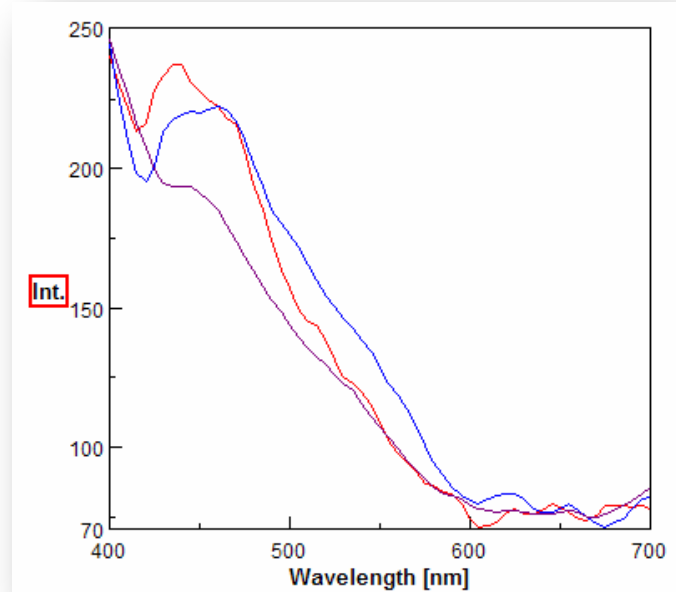


Figure 1 Scan of the background fluorescence of US, Japanese, and Canadian currency. All these monies have a similar background.

These security threads make it difficult to copy currency with a commercial color copier. Using a unique thread position for each denomination starting with the \$100 note prevents certain counterfeit techniques, such as bleaching ink off a lower denomination and using the paper to "reprint" the bill as a higher value note. Table 1 designates the color of the emitted fluorescence of the security threads.

Denomination	Fluorescence of Security Thread
\$100	Pink/Orange
\$50	Yellow
\$20	Green
\$10	Red
\$5	Blue

Table 1 Security threads in US Currency

Fluorescence Detection of Counterfeit US Currency

Experimental

A Jasco FP6200 fluorescence spectrophotometer equipped with a solid sample holder accessory was used for all analyses. The solid sample holder is kinematically mounted in the instrument sample compartment to provide the proper orientation of the sample to the excitation and emission ports. Bills of denomination \$5, \$10, \$20 and \$100 were placed in the sample holder such that the security thread was exposed to the excitation beam. Emission scans of both sides of each bill were collected and several locations on the security thread for each bill were also examined. The background fluorescence of the bill was subtracted from each scan of the security thread. Figure 2 illustrates the JASCO solid sample holder.



Figure 2 Jasco solid sample holder with \$20.00 bill.

Spectra were collected from 400-565nm. Instrument parameters were as follows:

- Band width (Ex) 5 nm (Em) 5 nm
- Measurement range 400 - 600 nm
- Data pitch 1nm
- Excitation Wavelength 365.0 nm
- Scanning speed 125 nm/min.

Representative scans of the security threads are shown in Figure 3. The emission bands are wide and distinctly identify each bill. The fluorescence intensity of the security threads appeared to decrease with apparent use and handling of the bills, as newer bills displayed a stronger fluorescence intensity. The fluorescent threads examined in this study did not have uniform intensity along the length of the thread. This suggests that fluorescence could be used for quality control of the production of these security devices.

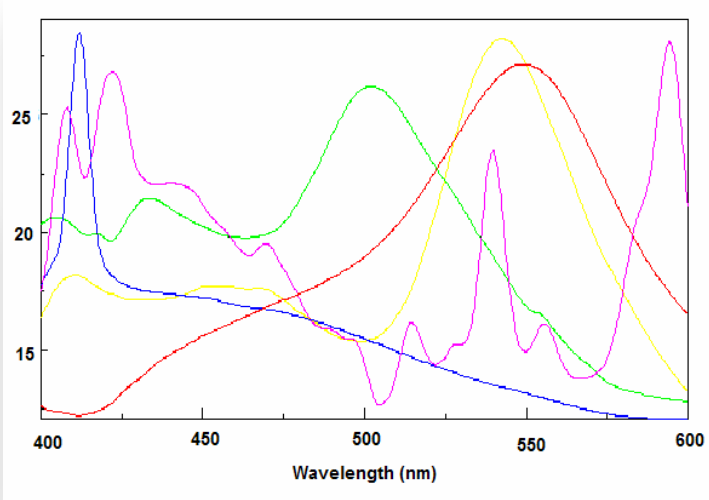


Figure 3 Spectral scans of the fluorescent strands in a 5, 10, 20, and 100 dollar bill

Conclusions

Simple fluorescence instrumentation can be used to evaluate the authenticity of U.S. currency. Using a fluorescence instrument as shown, the signal from the bill and its inherent security thread can be monitored to ensure currency validity and possibly provide a method for the examination of aging of a bill.

Absolute quantum yield measurement of solution using FP-8000 series

Introduction

Fluorescence quantum yield is defined as the ratio of the number of photons emitted from sample as fluorescence to the number of photons in the excited light absorbed. Absolute method and relative method are known as measuring methods. Relative method is comparing the intensity of standard fluorescence with unknown sample to calculate quantum yield of the unknown sample. Therefore obtained results depend on the accuracy of standard sample's quantum yield value. On the other hand, quantum yield can be obtained directly by the absolute method, because the absolute method allows to detect all the fluorescence from the sample and integrates using integrating sphere, enabling more accurate quantum yield measurement. In this experiment, some examples will be shown for the calculation of solution sample's quantum yield of which published values from literature are known by the absolute method.

Measuring system

- FP-8500 Spectrofluorometer*1)
- ILF-835 100mmF Integrating sphere unit
- 1 mm pathlength solution cell
- FWQE-880 Quantum yield calculation program

*1) Emission spectrum to which spectral correction is performed is required for quantum yield calculation. The spectra correction was performed using Rhodamine B on EX side, and was also performed on EM side using standard white plate for synchronous spectrum (250-450 nm) and ESC-842 (450-700 nm).

Samples

- 200 ppm Quinine sulfate (Solution: 1.0 N H₂SO₄)
- 15 ppm Fluorescein (Solvent: 0.1 N NaOH aq)
- 200 mg/mL tryptophan (Solvent: Ultra pure water)

Measuring method for absolute quantum yield

1) Measuring incident light

Confirm nothing is set on the sample cell holder in the integrating sphere, and measure spectrum of the incident light. Obtained peak area is defined as area from incident light, S₀ (equivalent number of photons in the incident light).

2) Measuring sample

Set the sample on the sample holder, and measure scattering and emission spectra of the sample. Obtained excitation wavelength peak area is defined as area scattered from sample, S₁ (equivalent number of photons which were not absorbed), and peak area in the emission wavelength range is defined as area emitted from sample, S₂.

3) Calculating quantum yield

Calculate in accordance with the following.

Sample absorption [%] = $(S_0 - S_1) / S_0 \times 100$

External quantum yield [%] = $S_2 / S_0 \times 100$

Internal quantum yield [%] = $S_2 / (S_0 - S_1) \times 100$

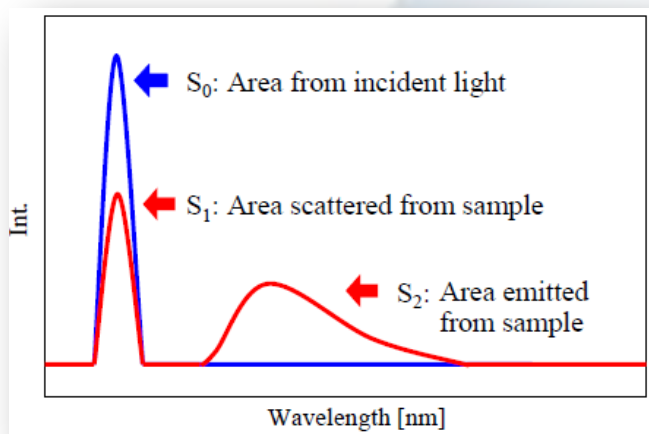


Figure 3 Image of S₀, S₁, S₂

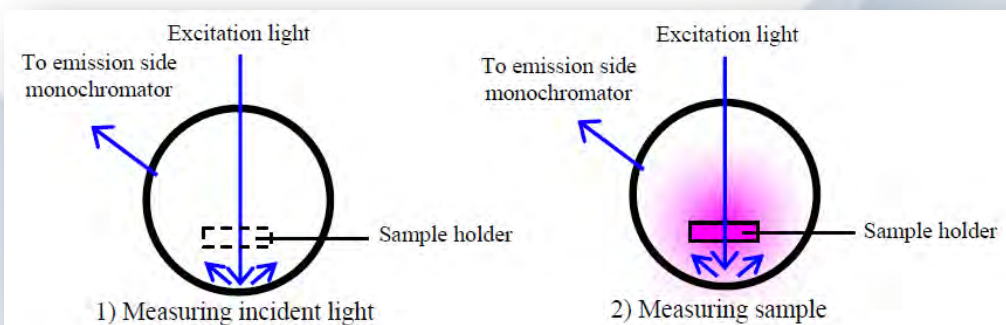


Figure 2 Diagram of integrating sphere for measuring incident light and measuring sample

Absolute quantum yield measurement of solution using FP-8000 series

Measurement results

Sample spectra measurement results are shown in the Figure 4 ~ 6.

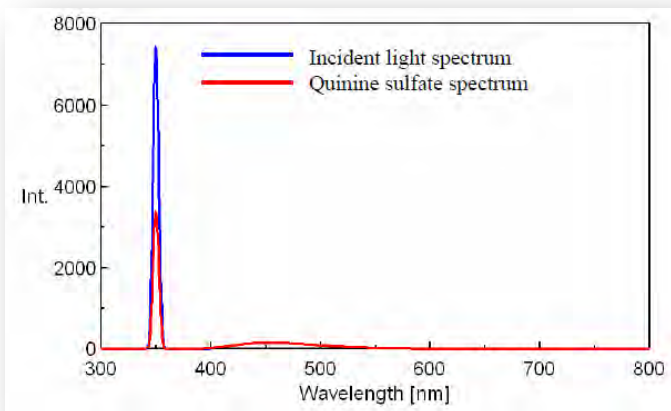


Figure 4 Emission spectrum of quinine sulfate

[Measurement condition]

- Mode: Emission
- Ex bandwidth: 5 nm
- Em bandwidth: 5 nm
- Ex wavelength: 350.0 nm
- Measurement range: 300 - 800 nm
- Scan speed: 200 nm/min
- Data interval: 0.1 nm
- Response: 0.5 sec
- PMT voltage: 350 V

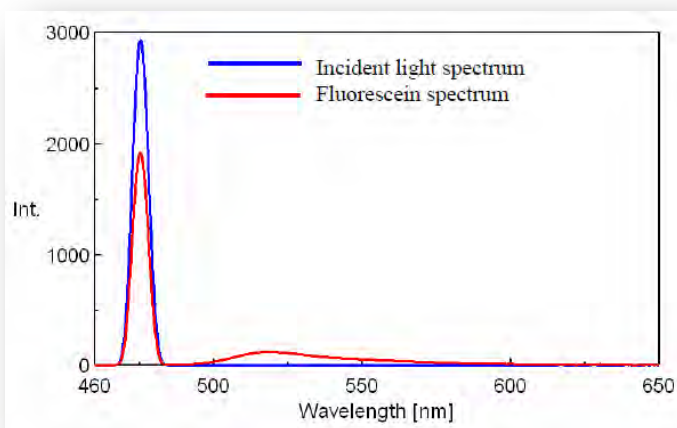


Figure 5 Emission spectrum of fluorescein

[Measurement condition]

- Mode: Emission
- Ex bandwidth: 5 nm
- Em bandwidth: 5 nm
- Ex wavelength: 475.0 nm
- Measurement range: 460 - 650 nm
- Scan speed: 200 nm/min
- Data interval: 0.1 nm
- Response: 0.5 sec
- PMT voltage: 250 V

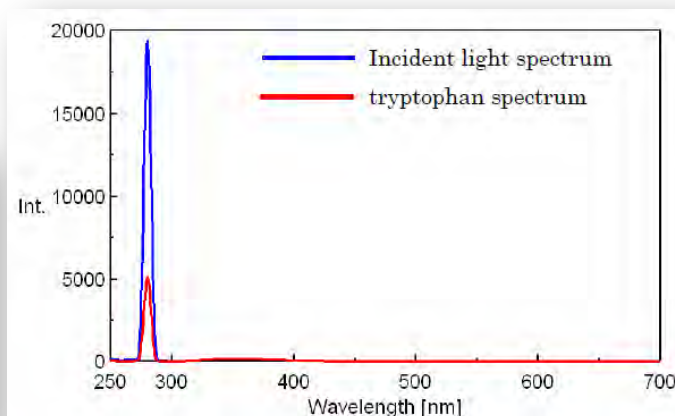


Figure 6 Emission spectrum of tryptophan

[Measurement condition]

- Mode: Emission
- Ex bandwidth: 5 nm
- Em bandwidth: 5 nm
- Ex wavelength: 280.0 nm
- Measurement range: 250 - 700 nm
- Scan speed: 200 nm/min
- Data interval: 0.1 nm
- Response: 0.5 sec
- PMT voltage: 400 V

Analysis results

Table 1 shows area from incident light (S0), area scattered from sample (S1), area emitted from sample (S2) calculated by each of sample's spectra and wavelength range. Calculation results of quantum yield using the values on the Table 1 and equations on the 3) are shown in the Table 2. Obtained results are within the range of published values from literatures for any samples.

Table 1 Detail of quantum yield calculation

	Area from incident light [S0]	Area scattered from [S1]	Area emitted from [S2]	Scattered WL Range [nm]	Emitted WL Range [nm]
Quinine sulfate	48267	22538	14304	320-365	365-750
Fluorescein	19174	12515	6116	465-485	485-630
Tryptophan	136135	35842	12101	270-290	290-550

Table 2 Calculation results of quantum yield

	Sample Absorbance	External quantum yield	Internal quantum yield	Internal quantum yield (published values)
Quinine sulfate	53.3%	29.6%	55.6%	50-57% ^{*2)}
Fluorescein	34.7%	31.9%	91.8%	85-92% ^{*2)}
Tryptophan	73.7%	8.9%	12.1%	12-14% ^{*3)}

*2) Literature: The Spectroscopical Society of Japan, (Japan Scientific Societies Press)

*3) Literature: Principles of fluorescence spectroscopy, Joseph R. Lakowicz, Springer

System evaluation of spectrofluorometer FP-8500 with optical fiber

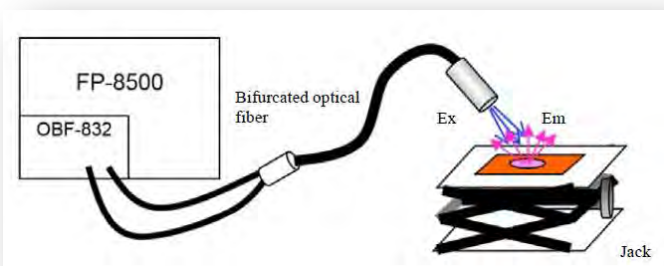
Introduction

By using OBF-832 optical fiber unit, it becomes easy to use an optical fiber as a fluorescence detection unit of the analyzer. With the use of the optical fiber, the measurement can be performed by just approaching a probe to a sample. It is possible to measure a sample which is larger than sample chamber, to trace in vivo reaction, to measure under the severe environment where people can not approach such as high/low temperature and high pressure.

In this application note, part of fluorescent samples were measured by using FP-8500 spectrofluorometer and OBF-832 optical fiber unit.

Measurement System and condition

- FP-8500 Spectrofluorometer
- OBF-832 Optical fiber unit
- Calibration Calibration light source / standard white plate
- Samples Red and Yellow referee cards



Sample measurement

Calibrated light source measurement under dark room condition

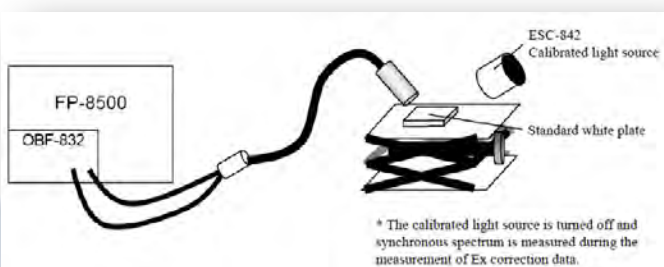


Figure 1 Measurement system

Measurement Condition

- Measurement mode: fluorescence
- Excitation bandwidth: 10 nm
- Emission bandwidth: 10 nm
- Excitation wavelength: 310 nm
- Measurement range: 400 - 800 nm
- Scan speed: 100 nm/min
- Data interval: 0.5 nm
- Response: 1 sec
- PMT voltage: 350 V (yellow card), 550 V (red card)

Measurement Results

Figure 2 and 3 show the measurement results. The profiles of each spectra measured with the optical fiber and with FLH-809 film holding block were consistent with each other. From the result, this system is effective in the case such as the measurement of a sample which is larger than sample chamber and the measurement under the severe environment.

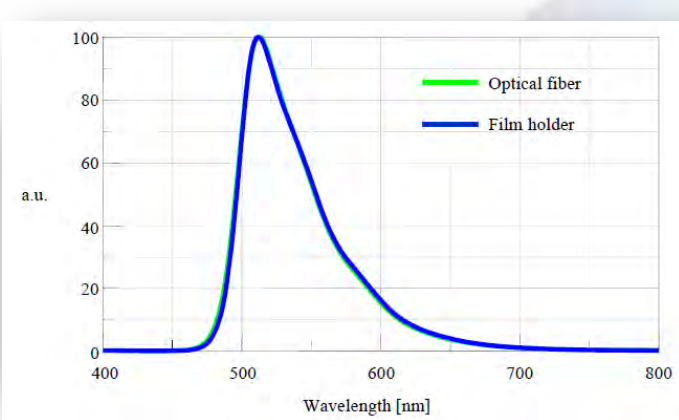


Figure 2 Peak normalized fluorescence spectrum of the yellow card

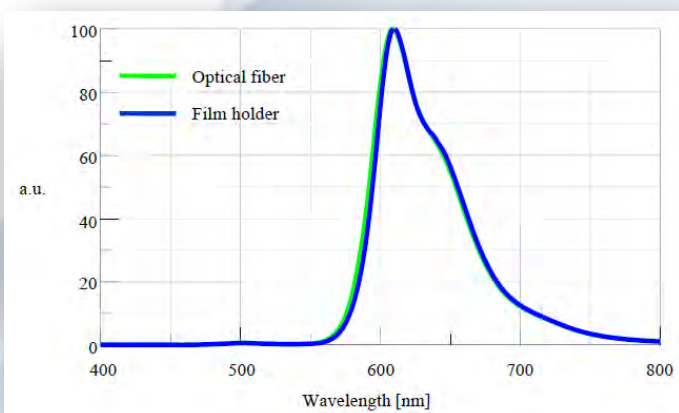


Figure 3 Peak normalized fluorescence spectrum of the red card

Automated Sun Protection Factor (SPF) Analysis of Sunscreen using UV-Vis

Dr. Amanda L Jenkins, and Dr. Richard A. Larsen, Jasco Inc.

The increasing awareness of the risks of skin cancer with sun exposure requires that sunscreen products be appropriately tested and labeled. The numerous possible sunscreen formulations demands that a rigorous analysis method be available.

Introduction

Sunscreens work by either reflecting or absorbing the ultraviolet (UV) radiation before it reaches the skin. The UV-A and UV-B region (400 - 290 nm) is the spectral region that must be blocked for effectiveness of the sunscreen. Whether organic or inorganic, the active ingredient that shields the skin from the sun must be present in sufficient quantity and uniformity to ensure skin protection. The traditional method for sunscreen analysis is based on a quantitative analysis of a diluted sample. A series of standards based on different concentrations of the active ingredient are measured and a quantitative method developed based on Beer's Law, $A = abc$. Where, A = the absorbance value of an analyte band; a = the absorptivity coefficient of the analyte band - a constant; b = the pathlength - generally considered a constant; and c = analyte concentration.

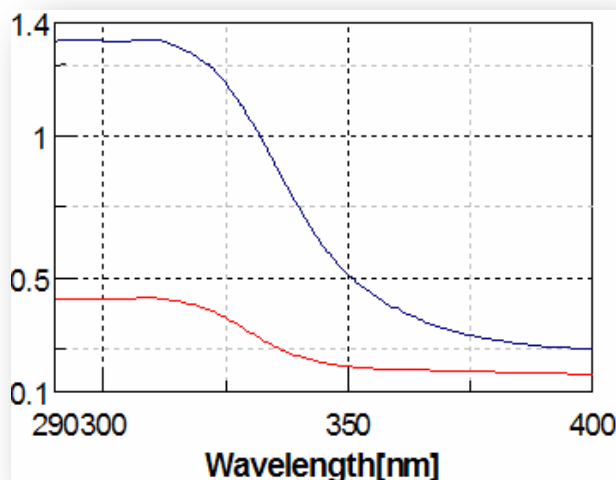


Figure 1 Sunscreen spectral scans

By contrast, the *in vitro* method developed by Diffey and Robson¹ uses a UV transparent substrate, 3M Transpore™ surgical tape, to examine the final sunscreen formulation.

No dilution and no standard preparation is necessary. Simply spread the sunscreen on the substrate, place the sample in the V-530 spectrophotometer and measure the spectrum.

Results and Discussion

Spectra of sunscreen formulations were collected over the spectral range 400 - 290 nm with a 0.5 nm data point resolution on a JASCO V-530 UV-Vis spectrophotometer. A fixed slit width of 2 nm was used with a 'Fast' detector speed and a scan speed of 400 nm/min. Sunscreen formulations were spread onto a 20 cm² piece of the 3M Transpore™ tape, the sunscreen covered substrate placed into the sample compartment and several spectra collected from different areas. Representative spectra of two different sunscreen formulations are presented as Figure 1.

product:	SPF 8 Trials				
company:	Sunscreen Maker, Inc.				
operator:	Working Everyday				
comments:	Latest Formulation				
wavelength [nm]	monochr. protective factor	measured transmittance	absorbance		
290	8.28	0.92	12.08		
295	8.37	0.92	11.95		
300	8.27	0.92	12.10		
305	8.28	0.92	12.11		
310	8.36	0.92	11.96		
315	7.89	0.90	12.60		
320	7.21	0.86	13.97		
325	6.13	0.79	16.31		
330	5.06	0.70	19.76		
335	4.39	0.64	22.78		
340	4.04	0.61	24.73		
345	3.73	0.58	26.37		
350	3.60	0.56	27.78		
355	3.44	0.54	29.05		
360	3.33	0.52	30.00		
365	3.17	0.50	31.69		
370	2.94	0.47	33.97		
375	2.76	0.44	36.18		
380	2.64	0.42	37.89		
385	2.41	0.38	41.47		
390	2.04	0.31	49.05		
395	1.72	0.24	57.99		
400	1.56	0.19	63.93		
				date (m/d/yr):	1/11/02
				UVA protection factor	3.5
				UVA / UVB ratio	0.69
				TOTAL UVA (320-400 nm AVG)	
				% released UVA radiation	23.10
				% shielded UVA radiation	66.90
				SHORT UVA (320-360 nm AVG)	
				% released UVA radiation	23.40
				% shielded UVA radiation	76.60
				SUNSCREEN PROTECTION FACTOR	7.1

An average sunscreen spectrum is calculated from the multiple sample spectra and the average submitted to a Windows Excel macro. The Excel macro calculates the SPF rating and other relevant data for the sunscreen sample (Figure 2) which is printed as a single page report. The results can be used during formula development or for quality control.

Conclusions

The Diffey Robson *in vitro* SPF calculation is a simple, rapid and universal analysis method for the determination of SPF values of sunscreens using either inorganic and organic screening components. The versatility of the JASCO V-530 spectrophotometer can accomplish the SPF calculation in addition to providing a full suite of UV-Vis analysis capabilities.

1.) B.L. Diffey, J. Robson, *J. Soc. Cosmet. Chem.*, 40, 127-133, 1989.

Countermeasure technique against heat island phenomenon - Evaluation of solar reflective paint material -

In recent years, solar reflective material attracts attention as one of remarkable countermeasure technique against heat island phenomenon and as sustainable household building material. These cutting edge sustainable materials have been evaluated by an independent organization as Environmental Technology Verification Project under Ministry of the Environment and its evaluation criterion is in process to be studied and to be established as standard regulation in JIS*. There is solar reflective paint material as sustainable material which has been approved by JIS (Japanese Industrial Standard) regulation. As shown in Fig.1, solar light has significant energy in near IR region. This solar reflective paint material has specific capability to reflect NIR region light of solar with higher efficiency than the other general paint materials. This capability reduces thermal energy on surface to penetrate into buildings, helping to improve an efficiency of air conditioner and contributes to saving energy.

In this Application Note, some example of evaluation about solar reflective paint material based on JIS K5602 is explained.

System configuration

V-670 UV/VIS/NIR Spectrometer
ISN-723 60 mm dia. Integrating sphere (UV/VIS/NIR)
Standard white plate for integrating sphere

Measurement/ Analysis programs

VWST-774 Solar/visible light measurement program
VWCD-790 Color diagnosis program



Figure 3 Integrating sphere unit

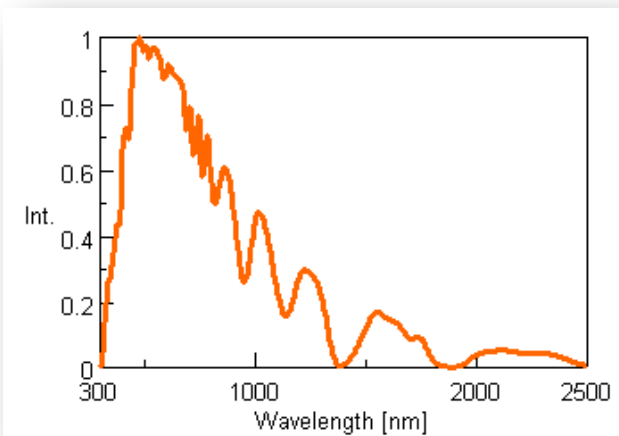


Figure 1 Standard solar intensity

Sample

Two aluminum plates were painted by both general water paint and solar reflective material paint in two different colors such as Gray and Red and dried completely for 7 days.



Solar reflective paint material General water paint

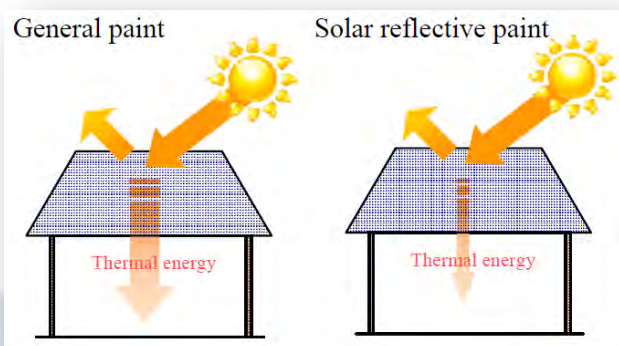


Figure 2 Conduction of solar thermal energy



Figure 4 Sample surface
(Left : Gray / Right : Red)

Countermeasure technique against heat island phenomenon - Evaluation of solar reflective paint material -

1. Spectral measurement result

Diffuse reflectance of samples was measured using [Spectral measurement] program under measurement condition shown in Table 1. By comparing the results shown in Figure 5, it is known that the solar reflective material paint has remarkably higher reflectance in NIR region than general water paint material.

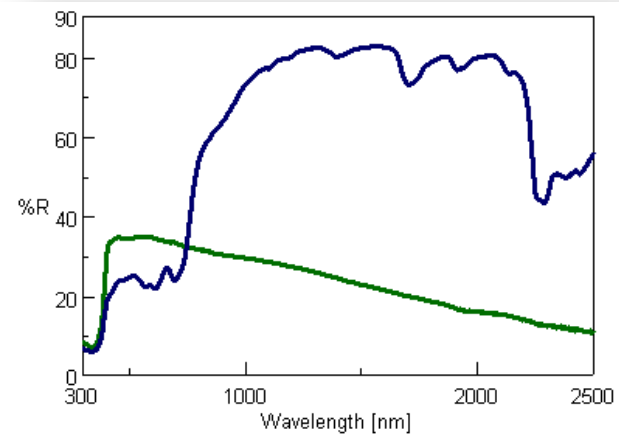
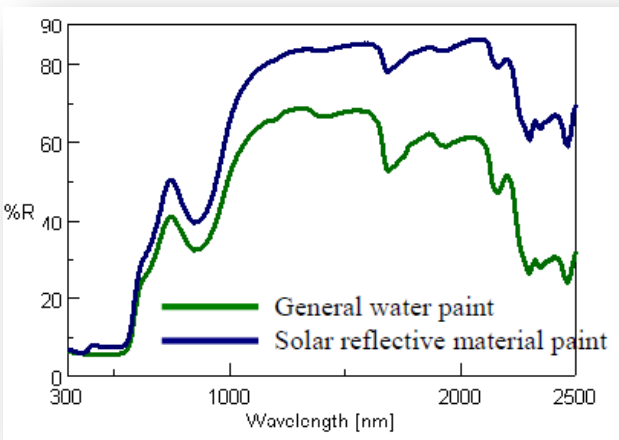


Figure 5 Diffuse reflectance spectra of solar reflective paint material and general water paint



2. Color Analysis result

By using the spectra obtained, the color analysis of both different paint materials was implemented using Color Analysis program and the results are shown in Figure 6, indicating the very similar color positions for both Gray and Red on chromaticity diagram. Even colors of two kinds of paint material are quite similar, the characteristics are completely different. Spectral measurement in UV/Vis/NIR region is a very useful method to obtain various important information to investigate such differences.

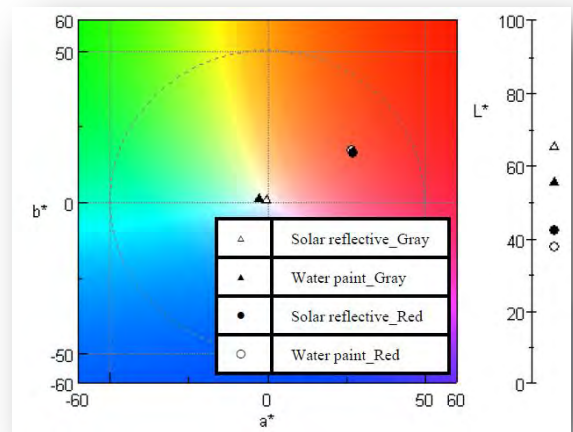


Figure 6 Chromaticity diagram

3. Calculation result of reflectance of solar light

Reflectance of solar light in three different wavelength ranges was calculated using Solar/visible light measurement program based on JIS K5602. It is clearly seen that solar reflective paint material has higher reflectance in all wavelength region and in NIR region.

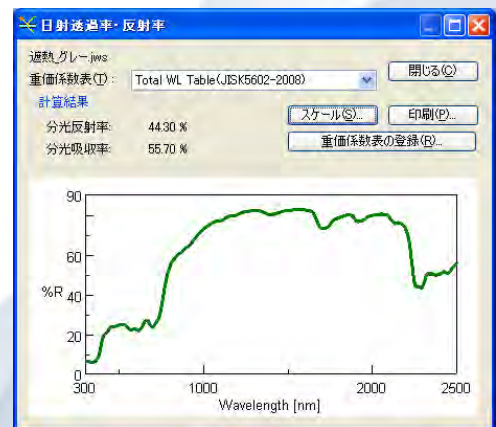


Table 1 - Measurement condition	
Measurement range	300 - 2500 nm
Data interval	1 nm
UV/Vis bandwidth	5.0 nm
NIR bandwidth	20.0 nm
Response	Fast
Scan speed	1000 nm/min
Correction	Base line / Dark

	Gray		Red	
	Solar reflective	Water paint	Solar reflective	Water paint
UV/Vis region	24.09	32.19	21.67	17.60
NIR region	70.39	26.68	64.98	50.61
All wavelength region	44.30	29.75	40.53	31.95

Evaluation of sun protection fabrics by using a UPF evaluation system

Introduction

UPF (UltraViolet Protection Factor) is used to indicate the UV shielding performance of sun protection for fabric products. The 'UPF value' represents the ratio of time for sunburn by UV with and without the protection of the fabric material or product. For example, in the case of skin irradiated by ultraviolet light in 10 minutes with a UPF 50 cloth, it takes 500 min (50 (UPF) x 10 min) to obtain the same amount of sunburn to the skin without using the cloth product. The test method of for UPF calculations when using a UV-Vis spectrophotometer is defined in AS/NZS 4399:1996, BS EN 13758-1:2002, the AATCC Test Method 183:2010, and GBT18830:2009.

In this application data, the evaluation of the UPF, UPF rating, UVA transmittance, and UVB transmittance of sun protection fiber products defined in AS/NZS 4399:1996 by using the UPF calculation system of a UV/Vis spectrophotometer is explained. Also, the fluorescence properties are explained by using a spectrofluorometer because fabric products sometimes emit fluorescence by UV light irradiation.

Calculation Method - UPF

UPF is calculated by equation (1).

$$UPF = \frac{\sum_{290}^{400} E(\lambda) \cdot S(\lambda)}{\sum_{290}^{400} E(\lambda) \cdot S(\lambda) \cdot T(\lambda)} \times 100 \quad (1)$$

$E(\lambda)$: CIE reference erythema dose spectrum
 $S(\lambda)$: radiation intensity distribution of sunlight
 $T(\lambda)$: diffuse reflectance spectra (%T)

UPF rating

To calculate the UPF rating measure the transmittance spectrum at more than four different points for the same sample and round down the value, calculated by equation (2), by 5.

$$UPF \text{ rating} = UPF_{AVE} - E \quad (2)$$

$$UPF_{AVE} = \frac{UPF_1 + UPF_2 + \dots + UPF_N}{N}$$

$$E = \frac{t_{k,a}}{\sqrt{N}} \times SD$$

$$SD = \sqrt{\frac{\sum_{i=1}^N (UPF_i - UPF_{AVE})^2}{N-1}}$$

UPF_i : UPF of i_{th} point on a sample

$t_{k,a}$: The value which provides 0.5 % as the border value of probability of one side in the t distribution

a: Probability of one side (0.005)

k: Degree of freedom (N-1)

If the UPF rating is smaller than the minimum of each UPF, the value which is calculated by equation (3) are rounded down by 5.

$$UPF \text{ rating} = \text{lowest UPF} \quad (3)$$

if UPF rating is more than 50, UPF rating is defined as 50+

UVA transmittance, UVB transmittance

UVA transmittance is calculated by equation (4) by using the average of the transmittance in the range from 315 nm to 410 nm.

UVB transmittance is calculated by equation (5) by using the average of the transmittance in the range from 290 nm to 315 nm.

Evaluation of sun protection fabrics by using a UPF evaluation system

$$UVA = \frac{T_{315} + T_{320} + T_{325} + \dots + T_{400}}{18} \quad (4)$$

$$UVB = \frac{T_{290} + T_{295} + T_{300} + \dots + T_{315}}{6} \quad (5)$$

Sample

T shirt (black)	polyester 100%
Sports shirt (black)	polyester 100%
Arm cover (black)	rayon 55% polyester 45%

Measurement

3D fluorescence measurement

3D fluorescence measurements of the samples were conducted using a spectrofluorometer to identify the fluorescence property using excitation wavelengths in the range from 290 nm to 400 nm.

Transmittance spectra measurement

1. Baseline measurements were performed using a Spectralon reference tile.
2. Transmittance spectra measurements were performed at 4 different points in the same sample.

* If fluorescence was observed in the 3D fluorescence measurement, a Fluorescence Cut Filter Block and a Fluorescence Cut Filter (U-330) are required to measure samples which emit fluorescence in the wavelength range from 450 to 650 nm.

Measurement parameters

Spectrofluorometer

Excitation bandwidth: 5 nm
Emission bandwidth: 5 nm
Scan speed: 5000 nm/min
Response: 10 msec
Data interval: 0.5 nm
Spectra correction: ON

Spectrophotometer

UV/Vis bandwidth: 5.0 nm
Scan speed: 100 nm/min
Response: 0.96 sec
Data interval: 1 nm

Results of 3D fluorescence measurements

Figure 1 illustrates the 3D fluorescence measurement of the T shirt. No fluorescence was observed for the excitation wavelengths from 290 to 400 nm. No fluorescence was observed for the sports shirt and arm cover samples.

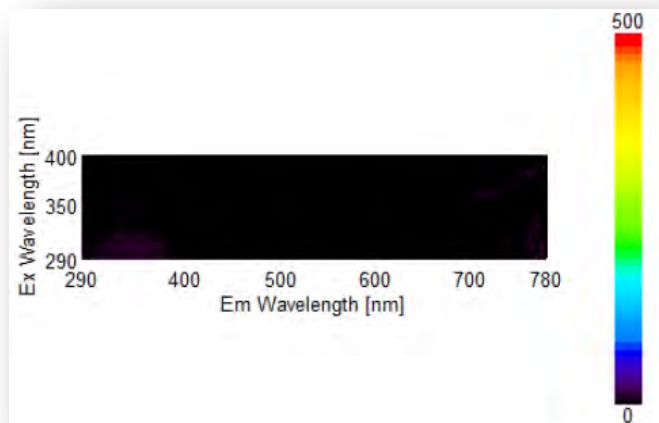


Figure 1 3D fluorescence spectra of T shirt

Results of transmittance measurements

Figure 2 shows the transmittance spectrum of each sample.

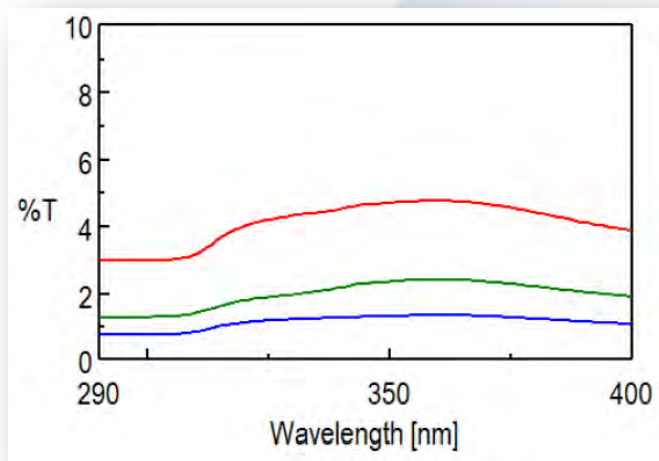


Figure 2 Transmittance spectrum of each sample
Red line: T shirt
Blue line: Sports shirt
Green line: Arm cover

Evaluation of sun protection fabrics by using a UPF evaluation system

Figure 3 illustrates the UPF measurement software display and Table 1 provides the analysis results for the samples. As shown in Figure 3, the [UPF measurement] program can objectively compare the performance of the ultraviolet shielding as a result of the numerical calculation of the UV shielding performance of fabric products. Moreover, the program corresponds to various standards including BS EN 13758-1:2002, AATCC Test Method 183:2010, and GBT18830:2009.

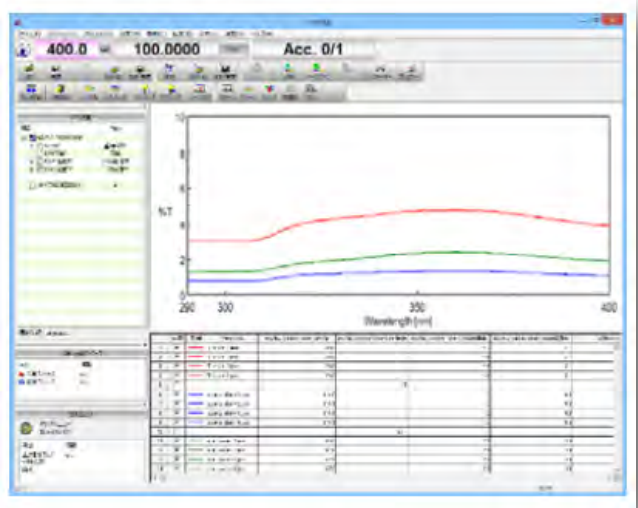


Figure 3 UPF Measurement Program

Sample	No.	UPF	UPF rating	UVA Transmittance (%)	UVB Transmittance (%)
T shirt	1	30.0	25	4.4	3.1
	2	30.0		4.4	3.1
	3	30.0		4.3	3.1
	4	30.0		4.4	3.1
Sports shirt	1	114.3	50+	1.2	0.8
	2	114.2		1.2	0.8
	3	114.1		1.2	0.8
	4	114.4		1.2	0.8
Arm cover	1	68.2	50+	2.1	1.3
	2	68.0		2.1	1.3
	3	68.1		2.1	1.3
	4	68.0		2.1	1.3

Table 1 Analysis result based on AS/NZS 4399:1996

Evaluation of the privacy film using an automated absolute reflectance measurement accessory

Introduction

A privacy film which is used for smartphone displays has a characteristic structure in which clear layers and light shielding layers are interlaminated. This structure prevents a smartphone display from bystanders 'peeking' at the screen while the viewing angle depends on the height and pitch of the light shielding layers in the louver layers. To evaluate the viewing angle or the transmittance of the louver layer, an absolute reflectance measurement accessory is an effective tool. The accessory can be used to set samples at a specified angle by rotating the sample to the source incidence and/or detector angles. In this application, the angle dependence of the transmittance spectra of the privacy film for a smartphone is explored.

Sample

Privacy film for smartphones (Figure 2)
Specification: View angle 65° Anti-glare processing

Measurement condition

- Position: transmittance, asynchronous
- Detection angle: 0°
- Incidence angle: -60° to 60°
- Measurement interval: 2°
- Measurement mode: %T
- Wavelength range: 380 to 780 nm
- Bandwidth: 5 nm
- Scan speed: 400 nm/min
- Response: 0.96 sec

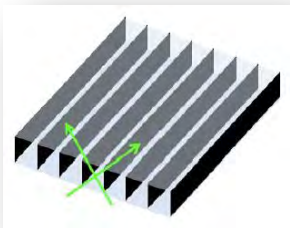


Figure 1 Structure of louver layer

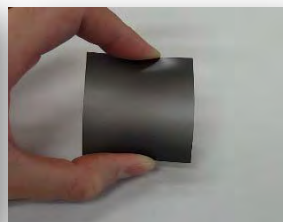


Figure 2 Privacy film sample

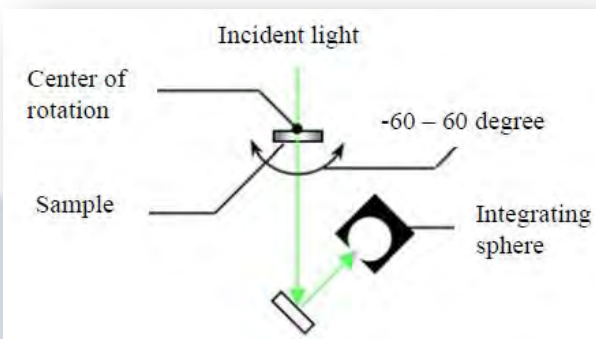


Figure 3 Measurement image

Result

Figure 5 illustrates the interval data in which spectra were acquired every 2° from -60° to 60°. Figure 6 outlines the transmittance spectra at 0°, 10°, 20°, 30°, 40°, 50°, and 60°. Figure 7 provides the angle scanning transmittance data from -60° to 60° at 550 nm. Figures 5 and 6 indicate that the film absorbs blue light at less than 400 nm and keeps the transmissivity constant at more than 400 nm, which means that the film displays the light to eyes without a large color change. As illustrated in Figure 7, the transmittance is approximately 5% near the nominal view angle of ±32.5°. This characteristic is quite suitable for user privacy. As indicated in this report, the absolute reflectance measurement system is best suited to evaluate the incident angle dependence properties of various transmittance spectra.

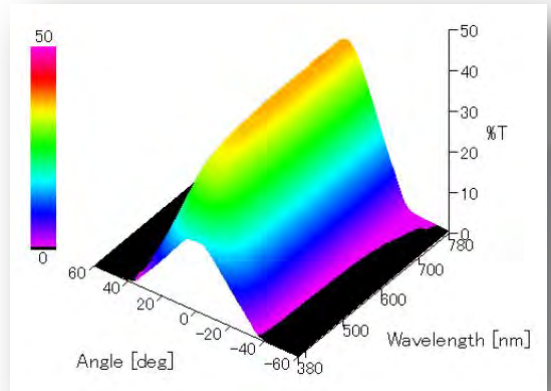


Figure 5 Interval data of the privacy film

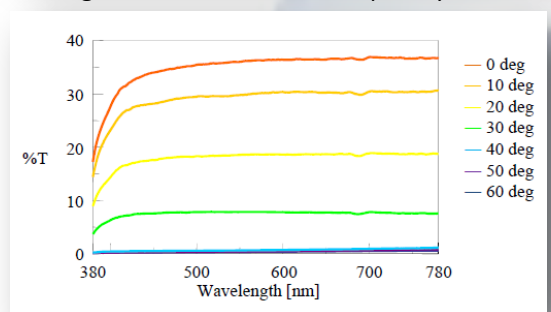


Figure 6 Transmittance spectrum at every 10° from 0° to 60°

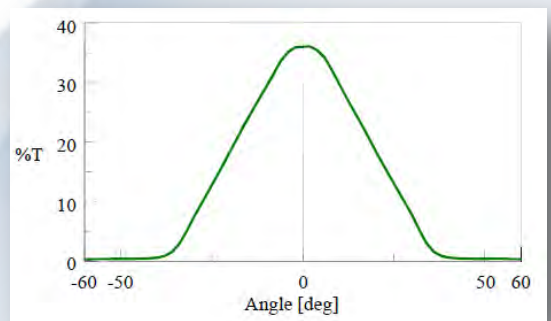


Figure 7 Angle dependence of transmittance spectra at 550 nm

Thickness Analysis of natural oxide film on microscopic Si pattern

Introduction

The MSV-5000 series microscopic spectrophotometer is for transmission/reflection measurement in a wide wavelength range from ultraviolet to near-infrared. It allows the measurement of the area of as small as 10 μm diameter and the built-in high-resolution camera enables to observe the samples precisely to determine the area to be measured. This instrument is most suitable to measure the minute samples or samples having microstructure. This time, the sample on which Si patterns of 35 μm widths are lined up on Ti substrate with 14 μm intervals was measured as a microstructure sample. Actually, the thickness of SiO₂ formed upon Si was analyzed from the obtained reflectance spectrum, because Si is easily oxidized in the air to form thin oxide film of SiO₂.

Measurement System

MSV-5200 Microscopic spectrophotometer
VWML-791 [Multi-Layer Analysis] program

Sample: Si and Si oxide film on the Ti substrate

Measurement condition

UV/Vis spectral bandwidth: 5.0 nm
NIR spectral bandwidth: 20.0 nm
Scan speed: 100 nm/min
Response: Slow
Data interval: 0.5 nm
Cassegrain objective mirror: 16x
Incidence angle: 23°
IN aperture: 10 $\mu\text{m}\phi$
OUT aperture: 10 $\mu\text{m}\phi$

Measurement

1. Baseline: Al vapor-deposited mirror as a reference is used for baseline measurement.
2. Measurement area: The sample is observed by the high-resolution camera to determine the measurement area (Figure 1). The red spot in Figure 1 shows the size and position of detected light.
3. Sample measurement: The reflectance spectrum is measured.
4. Transforming into absolute reflectance: The absolute reflectance spectrum of the sample is calculated by multiplying the obtained relative reflectance by the absolute reflectance of Al vapor-deposited mirror.

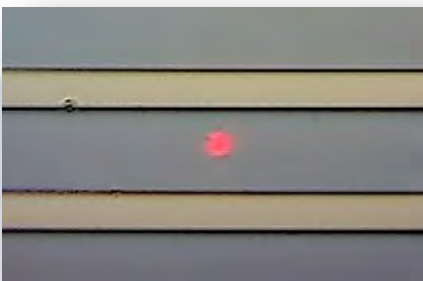


Figure 1 Observation figure of measurement position

Analysis

Reflectance(R) is expressed by the equation of refractive index of the film (n_i), extinction coefficient (k_i), the angle of incidence (θ_i), wavelength (λ) and the film thickness (d_i). This time, optical constants of Si and SiO₂ are used from the literature value. and then the film thickness of SiO₂ is estimated by using [Multi-Layer Analysis] program by fitting the calculated reflectance spectrum to the measured one to make the thickness value reasonable.

Measurement Results

Measured absolute reflectance spectrum is shown in Figure 2. MSV-5000 series adopts the confocal optical system, which enables the measurement eliminating the influence of back side reflection. In the range over 1100 nm where the light passes through Si, the spectrum would not be influenced by the back side reflection.

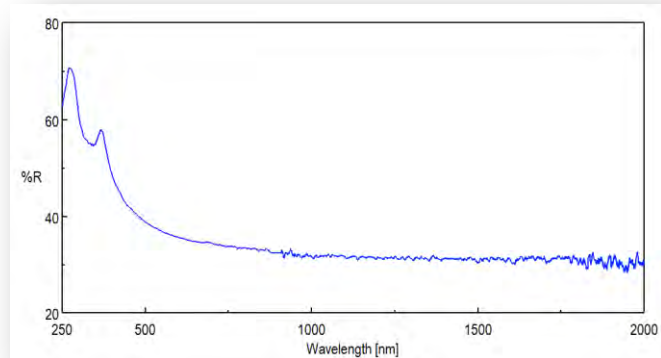


Figure 2 Absolute reflectance spectrum of sample

Analysis Results

The result of fitting the reflectance spectra using [Multi-Layer Analysis] program is shown in Figure 3. The error between measured spectrum and calculated one was within 2% (Figure 3) and the film thickness of SiO₂ was calculated to be 7.6 nm.

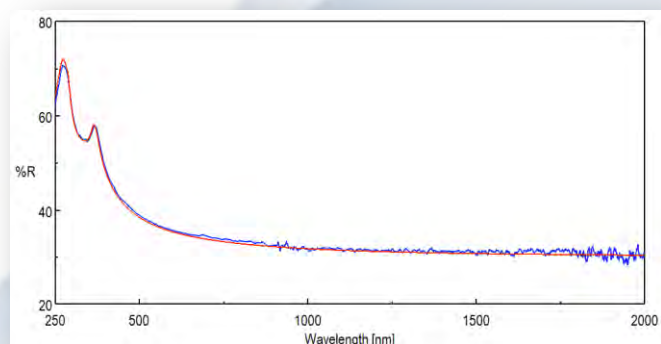


Figure 3 Fitting result of reflectance spectra

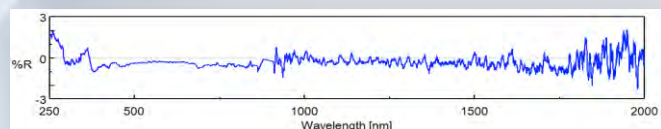


Figure 4 The error between measured spectrum and calculated one

Luminous Color Measurement by using UV/Vis Spectrophotometer

Lately, products such as LEDs, Organic EL displays, and plasma display panels (PDP) that applied luminous phenomenon are in widespread use and the developments in this field are rapidly proceeding. Starting with the blue LED developed in 1993, engineers finally succeeded in developing the white LED that is now the mainstream illuminant of the mobile phone backlight, flashlight, and so on. In display field, next-generation display with luminous body, such as the Organic EL displays having superior performances on luminous efficacy, flat-screen, and power consumption and the PDP for large-sized flat TV screen are actively developing.

For these developments, numeric evaluations of colors and color rendering of the luminous body itself and of the manufactured display are required. Here, the methods of evaluating luminous colors and color rendering by JASCO spectrophotometer are introduced for the cutting edge technologies of LED, Organic EL, and PDP. Moreover, the method of evaluating colors of the liquid crystal display (LCD) by the same system is also introduced.

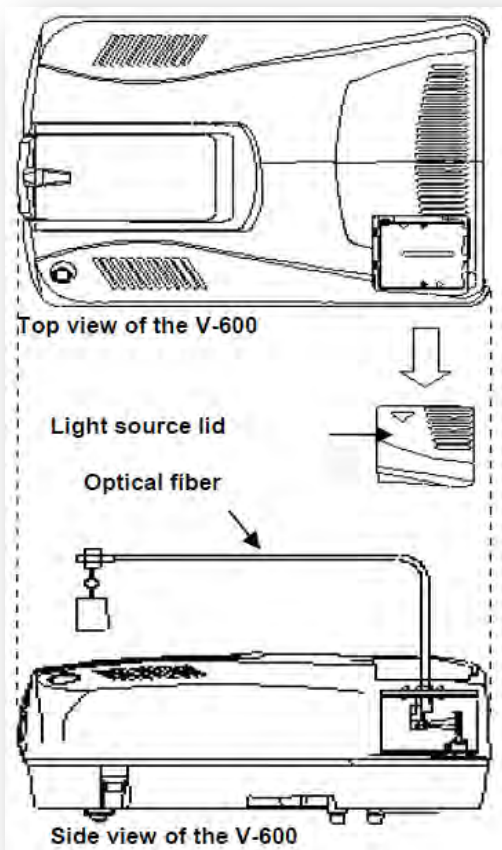


Figure 1

V-600 series spectrophotometer with the external source fiber optic interface

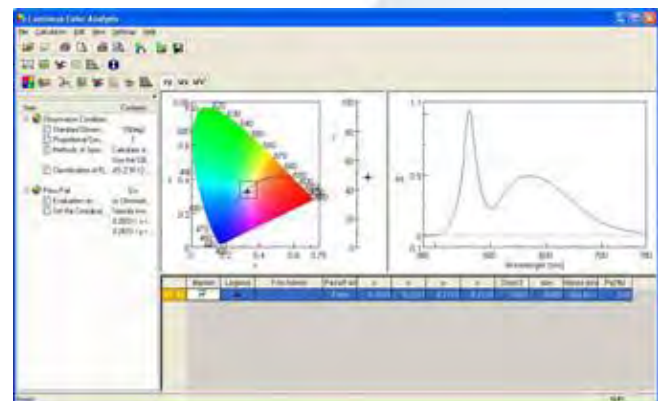
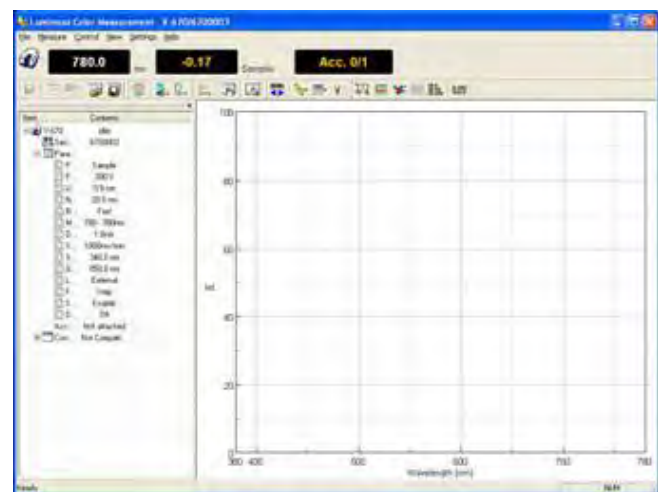


Figure 2

[Luminous Color Measurement] (Top)
[Luminous Color Analysis] (Bottom)

System Configuration for the Measurement/Analysis

- V-650/660/670 UV/Vis/NIR spectrophotometer
- Model ELM-742 External Source Fiber Optic Interface
- Calibrated lamp unit
- VWLU-788 Luminous Color Measurement/Analysis Program

Luminous Color Measurement by using UV/Vis Spectrophotometer

Main Functions of the

[Luminous Color Measurement/Analysis]

- Color Calculation Functions
 - Tristimulus Values X, Y, Z JIS Z 8701-1999
 - Chromaticity coordinate (x, y), (u, v), (u', v') JIS Z 8701-1999
 - Dominant Wavelength λ_d (Complementary Wavelength λ_c), Excitation purity p_e JIS Z 8701-1999
 - Correlated Color Temperature T_{cp} and Deviation duv JIS Z 8725-1999
 - Color Rendering Index R_a , R_1 to R_{15} JIS Z 8726-1990
 - Classification of the Fluorescent lamps JIS Z 9112-1990, 2004
- Pass/Fail Criteria Function

Measuring Method

1. Correction Coefficient Spectrum Measurement

Spectrophotometer has different grating efficiency and detector sensitivity according to the wavelength, so a gained spectrum reflects the instrument characteristics. To remove the instrument characteristics, measure the standard light source having a known emitting pattern in order to obtain the instrument characteristics (Correction Coefficient Spectrum). Here, the emitting pattern of the standard light source is called as the "Standard light source data", and a spectrum of the standard light source measured by the spectrophotometer is a "Standard light source spectrum". "Correction Coefficient Spectrum" can be calculated by dividing "standard light source raw spectrum" by "Standard light source data" (Figure 3).

2. Sample Measurement

Measure sample after obtaining the Correction Coefficient Spectrum. Here, a spectrum measured by spectrophotometer is called as a "Raw spectrum of sample", and the "Spectrum Correction" means removing the instrument characteristics from the spectrum. The "Spectrum Correction" is executed by dividing the "Raw spectrum of sample" by the "Correction Coefficient Spectrum".

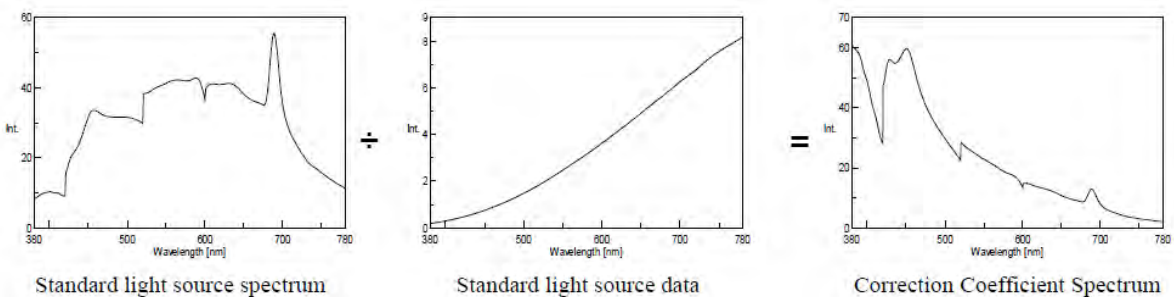


Figure 3 Calculation of the Correction Coefficient Spectrum

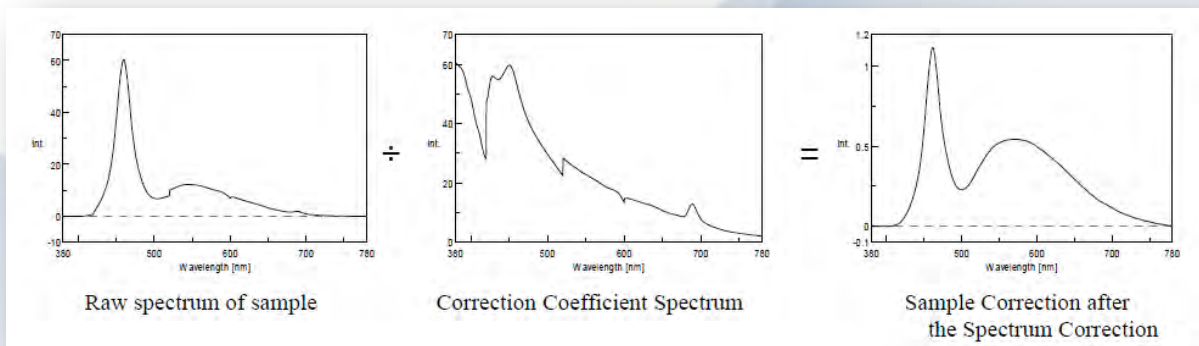


Figure 4 Methods of the Spectrum Correction

Luminous Color Measurement by using UV/Vis Spectrophotometer

Example 1 - Color Rendering and Correlated Color Temperature of Illuminations

White LED, fluorescent lamp, and sunlight were measured to calculate the Color Rendering Index and the Correlated Color Temperature. The white LEDs show relatively favorable Color Rendering Index (Ra) with high Correlated Color Temperature (Tcp). The color of the white LEDs differs according to their types, some of them show deeper blue color. Sunlight shows almost Ra 100 and the fluorescent lamp shows smaller Ra.

No.	Illumination (Spectrum Color)	Tcp (K)	duv	Ad (nm)	Pe (%)	Reference Illuminants	Ra	Classification of FL
1	White LED1 (Blue)	9055	-0.013	469.37	19.28	D9055	86	-----
2	White LED2 (Light Blue)	8563	0.003	482.54	17.62	D8563	80	-----
3	White LED3 (Yellow Green)	19359	-0.014	470.37	31.23	D19358	80	-----
4	Fluorescent lamp (Green)	4632	0.005	572.78	19.05	P4632	82	N
5	Sunlight (Red)	5158	0.003	566.74	9.1	D5158	98	N

Table 1 Correlated Color Temperature and Color Rendering for each illumination

Example 2 - Color Calculation of Liquid Crystal Display

The screens of a liquid crystal display were measured when it shows white, red, blue, green, yellow, light blue, and deep red. The spectra were calculated by the color calculation program.

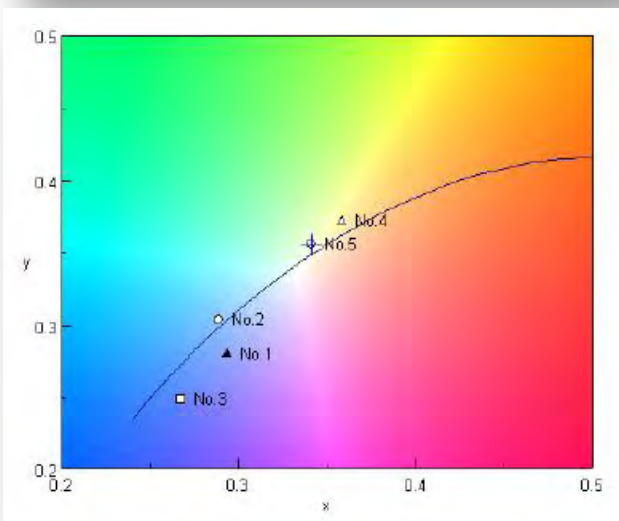
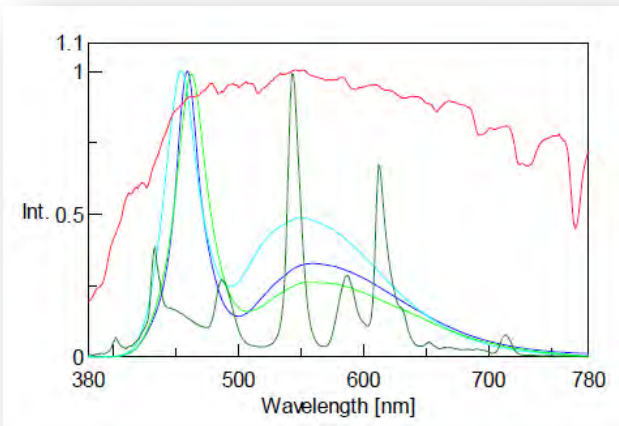


Figure 5

Emitting spectra of the illuminations (above) data plotted on the chromaticity diagram (below)

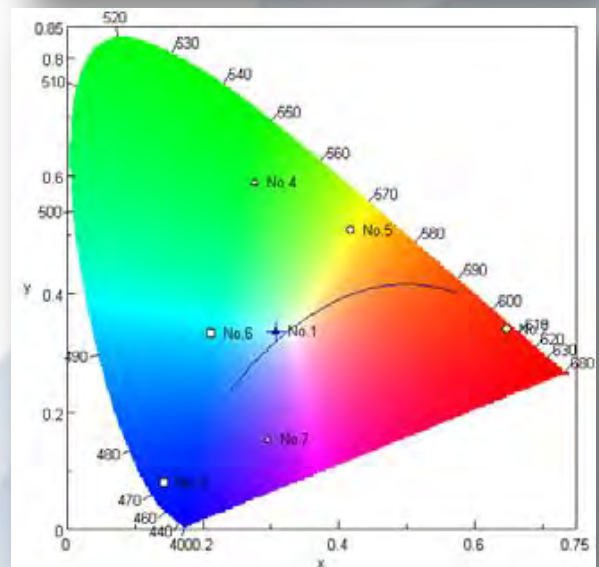
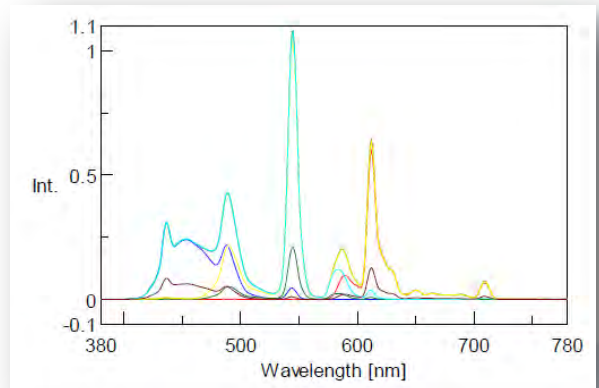


Figure 6

Spectra for each screen and (above) data plotted on the chromaticity diagram (below)

Luminous Color Measurement by using UV/Vis Spectrophotometer

The XYZ values were converted into RGB values, and compared the values with that of display settings. Although the values G and B showed relatively higher number than set value, we consider the results match reasonably.

No.	Color	X	Y	Z	x	y	Tcp (K)
1	White	18.95	20.56	22.01	0.308	0.3342	6714
2	Red	8.66	4.51	0.19	0.648	0.3376	-----
3	Blue	3.56	1.95	19.37	0.1431	0.0784	-----
4	Green	1.37	2.9	0.67	0.277	0.5868	-----
5	Yellow	15.3	18.54	2.82	0.4173	0.5057	-----
6	Light Blue	10.2	15.96	22.06	0.2115	0.331	-----
7	Deep Red	2.74	1.4	5.1	0.2963	0.1518	-----

Table 2 Color Calculation Result for each color
(Two-degree standard observer is applied to the calculation)

The conversion of the XYZ values into RGB values is executed according to the method of Colors & Dyeing Club in Nagoya/Osaka.
(<http://www005.upp.so-net.ne.jp/fumoto/index.htm>).

Color	Display' RGB settings			RGB converted from XYZ		
	R	G	B	R	G	B
White	255	255	255	247	262	256
Red	255	0	0	269	0	0
Blue	0	0	255	0	57	256
Green	0	128	0	0	127	32
Yellow	255	255	0	254	257	30
Light Blue	0	255	255	0	263	259
Deep Red	128	0	128	128	11	139

Table 3 RGB values comparison between display settings and converted XYZ values

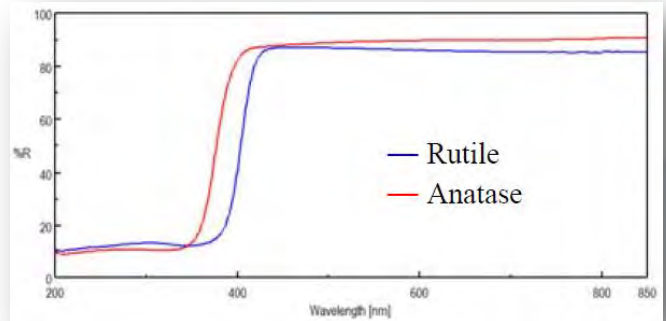
Bandgap Measurements for Titanium Dioxide Powder

Introduction

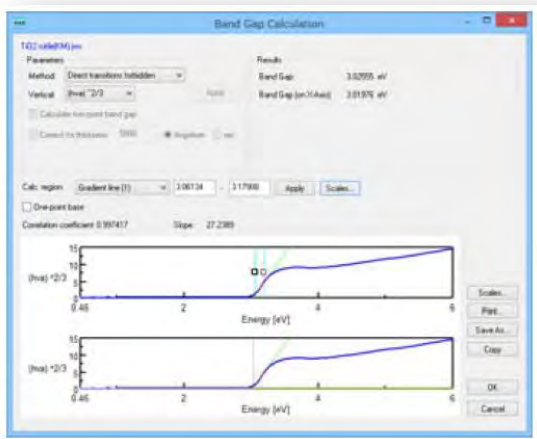
The bandgap energy for semiconductor materials can be determined from the transmittance or reflectance spectrum using a JASCO spectrophotometer.

Diffuse transmittance spectra for rutile and anatase titanium dioxide powder were measured. Since for titanium dioxide, absorption occurs due to forbidden direct transitions, plotting $h\nu$ against $(h\nu\alpha)^{2/3}$ allows the bandgap energy to be determined.

Although, in principle, the bandgap should be calculated using the absorption coefficient, when only bandgap absorption occurs, the bandgap energy can be determined directly from the transmittance or reflectance spectrum. If the sample is a thin film and an interference pattern is present in the transmittance or reflectance spectrum, use an absolute reflectance measurement unit to measure the spectrum. The interference effect can be eliminated by calculating $100\%T-\%R$.



Diffuse transmittance spectrum for TiO₂



VWBG-773 [Band Gap Calculation] program

Apparatus

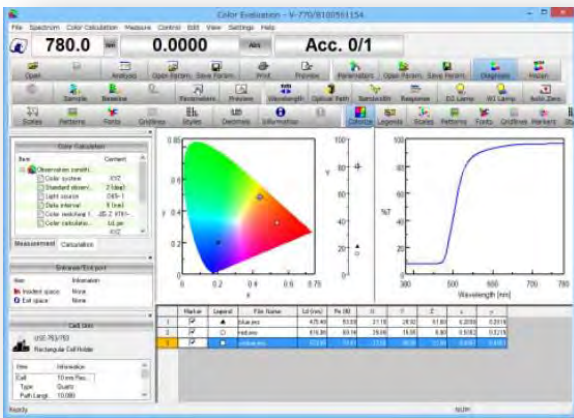
- V-770 - UV/Vis/NIR Spectrophotometer
- ISN-923 - Integrating sphere unit
- PSH-002 – Powder Cell
- VWBG-773 - Band Gap Calculation program

Reflection Object Color Measurements using Color Diagnosis System

Introduction

The color diagnosis system for the V-700 series can evaluate the reflection or transmission object color determined based on the CIE (Commission Internationale de l'Éclairage) standard.

Reflectance spectra for colored plastic reflective plates were measured with or without the specular component using an integrating sphere unit. If the spectrum includes the specular component, it is found that the lightness is exaggerated and the chroma is diminished. Accordingly, to evaluate the color of a mirror or a mirror-like sample surface, it is necessary to remove the specular component during measurement.

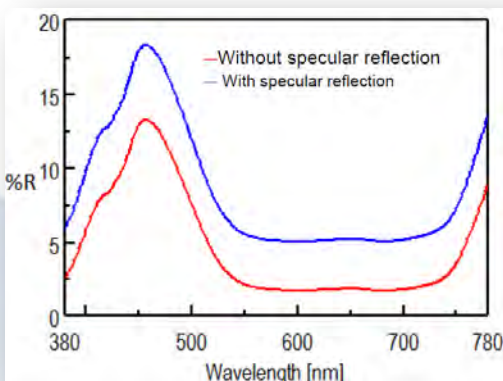


VWCD-960

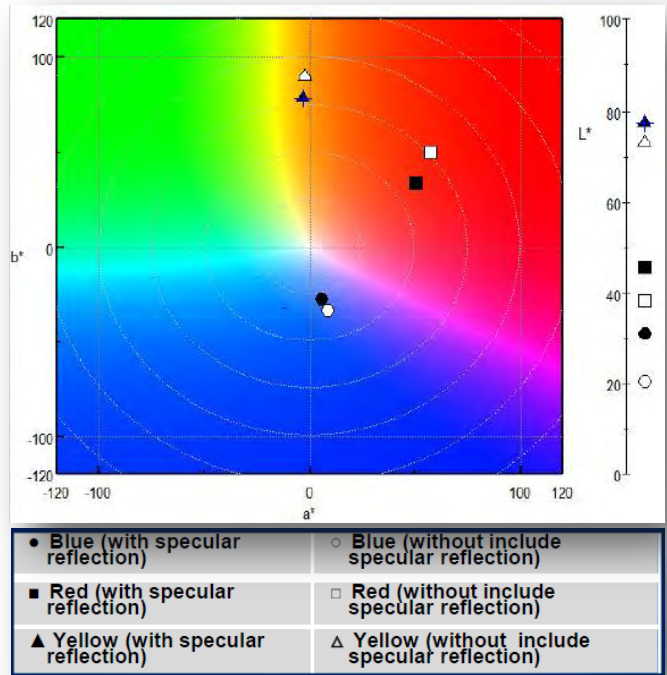
[Color Evaluation (Color Diagnosis)] program



Colored plastic reflective plates



Reflectance spectrum
for blue reflective plate



L*a*b* chromaticity diagram

Standard	Standard Name	Remarks
JIS Z 8722:2009	Methods of colour measurement -- Reflecting and transmitting objects.	Reflection object color: the φ60-mm or φ150-mm integrating sphere unit corresponds to geometric condition d. Transmission object color: the standard cell holder or film holder corresponds to geometric condition e.
CIE No.15:2004	COLORIMETRY, THIRD EDITION	The φ60-mm or φ150-mm integrating sphere unit corresponds to geometric condition f.

Light Source	Standard
D65, A	JIS Z 8781-2: 2012, CIE 15: 2004, ISO 11664-2:2007 / JIS Z 8701: 1999, JIS Z 8720: 2000, ASTM E308: 2008
B	JIS Z 8701: 1982
C	JIS Z 8701: 1999, JIS Z 8720: 2000, CIE 15: 2004, ASTM E308: 2008
D50, D55, D75	CIE 15: 2004 / JIS Z 8720: 2000, ASTM E308: 2008
F1, F3, F4, F5, F6, F8, F9, F10	CIE 15: 2004
F2, F7, F11, F12	CIE 15: 2004, ASTM E308: 2008

Reflection Object Color Measurements using Color Diagnosis System

Color System	Standard
XYZ	JIS Z 8701: 1999, CIE No.15: 2004, ISO 11664-1: 2007, ASTM E308: 2008
L*a*b*	JIS Z 8781-4: 2013, CIE No.15:2004, ISO 11664-5: 2009, ASTM E308: 2008
Lab	JIS Z 8730: 2002, ASTM D2244:2011
L*u*v*	JIS Z 8781-5: 2013, CIE No.15: 2004, ISO 11664-5: 2009, ASTM E308: 2008
Munsell	JIS Z 8721: 1993



Color-matching Function

JIS Z 8781-1: 2012, ISO 11664-1: 2007 / JIS Z 8701: 1999,
ASTM E308: 2008 / JIS Z 8701: 1982, CIE 15: 2004

Color Difference	Standard
$\Delta E^*_{abr}, \Delta L^*, \Delta a^*, \Delta b^*$	JIS Z 8730: 2009, CIE 15: 2004, ISO 7724/3: 1984, ASTM D2244: 2011
$\Delta E^*_{abr}, \Delta L^*, \Delta C^*_{abr}, \Delta H^*_{ab}$	JIS Z 8730: 2009, CIE 15: 2004, ISO 7724/3: 1984, ASTM D2244: 2011
$\Delta E_{00}, \Delta E_{00}, \Delta L', \Delta C', \Delta H'$	JIS Z 8730: 2009, CIE 15: 2004, ASTM D2244: 2011
$\Delta E_{94}, \Delta L^*, \Delta C^*_{abr}, \Delta H^*_{ab}$	JIS Z 8730: 2009, CIE 15: 2004 / ASTM D2244: 2011
$\Delta E_{CMC(l,C)}, \Delta L^*, \Delta C^*_{abr}, \Delta H^*_{ab}$	JIS Z 8730: 2009, ISO 105-J03: 2009, ASTM D2244: 2011
$\Delta E^*_{Hr}, \Delta L, \Delta a, \Delta b$	JIS Z 8730: 1980, ASTM D2244: 2011
$\Delta E^*_{uv}, \Delta L^*, \Delta u^*, \Delta v^*, \Delta C^*_{uv}, \Delta H^*_{uv}$	JIS Z 8730: 2009, CIE 15: 2004, ASTM D2244: 2011

Calculation Items	Standard
Tri-stimulus values: XYZ	JIS Z 8701: 1999, CIE 15:2004, ISO 11664-1: 2007, ASTM E308: 2008
Chromaticity coordinates: x, y	JIS Z 8701: 1999, CIE 15: 2004, ASTM E308: 2008
Dominant wavelength: λ_d , excitation purity: p_e	JIS Z 8701: 1999, CIE 15: 2004
Lightness index: L*, Chromaticity coordinates: a*, b*	JIS Z 8781-4: 2013, CIE 15: 2004, ISO 11664-4: 2009, ASTM E308: 2008
ab Chroma: C^*_{abr} , ab Hue angle: h_{ab}	JIS Z 8781-4: 2013, CIE No.15: 2004, ISO 11664-4: 2008, ASTM E308: 2008
Lightness index: L, chromaticity coordinates: a, b	JIS Z 8730: 2002, ASTM D2244: 2011
Lightness index: L*, chromaticity coordinates: u*, v*	JIS Z 8781-5: 2013, CIE 15: 2004, ISO 11664-5: 2009, ASTM E308: 2008
Hue: H, lightness: V, chroma: C	JIS Z 8721: 1993
Whiteness index: WI	JIS Z 8715: 1999 / CIE 15: 2004 / ASTM E313: 2010 / ASTM E313: 1996 / ASTM E313: 1973
Tint: T_w	JIS Z 8715: 1999 / CIE 15: 2004 / ASTM E313: 2010 / ASTM E313: 1996
Yellowness: YI	JIS K 7105: 1981 / JIS K 7373: 2006, ASTM E313: 2010

Gardner Color Measurement System

Introduction

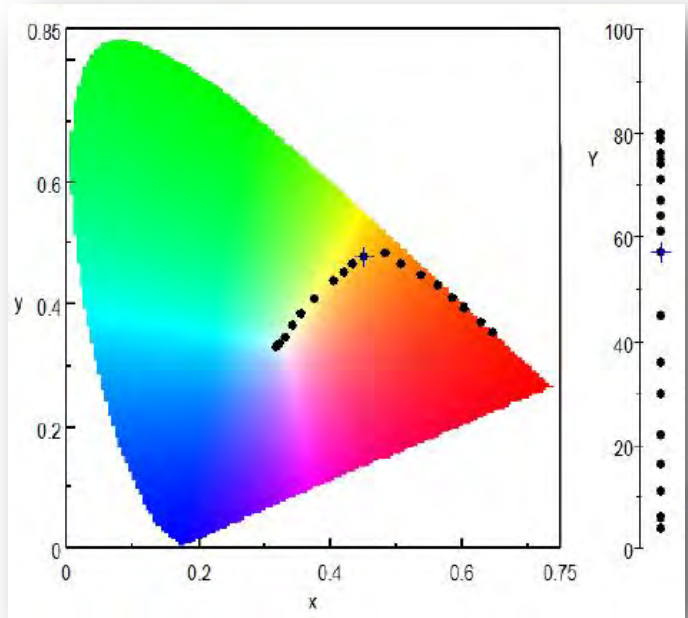
The Gardner color measurement system can evaluate the Gardner color as a measure of the degree of coloration of samples such as boiled oil, varnish, petroleum, liquids used in the production of chemicals, and substances that become molten when heated.



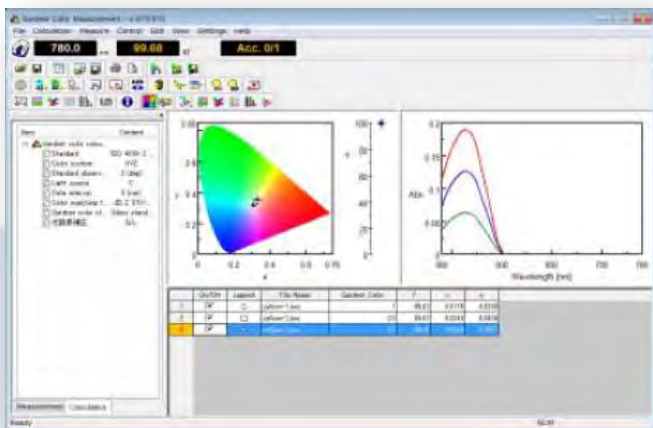
V-750 UV/Vis spectrophotometer

The Gardner scale is defined based on the chromaticity of glass or liquid standards numbered from 1 for the lightest (light yellow) to 18 for the darkest (brownish red). By identifying the standard solution that is closest in color to the sample solution, the standard color number for the sample can be evaluated. In this program, the chromaticity coordinates x and y , and the tristimulus value Y for the standard samples can be registered by entering them directly or by calculating them from the spectrum for the standard sample. The sample spectrum is then measured and its Gardner color is calculated either from the color difference between the sample and the standard, or by comparing their x and y values.

This system is compliant with ISO 4630-2:2004 Clear liquids - Estimation of colour by the Gardner colour scale - Part 2: Spectrophotometric method.



XYZ color system with standard solution coordinates plotted

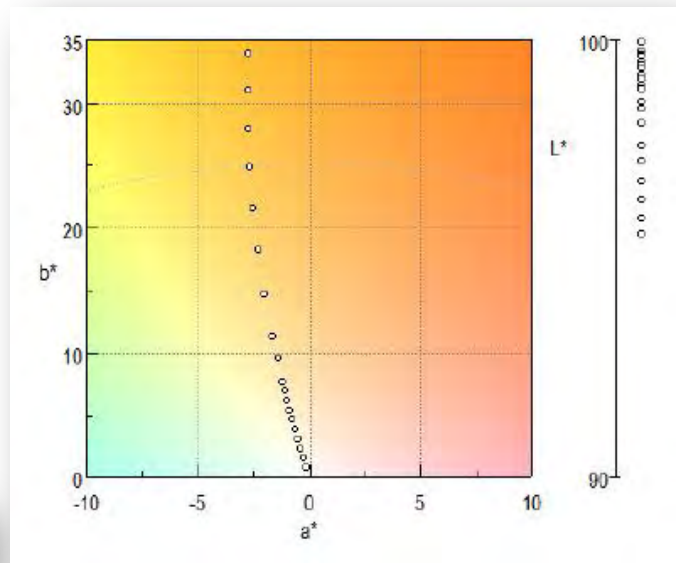


[Color Evaluation-Gardner Color] program (example)

Hazen Color Measurement System

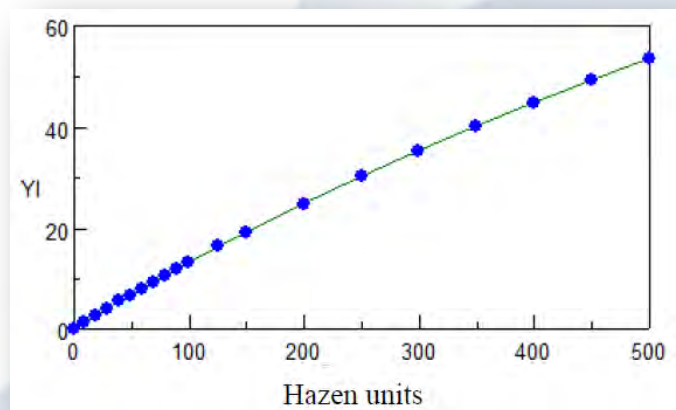
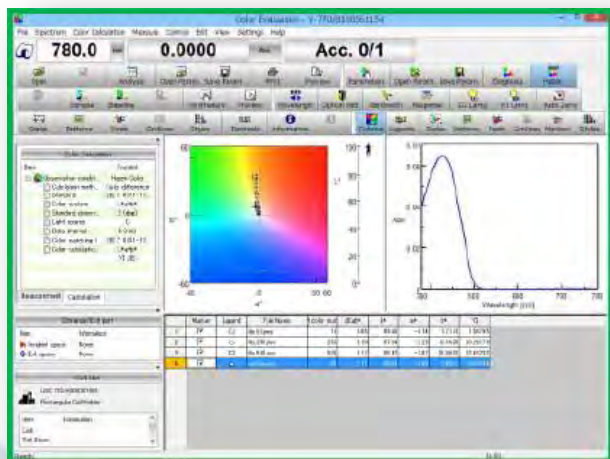
Introduction

The Hazen color measurement system can evaluate the Hazen color of samples such as drying oil, varnish, petroleum, liquids used in the production of chemicals, and substances that become molten when heated.



The Hazen scale is defined based on the chromaticity of numbered standard solutions with different concentrations and yellow hues. By identifying the standard solution that is closest in color to the sample solution, the standard color number for the sample can be evaluated. In the [Color Evaluation-Hazen Color] program, any of the following methods can be used to determine the color in Hazen units.

1. The color difference between standard and sample solutions
2. A calibration curve for the relation between the yellowness index YI and Hazen units for standard solutions
3. A calibration curve for the relation between the chromaticity coordinates b^* and Hazen units
4. A calibration curve for the relation between the absorbance at a specified wavelength and Hazen units for standard solutions



This system is compliant with ISO 6271-2:2004 Clear liquids - Estimation of colour by the platinum-cobalt scale-Part 2: spectrophotometric method. In this program, the visual test defined in JIS K 0071-1:1998, ISO 6271-1:2004 or ASTM D 1209-05 is applied to the UV/Vis spectrophotometer.

Evaluation of antireflection film by using absolute reflectance measurement accessory

Introduction

Antireflection film is widely used in many different products of various fields. For example, it is used for window and lens in visible region and also for near IR region laser diode in optical communication purpose and optical materials. The performance of antireflection film is getting higher recently, which is less than 0.1% reflectance level. And it is the one of reason for above expanded markets and fields. This application note proved that JASCO Automated absolute reflectance measurement accessory can be applied to the reflectance measurement with less than 0.1%. For this proof statement, several measurement data are shown in below about film sample which has been designed less than 0.1% reflectance both in visible and near infrared regions.

Sample

1) Measurement for linearity

- Visible region: KMnO₄ solution (66.7, 133.3, 200.0, 266.7 mg/L)
- Infrared region: ND filter A, ND filter B

2) Reflectance measurement of antireflection film*¹⁾

- AR coat VIS (430 - 600 nm)
- AR coat NIR-1 (980 - 1140 nm)
- AR coat NIR-2 (1320 - 1600 nm)

*1 The base of antireflection film is quartz.

Measurement

Measurement for linearity

1.1 Visible region

- (1) Dark measurement is carried out with setting the masking shield to the cell holder of Automated absolute reflectance measurement accessory.
- (2) Baseline measurement is carried out with setting water set into the rectangular cell holder.
- (3) Sample measurement is carried out with setting sample into the rectangular cell holder.

1.2 Near infrared region

- (1) Dark measurement is carried out with setting the masking shield to the sample holder of Automated absolute reflectance measurement accessory.
- (2) Baseline measurement is carried out with air.
- (3) Sample measurement is carried out with ND filter A set into the sample holder.
- (4) Sample measurement is carried out with ND filter B, not parallel to ND filter A.
- (5) Sample measurement is carried out with setting off ND filter A.

2.0 Reflectance measurement of antireflection film

- (1) Dark measurement is carried out with setting the masking shield to the sample holder of Automated absolute reflectance measurement accessory.
- (2) Baseline measurement is carried out with air.
- (3) Sample measurement is carried out with setting sample to sample holder.

Result

(1) Measurement for linearity

1.1 Visible region

Figure 1 shows the absorption spectra of KMnO₄ solution, and Figure 2 shows the calibration curve at 526 nm where is peak wavelength. As shown in Figure 2, in absorbance range from 1 to 4, R₂ shows the high correlation (more than 0.999). This indicates that Automated absolute reflectance measurement accessory can provide absorbance up to 4, which means that transmittance and reflectance are obtained up to 0.01%.

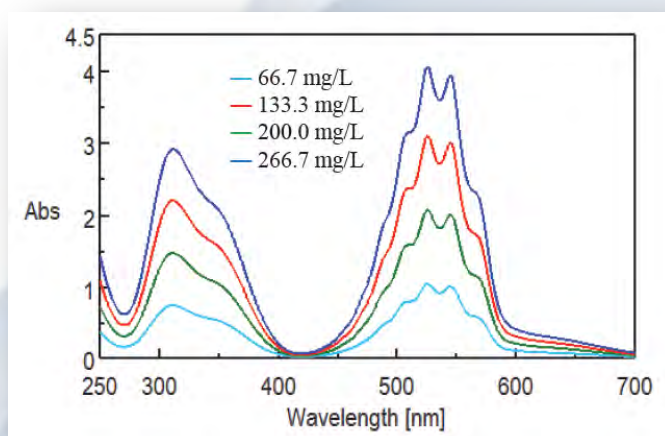


Figure 1 Absorbance spectrum KMnO₄ solution

Evaluation of antireflection film by using absolute reflectance measurement accessory

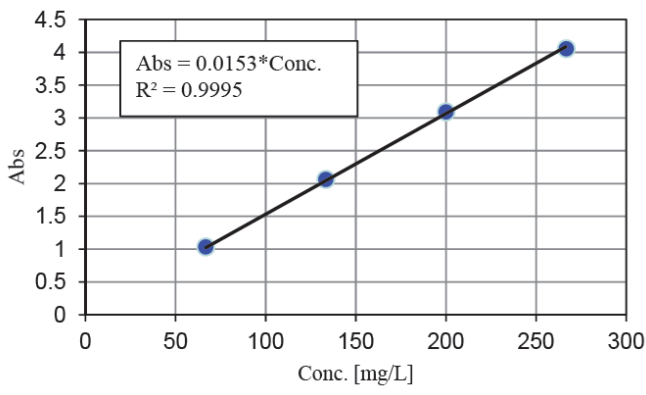


Figure 2 Calibration curve at 526 nm

1.2 Near infrared region

Figure 3 shows the absorbance spectrum of ND filter. The spectrum of ND filter A and B agrees in that of sum of filters. This indicates that Automated absolute reflectance measurement accessory can provide absorbance up to 4, which means that transmittance and reflectance are obtained up to 0.01 %.

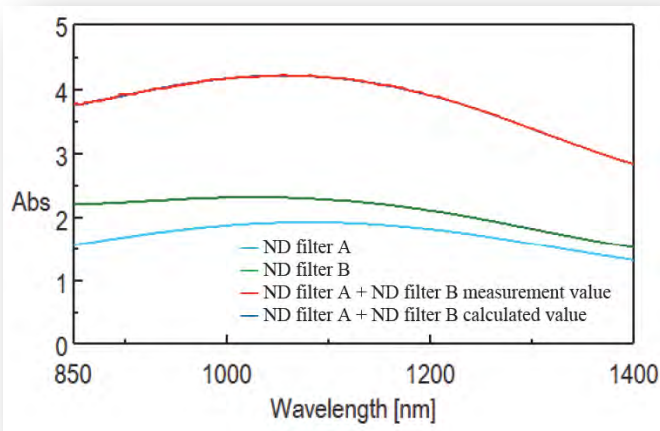


Figure 3 Absorbance spectra of ND filter

2) Reflectance measurement of antireflection film Figure 4 shows the reflectance spectrum of antireflection film in visible region and Figure 5, 6 show in near infrared region. Table 1 shows the reflectance of the bottom peak. As shown in Figure 4, 5, and 6, V-770/780 allow measurement with less than 0.1 % reflectance in the wavelength range from visible to near infrared. V-770 and V-780 provides almost similar spectrum in terms of S/N ratio in the wavelength range from 980 nm to 1140 nm. But, in wavelength range from 1320 nm to 1600 nm, V-780 provides the more high-quality spectrum with high S/N ratio due to the difference of installed detector. V-770 equips the PbS detector which has high sensitivity in the wide wavelength range. On the other hand V-780 equips the InGaAs detector which has more high sensitivity. Thus, this means V-770 is suitable for measurement with wide wavelength range and V-780 is suitable for high sensitivity measurement.

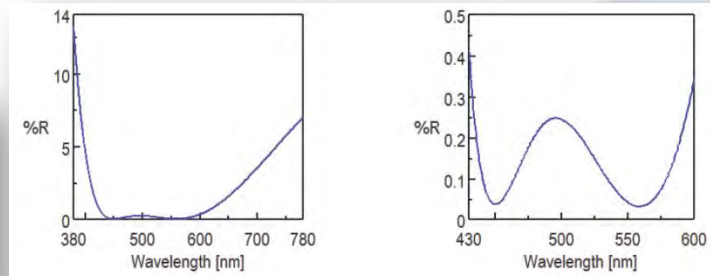


Figure 4 Reflectance spectrum of AR coat VIS

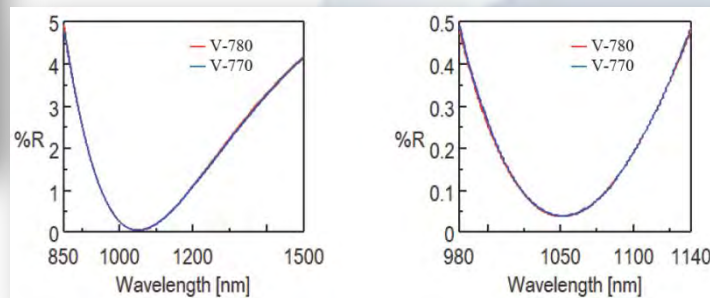
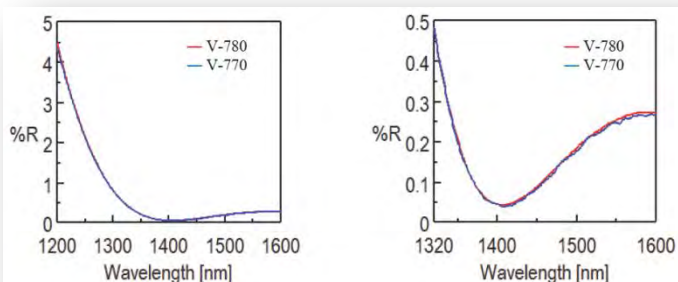


Figure 5
Reflectance spectrum of AR coat in visible region NIR-1

Evaluation of antireflection film by using absolute reflectance measurement accessory


Figure 6

Reflectance spectrum of AR coat in visible region NIR-2

AR coat VIS		
	Wavelength [nm]	Reflectance [%]
V-770	450.5	0.03681
	558.0	0.03144

AR coat NIR-1		
	Wavelength [nm]	Reflectance [%]
V-770	1049	0.03655
V-780	1049	0.03655

AR coat NIR-2		
	Wavelength [nm]	Reflectance [%]
V-770	1406	0.03703
V-780	1406	0.04235

Table 1

 Reflectance of bottom peak
in reflectance spectrum

Measurement parameters

1 Measurement for linearity

1.1 Visible

- UV/Vis bandwidth L5.0 nm
- UV/Vis response 3.84 sec
- Scan speed 100 nm/min
- Data interval 1 nm

1.2 Near-infrared

- NIR bandwidth 40.0 nm
- NIR response 3.84 sec
- Scan speed 100 nm/min
- Data interval 1 nm

2 Reflectance measurement of antireflection film

AR coat VIS

- UV/Vis bandwidth L5.0 nm
- UV/Vis response 0.96 sec
- Scan speed 200 nm/min
- Data interval 0.5 nm
- Incident angle 5°
- Polarization N-polarized light

AR coat NIR-1/NIR-2

- NIR bandwidth 40 nm (V-770)/ 10.0 nm (V-780)
- NIR response 3.84 sec
- Scan speed 100 nm/min
- Data interval 1 nm
- Incident angle 5°
- Polarization N-polarized light

Introduction of Haze value measurement system for UV/Vis spectrophotometer

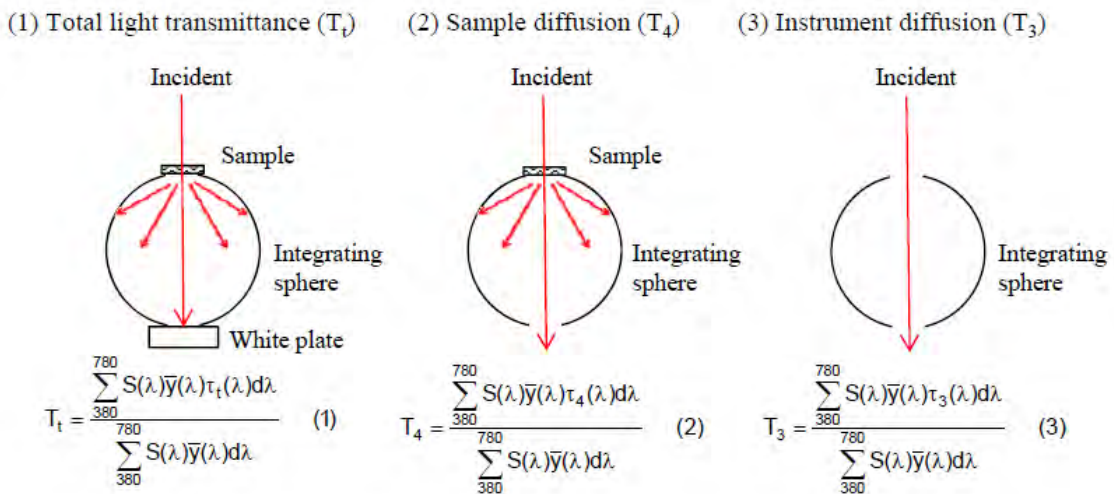
Introduction

Haze value is an indicator to show fogged degree of samples and recently is often used to evaluate the transparency and diffuseness of touch panel and solar cell materials.

In this application note, the measurement method of Haze value and total light transmittance, and measurement of Haze value in diffuser panels are reported. Measurement methods on JIS, ISO, and ASTM applied to the UV-visible spectrophotometer in this application.

Measurement Method

With using integrating sphere, total transmittance (T_t), sample diffusion rate (T_4) and scattering rate (T_3) which is required to calibrate the diffusion by instruments are measured in the wavelength range from 380 to 780 nm (figure 1). Using equation (4) provides the diffuse transmittance (T_d) of sample, and Haze value can be calculated by the ratio between T_t and T_d (equation (5)).



$\tau_t(\lambda), \tau_3(\lambda), \tau_4(\lambda)$: Transmittance spectrum in each measurement

$S(\lambda)$: Spectral characteristics of light source

$\bar{y}(\lambda)$: Luminosity factor

Fig.1 Image of Haze value measurement

Diffuse transmittance (T_d):
$$T_d = T_4 - T_3 \left(\frac{T_t}{100} \right) \quad (4)$$

Haze value:
$$\text{Haze} = \frac{T_d}{T_t} \quad (5)$$

Sample

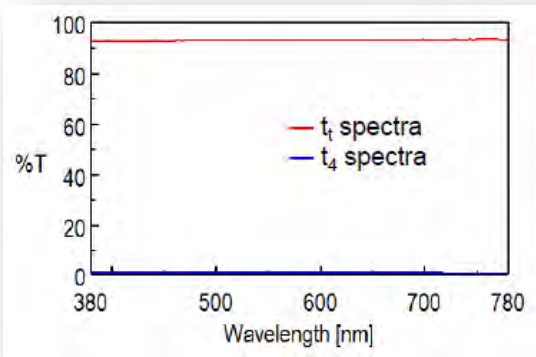
Six quartz diffuser panels.



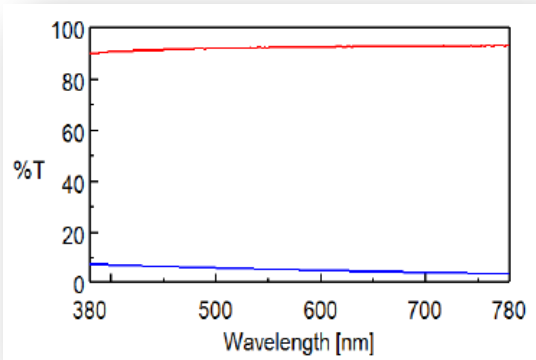
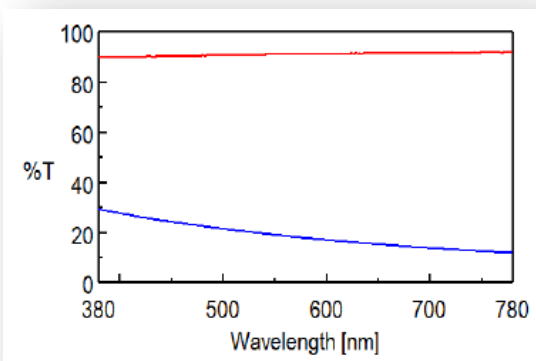
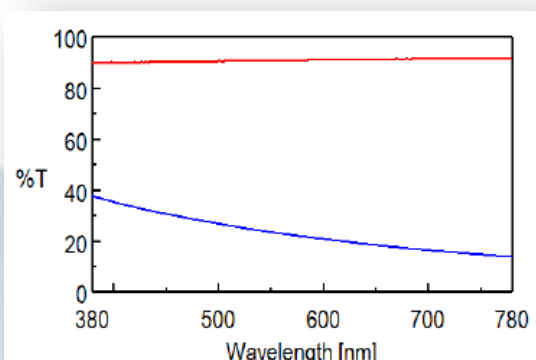
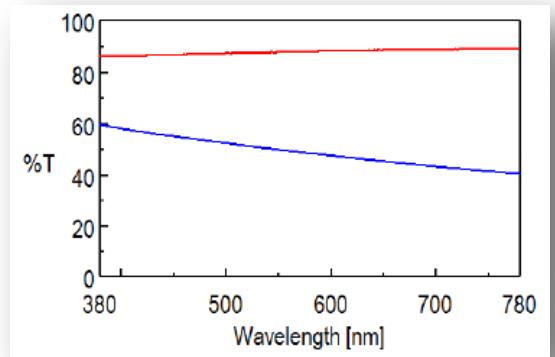
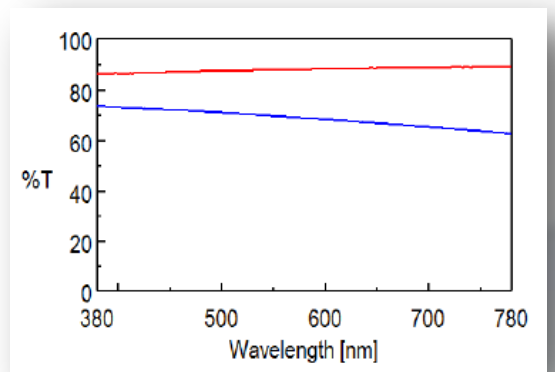
Measurement Results

The spectrum of total light transmittance (τ_t) and of sample diffusion rate (τ_4) are shown in figure 3. The calculated Haze value is shown in table 1. As shown in the figure and the table, the difference of fog degree between 3 and 4, 5 and 6 are distinguish clearly. As result, in this system, the fogged degree of samples which is difficult to be detected by visual observation can be evaluated by numerical value. So, this system can be effective to comparison of products or control of quality.

Introduction of Haze value measurement system for UV/Vis spectrophotometer


Figure 3a

Transmittance spectrum of six plate samples -
Sample 1


Figure 3b - Sample 2

Figure 3c - Sample 3

Figure 3d - Sample 4

Figure 3e - Sample 5

Figure 3f - Sample 6

No.	T ₃ [%]	T _t [%]	T ₄ [%]	T _d [%]	Haze [%]
1	0.08	93.06	0.71	0.63	0.7
2	0.08	92.13	4.94	4.86	5.3
3	0.08	90.88	18.7	18.62	20.5
4	0.08	90.7	23.12	23.04	25.4
5	0.08	87.75	69.34	69.27	78.9
6	0.08	85.46	70.56	70.49	82.5

Table 1 Calculation results of Haze value

Measurement Condition

Band width 5.0 nm
Scan speed 400 nm/min
Response 0.24 sec
Data interval 1 nm

Calculation Condition

Light source D65
Color-matching function JIS Z 8781-1
View angle 2°

Example of the measurement of a highly reflective material, a dielectric multi-layer mirror using absolute reflectance spectroscopy

Introduction

Dielectric multi-layer mirrors are laminated optics comprising of a combination of high refractive index and low refractive index materials. Using the interference effect, this mirror can provide extremely high reflectance (near 100%) in a specific wavelength range. (Figure 1)

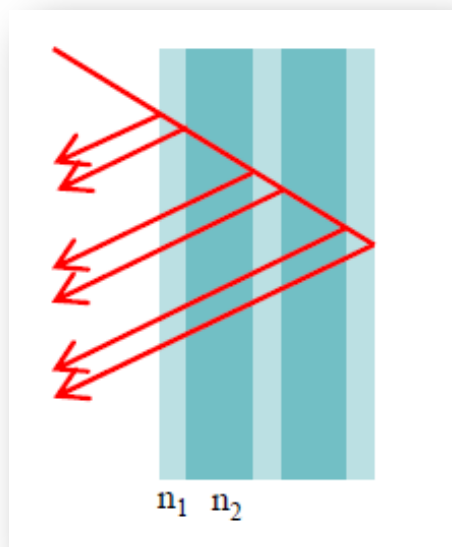


Figure 1 Diagram of the dielectric multi-layer mirror
 n_1 : high refractive index
 n_2 : low refractive index

This type of mirror is widely used in cameras, telescopes and optics for optical communication to reduce loss in light intensity. Therefore, in the quality control and R&D of dielectric multi-layer mirrors, it is very important to evaluate the reflectance with very high accuracy. JASCO provides a high performance absolute reflectance measurement system using the V-700 series UV/Vis spectrophotometer with double-beam optical system, which has high photometric stability.

The absolute reflectance system can perform measurement at arbitrary and user-selectable incident angles; this allows the measurement of dielectric multi-layer mirrors at designated incident angles. As an example of high reflectance measurement using the JASCO absolute reflectance measurement system, this application note reports the results for a dielectric multi-layer mirror.

Sample

Dielectric multi-layer mirror

Measurement

1. Dark measurement is performed with a light shielding plate.
2. Baseline measurement is performed against air.
3. Sample measurement is performed.

The procedure detailed above was repeated three times.

Measurement Condition

- Bandwidth 5.0 nm
- Scanning speed 20 nm/min
- Response 3.84 sec
- Data interval 1 nm
- Incident angle 10 degree
- Polarization p-polarized light



Figure 2 Absolute reflectance measurement accessory

Example of the measurement of a highly reflective material, a dielectric multi-layer mirror using absolute reflectance spectroscopy

Measurement result

Figure 3 shows an overlay of the absolute reflectance spectra of the dielectric multi-layer film mirror, and Figure 4 shows a zoomed view of the same spectra. As shown in the Figure 4, the measurement repeatability around 100%R is better than 0.1%R, which demonstrates that this system has very high measurement repeatability. Table 1 shows the comparison between the expected values and the measured values. The difference between the average of the measurement value and the expected value is better than 0.15%, which shows that this system has high accuracy and good correlation for reflectance measurement close to 100%R.

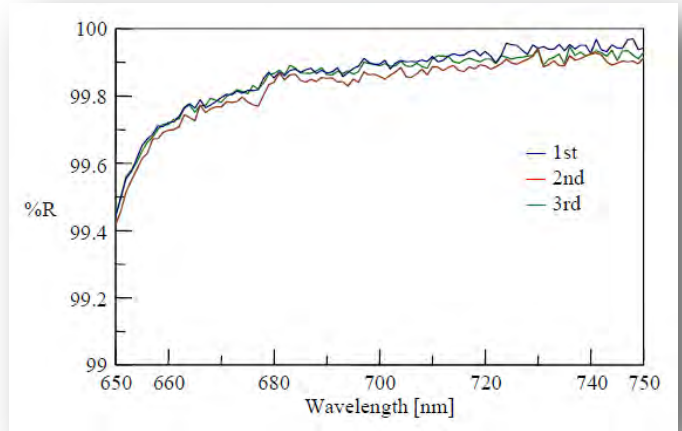


Figure 4 Absolute reflectance spectra of the dielectric multi-layer mirror at around 100%R

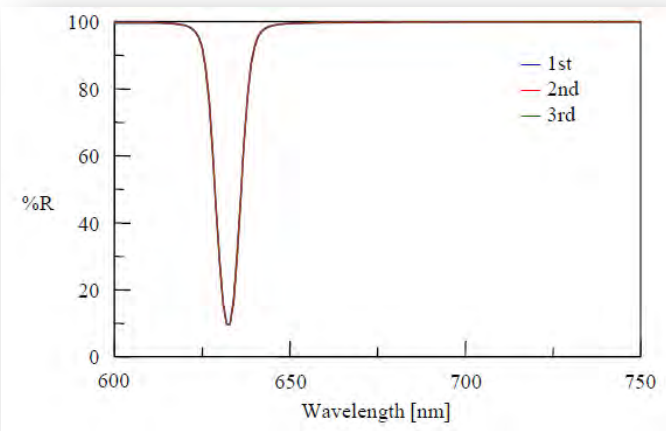


Figure 3 Absolute reflectance spectra of the dielectric multi-layer mirror

Wavelength [nm]	Expected value [%R]	Measurement value [%R]			Average value [%R]	Standard variation	Variation coefficient [%]	Difference between expected and average
		1	2	3				
680	99.9914	99.8663	99.8537	99.8407	99.8536	0.013	0.013	-0.1378
700	99.9918	99.8892	99.8943	99.8578	99.8804	0.020	0.020	-0.1114
720	99.9839	99.9094	99.9316	99.8889	99.9100	0.021	0.021	-0.0739

Table 1 Comparison of theoretical and measured values

Measurement reproducibility of Color Diagnosis System

Introduction

Color is a visually perceived property that is derived from the reflected or transmitted spectrum of light interacting with the eye (Figure 1).

It is important to evaluate and obtain measurable factors describing color for color management during the industrial processes used in the manufacture of products.

JASCO has developed various applications that use the V-700 Series of UV/Vis spectrophotometers for color analysis using both reflectance and/or transmittance spectra of samples. The V-700 spectrophotometer Figure 1 Mechanism of color recognition by human eye uses a double-beam optical system, which offers high measurement accuracy and stability. Because of the high performance of the V-700 UV/Vis spectrophotometer color coordinates (results for color calculation) can be determined with high reproducibility.

This application note illustrates the reproducibility of color calculations made using JASCO's proprietary color diagnosis system.

Sample

Color pellets (blue, red and yellow) (Figure 2)

Measurement

Measurement was performed using a V-750 UV-Vis spectrophotometer with ISV-922 integrating sphere and and VWCD-960 Color diagnosis program. Baseline measurement was performed using a standard white reference plate, then the sample was measured. Both reference and sample measurement was made with the specular reflection component included.

To confirm the measurement reproducibility 10 spectra were collected with the sample removed and replaced in between scans to assess the effects of changing the measurement position.

Measurement Condition

- Bandwidth 5.0 nm
- Scanning speed 400 nm/min
- Response 0.96 sec
- Data interval 1 nm

Measurement result

The reflectance spectra measured for each sample are shown in Figure 3. The right side of Figure 3 shows zoomed-in spectra in the wavelength range 740 - 780 nm.

As shown in each spectrum, the difference between maxima and minima of the photometric value is less than 0.15%R, this demonstrates that measurement system has high reproducibility.

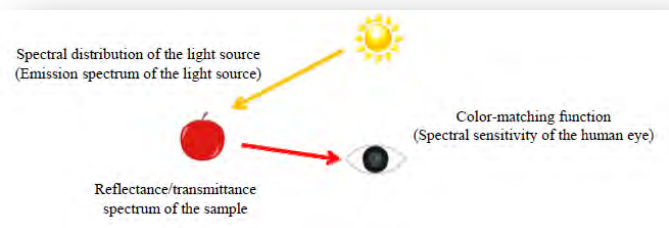
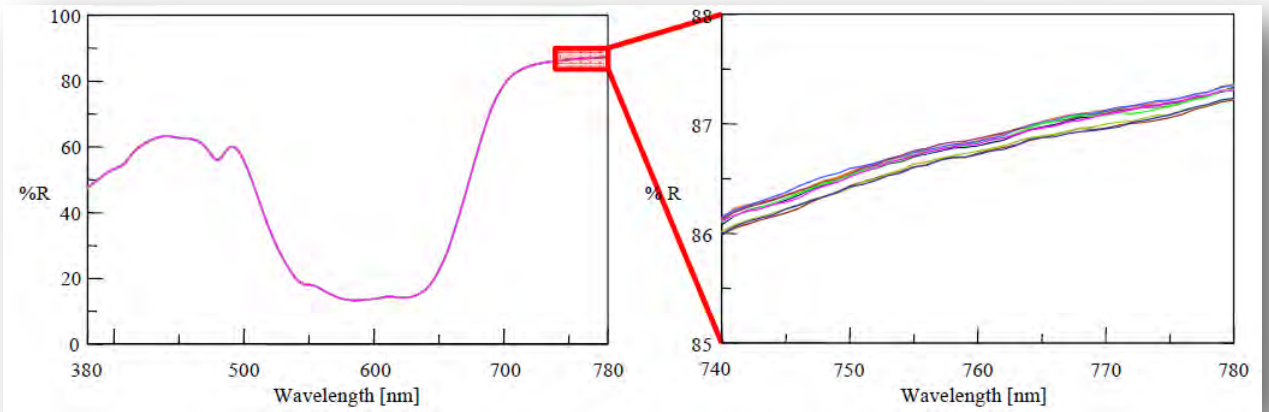


Figure 1 Mechanism of color recognition by human eye

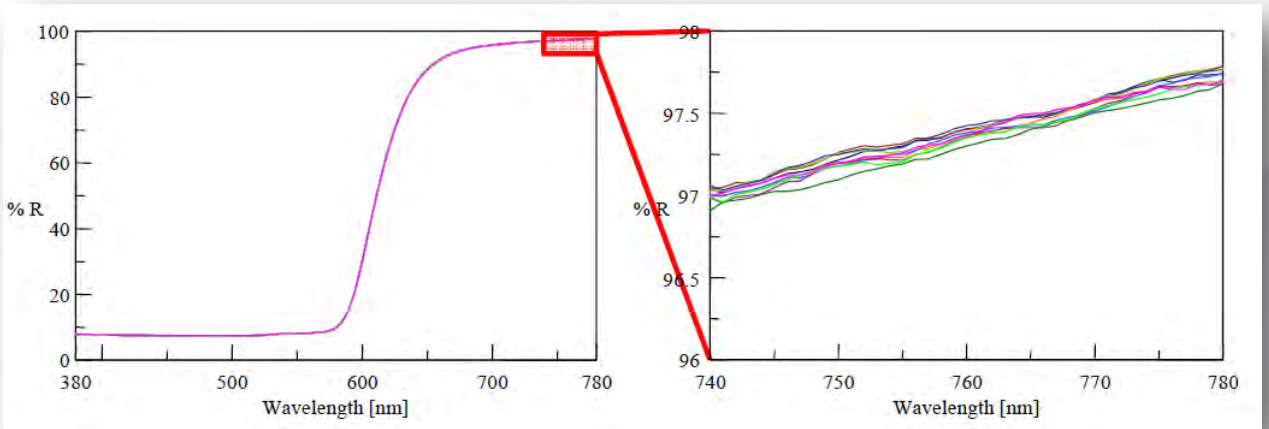


Figure 2 Sample

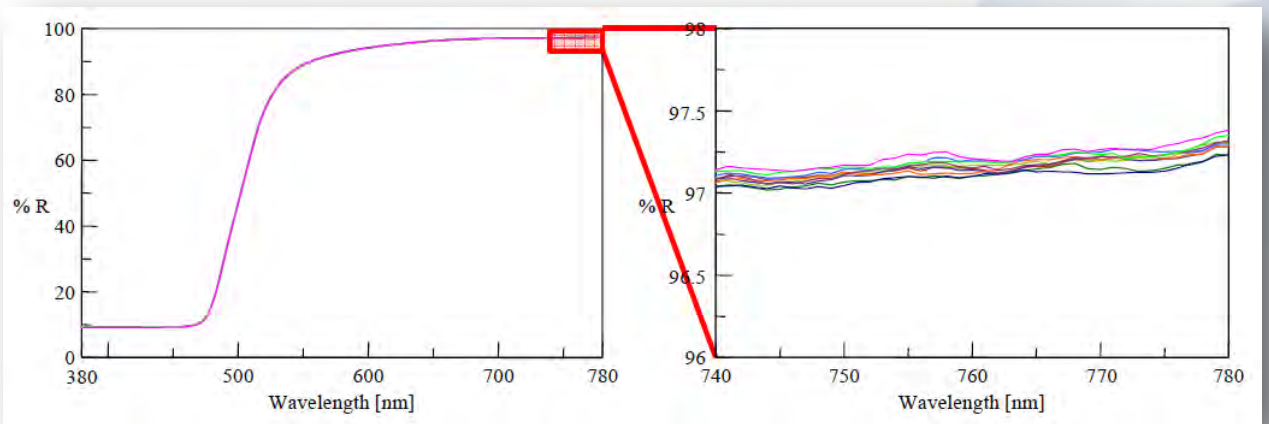
Measurement reproducibility of Color Diagnosis System



Color pellet (Blue)



Color pellet (Red)



Color pellet (Yellow)

Figure 3 Reflectance spectra of color pellets

Measurement reproducibility of Color Diagnosis System

Analysis Results

The Color Diagnosis Program (Fig.4) is used to calculate color coordinates from measured spectra. Figure 5 shows the results plotted on XYZ, L*a*b*, Lab and L*u*v* chromaticity diagrams. The calculated values are shown in tables 1, 2 and 3. For the color coordinates that represent chroma and hue (x, y, a^*b^*, ab, u^*v^*), the difference between maxima and the minima are; x and y , less than 0.0012, a^* and b^* , less than 0.31, a and b , less than 0.18, u^* and v^* , less than 0.50.

For the color coordinates that represent brightness (Y, L, L^*), the difference between the maxima and minima is less than 0.1.

As shown in these results the JASCO Color Diagnosis system offers high reproducibility.

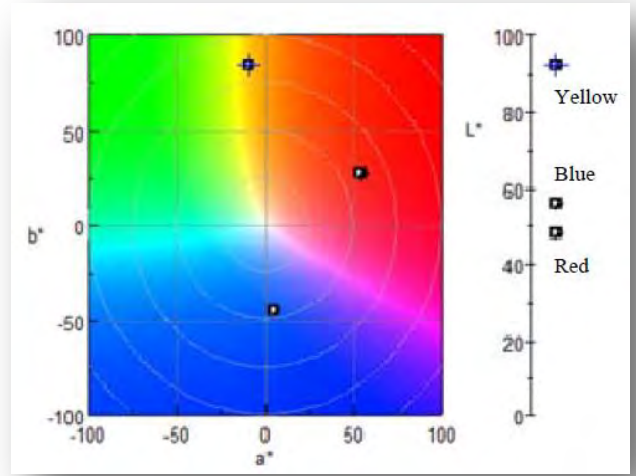


Figure 5b L*a*b* color system

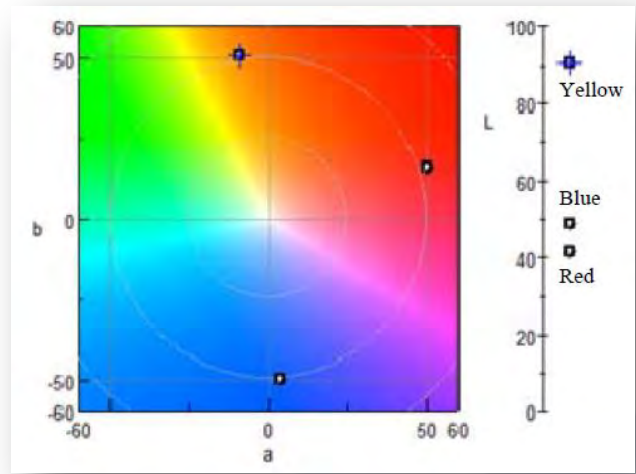


Figure 5c Lab color system

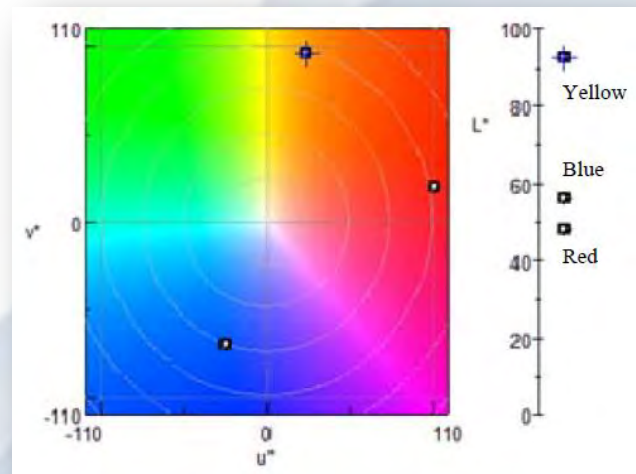


Figure 5d L*u*v* color system

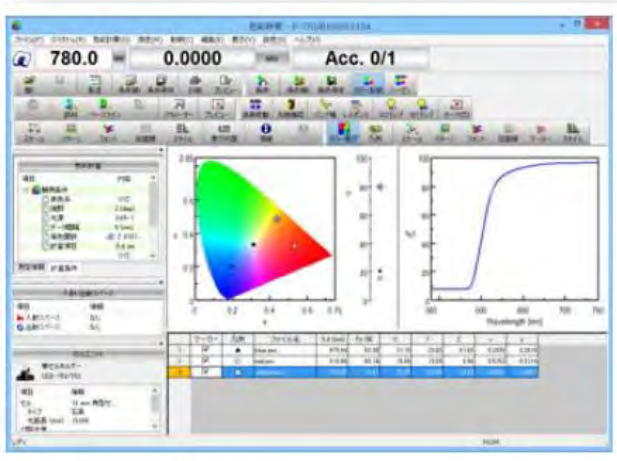


Figure 4 Color Diagnosis Program

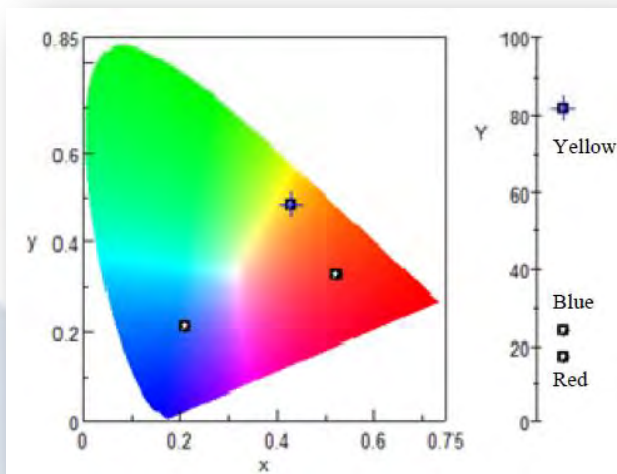


Figure 5a XYZ color system

Measurement reproducibility of Color Diagnosis System

Number of times	X	Y	Z	x	y	L*	a*	b*	L	a	b	u*	v*
1	23.77	23.94	65.84	0.2094	0.2108	56.03	4.58	-44.94	48.93	3.78	-50.19	-24.75	-70.73
2	23.77	23.94	65.81	0.2094	0.2109	56.03	4.57	-44.91	48.93	3.78	-50.15	-24.74	-70.69
3	23.74	23.91	65.70	0.2095	0.2109	55.99	4.57	-44.88	48.89	3.78	-50.09	-24.71	-70.62
4	23.76	23.93	65.72	0.2095	0.2110	56.01	4.57	-44.87	48.91	3.78	-50.08	-24.71	-70.60
5	23.76	23.92	65.71	0.2095	0.2110	56.01	4.56	-44.85	48.91	3.77	-50.06	-24.71	-70.58
6	23.79	23.96	65.85	0.2094	0.2109	56.04	4.57	-44.92	48.95	3.78	-50.16	-24.75	-70.70
7	23.80	23.97	65.85	0.2095	0.2110	56.06	4.55	-44.89	48.96	3.77	-50.12	-24.74	-70.65
8	23.81	23.98	65.83	0.2095	0.2111	56.07	4.55	-44.87	48.97	3.76	-50.08	-24.73	-70.62
9	23.80	23.97	65.79	0.2096	0.2111	56.06	4.55	-44.85	48.96	3.76	-50.06	-24.71	-70.58
10	23.80	23.97	65.81	0.2095	0.2111	56.06	4.55	-44.86	48.96	3.76	-50.08	-24.73	-70.61
Max-Min	0.07	0.07	0.15	0.0002	0.0003	0.07	0.03	0.09	0.07	0.02	0.13	0.05	0.14
Ave.	23.78	23.95	65.79	0.21	0.21	56.04	4.56	-44.88	48.94	3.77	-50.11	-24.73	-70.64
SD	0.02289	0.02509	0.05879	0.00006	0.00008	0.0252	0.0104	0.0312	0.0256	0.0083	0.0456	0.0168	0.0512
CV [%]	0.10	0.10	0.09	0.03	0.04	0.04	0.23	-0.07	0.05	0.22	-0.09	-0.07	-0.07

Table 1 Color calculation results of color pellet (blue)

Number of times	X	Y	Z	x	y	L*	a*	b*	L	a	b	u*	v*
1	27.74	17.16	8.17	0.5226	0.3234	48.47	53.78	26.78	41.43	49.99	15.67	101.05	19.17
2	27.78	17.17	8.09	0.5238	0.3237	48.47	53.94	27.08	41.44	50.17	15.80	101.55	19.40
3	27.76	17.15	8.10	0.5236	0.3236	48.45	53.92	27.02	41.41	50.14	15.77	101.46	19.34
4	27.75	17.15	8.08	0.5238	0.3237	48.45	53.92	27.06	41.41	50.13	15.79	101.48	19.37
5	27.73	17.14	8.10	0.5236	0.3236	48.43	53.90	26.99	41.40	50.11	15.75	101.39	19.31
6	27.70	17.11	8.10	0.5235	0.3235	48.40	53.89	26.94	41.37	50.10	15.73	101.35	19.27
7	27.76	17.18	8.13	0.5231	0.3237	48.49	53.80	26.97	41.45	50.01	15.76	101.21	19.34
8	27.72	17.14	8.11	0.5233	0.3235	48.43	53.85	26.93	41.40	50.06	15.73	101.27	19.27
9	27.72	17.14	8.11	0.5233	0.3235	48.43	53.86	26.93	41.40	50.06	15.73	101.28	19.27
10	27.77	17.19	8.13	0.5231	0.3238	48.50	53.78	26.97	41.46	50.00	15.76	101.18	19.35
Max-Min	0.09	0.08	0.08	0.0012	0.0004	0.10	0.16	0.31	0.09	0.18	0.13	0.50	0.23
Ave.	27.74	17.15	8.11	0.52	0.32	48.45	53.86	26.97	41.42	50.08	15.75	101.32	19.31
SD	0.0270	0.0230	0.0274	0.00038	0.00012	0.0288	0.0613	0.0852	0.0278	0.0640	0.0377	0.1545	0.0670
CV [%]	0.10	0.13	0.34	0.07	0.04	0.06	0.11	0.32	0.07	0.13	0.24	0.15	0.35

Table 2 Color calculation results of color pellet (red)

Measurement reproducibility of Color Diagnosis System

Number of times	X	Y	Z	x	y	L*	a*	b*	L	a	b	u*	v*
1	73.34	82.03	14.95	0.4306	0.4816	92.59	-9.44	84.03	90.57	-9.25	50.69	23.70	95.18
2	73.34	82.03	14.95	0.4306	0.4816	92.59	-9.43	84.03	90.57	-9.25	50.69	23.71	95.17
3	73.37	82.06	14.93	0.4307	0.4817	92.60	-9.44	84.11	90.59	-9.26	50.72	23.72	95.23
4	73.37	82.06	14.91	0.4307	0.4817	92.60	-9.44	84.15	90.59	-9.25	50.73	23.74	95.26
5	73.36	82.04	14.93	0.4307	0.4817	92.59	-9.42	84.10	90.58	-9.24	50.71	23.75	95.22
6	73.36	82.05	14.94	0.4307	0.4817	92.60	-9.44	84.09	90.58	-9.25	50.71	23.72	95.22
7	73.38	82.07	14.92	0.4307	0.4817	92.60	-9.44	84.13	90.59	-9.25	50.73	23.74	95.25
8	73.37	82.06	14.93	0.4307	0.4817	92.60	-9.44	84.11	90.59	-9.25	50.72	23.73	95.23
9	73.40	82.07	14.90	0.4308	0.4817	92.61	-9.41	84.18	90.59	-9.22	50.74	23.79	95.27
10	73.41	82.09	14.87	0.4309	0.4818	92.62	-9.41	84.26	90.60	-9.23	50.77	23.81	95.33
Max-Min	0.07	0.07	0.08	0.0003	0.0002	0.03	0.03	0.23	0.04	0.03	0.08	0.11	0.16
Ave.	73.37	82.06	14.92	0.43	0.48	92.60	-9.43	84.12	90.59	-9.24	50.72	23.74	95.24
SD	0.0218	0.0201	0.0232	0.00008	0.00006	0.0089	0.0118	0.0678	0.0111	0.0112	0.0241	0.0348	0.0457
CV [%]	0.03	0.02	0.16	0.02	0.01	0.01	-0.13	0.08	0.01	-0.12	0.05	0.15	0.05

Table 3 Color calculation results of color pellet (yellow)

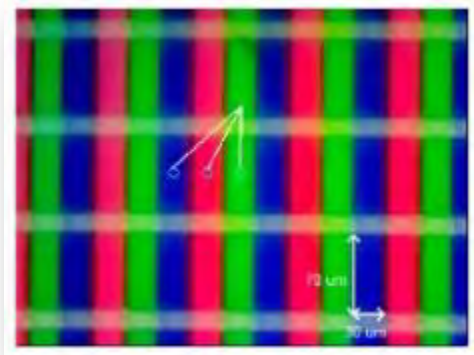
Analysis Conditions

- Light source D65 (CIE 15:2004, JIS Z 8781-1:2012, ISO 11664-2:2007)
- Color-matching function CIE 15:2004, JIS Z 8701:1982
- Viewing angle 2°
- Data interval 5 nm

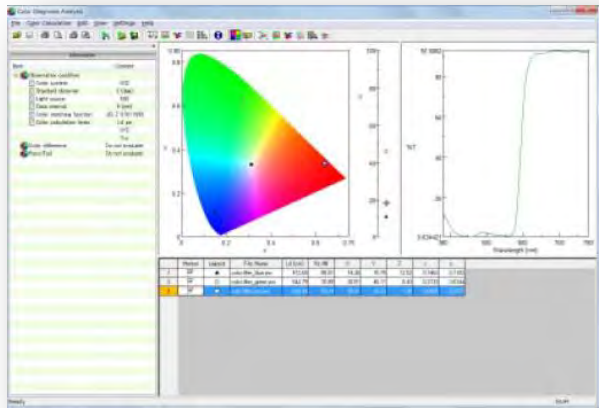
Color Analysis System for RGB Color Filters

Introduction

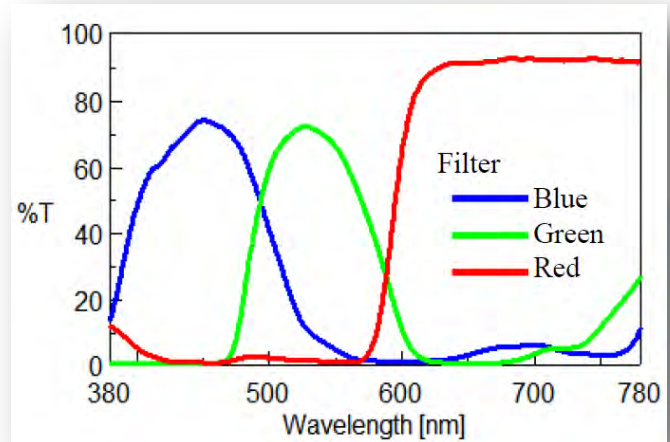
This system measures the transmittance for each pixel in RGB color filters used for flat panel displays, and analyzes the color. The transmittance spectrum for the three colors in the filter was measured, and the calculation results were plotted as a chromaticity diagram using the [Color Diagnosis Analysis] program



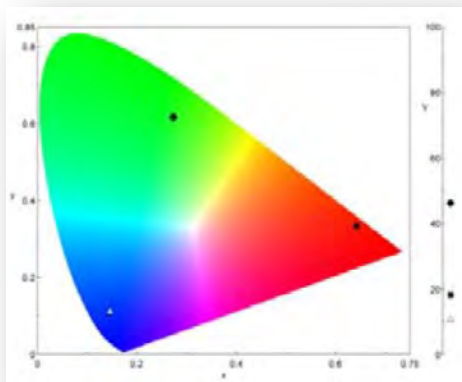
Observed image



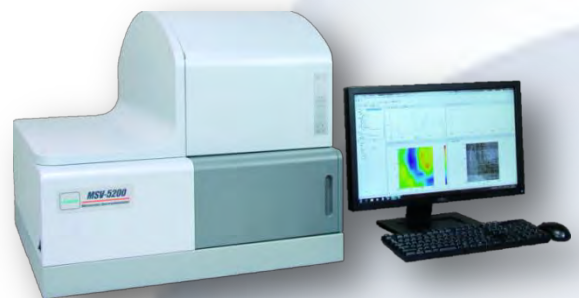
[Color Diagnosis Analysis] program



Transmittance spectrum



Chromaticity diagram (XYZ color system)



	Model No.	Product name	Remarks
Instrument	MSV-5200-16	UV/Vis/NIR Micro-spectrophotometer	<ul style="list-style-type: none"> Wavelength range: 200 to 2700 nm Supplied with 16x Cassegrain objective, converging mirrors, and manual stage.
Optional Program	MCAN-581	[Color Diagnosis Analysis] program	<ul style="list-style-type: none"> Dedicated analysis program for Spectra Manager Ver.2 Data in multiple file formats (*.jwa, *.jwb, *.jwd) can be analyzed.
Optional Accessories	MAXY-501-F	Automatic XYZ stage	<ul style="list-style-type: none"> Optionally installed in factory Movable distance*: X: 76 mm Y: mm, 52 mm, Z: 25 mm. * Varies depending on the magnification of the objective or convergence mirror, or the type of sample.
Description	Available models are the MSV-5100 (200 to 900 nm) and MSV-5300 (200 to 1600 nm). Using the automatic XYZ stage, mapping, line and multipoint measurements can be performed, in addition to automatic focusing and multiple-image acquisition. The joystick is an optional extra.		

Estimation of refractive index of monocrystalline sapphire by polarization measurement using MSV-5000 series

Introduction

The MSV-5000 series microscopic spectrophotometer is for transmission and reflection measurements of a sample as small as 10 μmφ in a wide wavelength range from ultraviolet to near-infrared. The MSV-5000 has a built-in the Glan-Taylor polarizer as standard and can obtain optical constant such as refractive index(n) and extinction coefficient(k) by measuring reflectance spectrum of small monocrystalline having birefringence. This time, the monocrystalline sapphire(measurement area size: 50 um in diameter), which has two types of crystal axis (c-axis or a-axis) and whose refractive index is already known, was measured and the dispersion of the refractive index was calculated.

Measurement system

MSV-5200 UV/Vis/NIR Microscopic spectrophotometer
VWML-791 Multi-layer analysis program

Sample

Monocrystalline sapphire

Measurement

1. Baseline: Two baselines of Al vapor deposited mirror were measured with polarizer angle at 0 and 90 degrees as a reference.
2. Determination of crystalline axis: Under the condition of the polarizer angle at 0 degree and wavelength at 550 nm, the sample was rotated to find the angle of sample where the sample showed maximum reflectance. Then c-axis was determined by this angle and as orthogonal of c-axis, a-axis was determined as.
3. Sample Measurement: After determination of c-axis, the reflection spectra were measured at polarizer angle at 0 and at 90 degree respectively.
4. Conversion into absolute reflectance: The absolute reflectance spectrum of the sample was calculated by multiplying the obtained relative reflectance by the absolute reflectance spectrum of Al vapor deposited mirror.

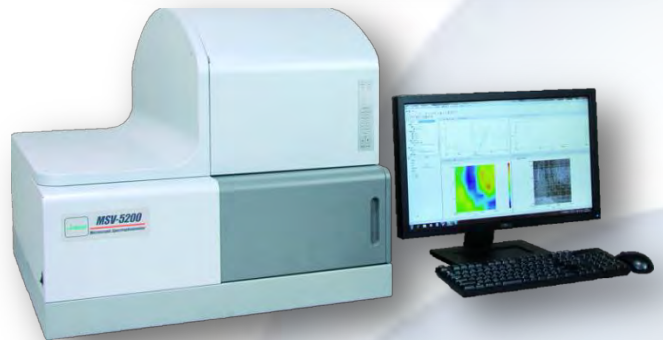
Analysis

Two kinds of calculation methods were used for obtaining the refractive index and the results were compared.

1. Method using [UVVIS K-K Conversion] Program: The refractive index(n) is expressed by specular reflectance spectrum(R) and phase change(φ) (Equation 1). Since the Kramers-Kronig(K-K) equation can be applied to specular reflectance spectrum(R) and phase change(φ) (Equation 2), phase change(φ) was calculated by K-K conversion of specular reflectance spectrum (R) and then, the refractive index(n) was calculated.

$$n = \frac{1 - R}{1 + R - 2\sqrt{R} \cos \phi} \quad \text{Equation 1}$$

$$\phi(\omega) = \frac{2\omega}{\pi} P \int_0^{\infty} \frac{\ln \sqrt{R(\omega')}}{\omega'^2 - \omega^2} d\omega' \quad \text{Equation 2}$$



2. Method using [Multi-layer Analysis] Program (Application of Fresnel equation): Reflectance spectrum is expressed by the refractive index of the air and the sample(n1, n2), the incident angle(θ1) and the reflection angle(θ2) (Equation 3). By applying this equation, the wavelength dispersion of the refractive index was calculated using [Multi-layer Analysis] Program by fitting the calculated reflectance spectrum using Equation 3 to the measured spectrum.

$$R = \frac{1}{2} \left\{ \left(\frac{n_1 \cos \theta_1 - n_2 \cos \theta_2}{n_1 \cos \theta_1 + n_2 \cos \theta_2} \right)^2 + \left(\frac{n_1 \cos \theta_2 - n_2 \cos \theta_1}{n_2 \cos \theta_1 + n_1 \cos \theta_2} \right)^2 \right\} \quad \text{Equation 3}$$

Estimation of refractive index of monocrystalline sapphire by polarization measurement using MSV-5000 series

Parameters

Spectral bandwidth: 5.0 nm
 Response: Slow
 Accumulation: 3 times
 Cassegrain objective : 16 times
 Angle of polarizer: 0, 90 degree
 Scan speed: 200 nm/min
 Data interval: 0.1 nm
 Incident angle: 23 degree
 IN aperture: 50 $\mu\text{m}\phi$
 OUT aperture: : 50 $\mu\text{m}\phi$

Measurement Results

Absolute reflectance spectrum of monocrystalline sapphire is shown in Figure 1. Reflectance of ordinary light (c-axis) is approximately 0.15% higher than that of extraordinary light (a-axis).

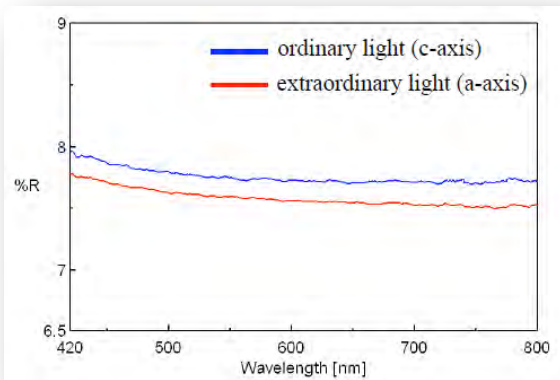


Figure 1 Absolute reflectance spectra of monocrystalline sapphire

Analysis Results

By using [UVVis K-K Conversion] and [Multi-layer Analysis] Program, the wavelength dispersion of the refractive index was obtained (Figure 2). Table 1 shows the result compared with the literature value of the refractive index of ordinary light and extraordinary light. The refractive index was determined with precision of two decimal places in a small area of several tens of microns, by either calculating method.

Table 1 Comparison with literature value of the refractive index of monocrystalline sapphire

above: by using [UVVis K-K Conversion] Program
 below: by using [Multi-layer Analysis] Program

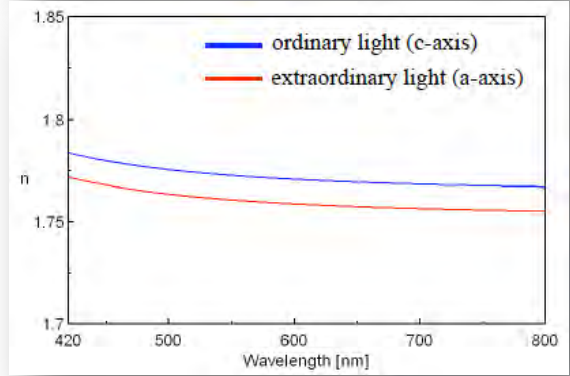
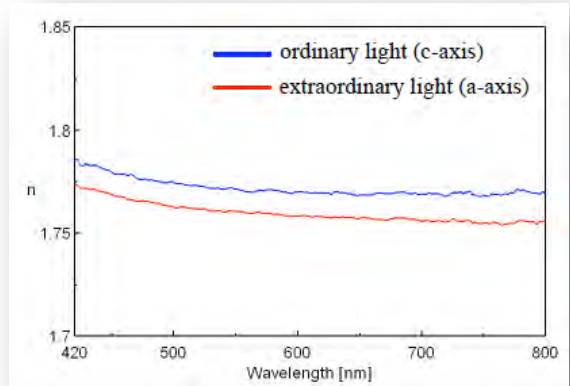


Figure 2 Wavelength dispersion of refractive index of monocrystalline sapphire
 above: by using [UVVis K-K Conversion] Program
 below: by using [Multi-layer Analysis] Program

Wavelength [nm]	Literature value	K-K transform		Multilayer analysis	
	Refractive index	Refractive index	Error	Refractive index	Error
632.8	1.766	1.770	0.0037	1.769	0.0036
589.3	1.768	1.770	0.0016	1.771	0.0028
546.1	1.771	1.772	0.0012	1.773	0.0018
532.0	1.772	1.771	-0.0005	1.773	0.0015
514.5	1.773	1.773	-0.0005	1.774	0.0011
488.0	1.775	1.775	-0.0005	1.776	0.0007

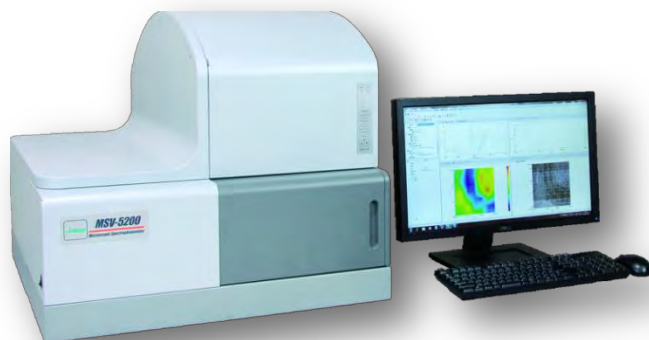
Wavelength [nm]	Literature value	K-K transform		Multilayer analysis	
	Refractive index	Refractive index	Error	Refractive index	Error
632.8	1.758	1.757	-0.0005	1.758	-0.0003
589.3	1.760	1.758	-0.0015	1.759	-0.0011
546.1	1.763	1.761	-0.0017	1.761	-0.0020
532.0	1.764	1.761	-0.0030	1.761	-0.0022
514.5	1.765	1.762	-0.0032	1.762	-0.0026
488.0	1.767	1.764	-0.0028	1.764	-0.0030

Transmittance and Reflectance Measurement System For Minute Lenses

Introduction

Small type lens is widely used in various products as smart phone , tablet, PC etc. This note show the transmittance and reflectance measurement for 1-mm-diameter lenses used in mobile-phone cameras.

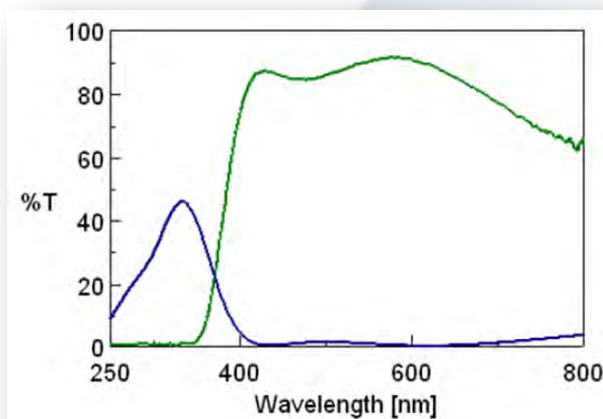
For samples that refract light such as lenses, the transmittance can be measured using an integrating sphere. The reflectance can also be measured if the aperture size is sufficiently reduced so that the area being analyzed can be considered to be flat.



1-mm-diameter
mobile-phone camera lens



Integrating sphere for MSV-5200



	Model No.	Product name	Remarks
<i>Instrument</i>	MSV-5200-16	UV/Vis/NIR Micro-spectrophotometer	<ul style="list-style-type: none"> Wavelength range: 200 to 2700 nm Supplied with 16x Cassegrain objective, converging mirrors, and manual stage.
<i>Optional Accessories</i>	MISP-552	Integrating sphere for MSV-5200	<ul style="list-style-type: none"> Wavelength range: 250 to 2000 nm Only for the dedicated manual stage for the integrating sphere. Not applicable for diffuse transmittance or reflectance measurements. Normal (non-diffuse) reflectance measurements can be performed using the reflectance optical path.
<i>Description</i>	Available models are the MSV-5100 (200 to 900 nm) and MSV-5300 (200 to 1600 nm). The type of integrating sphere varies depending on the instrument model, and determines the wavelength range that can be used.		

Verification of [Wavelength Accuracy] and [Wavelength Repeatability] using mercury emission line spectrum

Introduction

For high-precision CD spectrum measurement, [Wavelength Accuracy] and [Wavelength Repeatability] are important parameter to obtain precise spectrum. J-1000 CD spectrometer has high [Wavelength Accuracy] and [Wavelength Repeatability], and these features can realize high-precision CD spectrum measurement. In this application data, [Wavelength Accuracy] and [Wavelength Repeatability] are verified by measuring the 253.652 nm emission line spectrum of the mercury lamp, which is installed in J-1000 series CD spectrometer for validation.

Repeat count	Peak wavelength
1	253.650 nm
2	253.650 nm
3	253.650 nm
4	253.650 nm
5	253.650 nm

Table 1 Wavelength repeatability

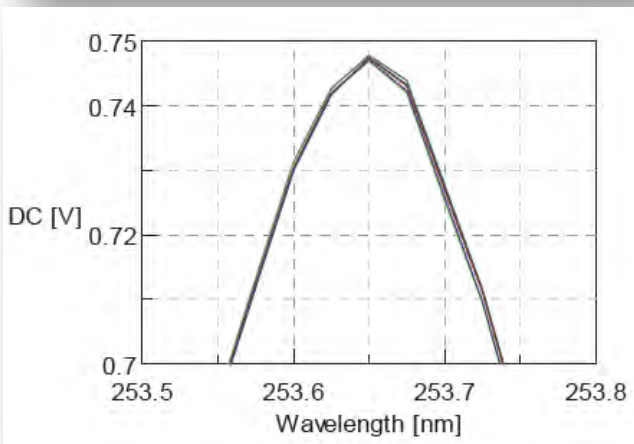
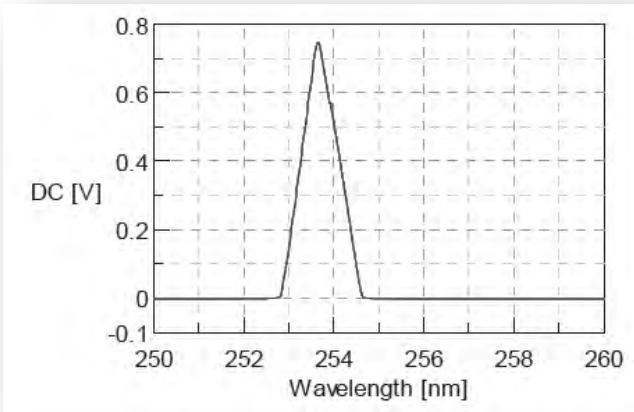


Figure 1 Mercury Lamp emission line spectra (bottom: Zoom View)



JASCO J-1500
Circular Dichroism Spectropolarimeter

JASCO Europe S.r.l.

Via Cadorna, 1 - 23894 Cremella (LC)

jasco@jasco-europe.com

www.jasco-europe.com

DISCLAIMER

The contents of this publication are for reference and illustrative purposes only. Information, descriptions, and specifications in this document are subject to change without notice and cannot be used from third parts for data comparison and/or performance comparison. JASCO assumes no responsibility and will not be liable for any errors or omissions contained herein or for incidental, consequential damages or losses in connection with the furnishing, performance or use of this material.